BINARY COLLISION-INDUCED LIGHT SCATTERING BY MOLECULAR GASES

A Thesis

Submitted to

the Faculty of Graduate Studies

University of Manitoba

In Partial Fulfillment

of the Requirements for the Degree

Doctor of Philosophy

by

David Peter Shelton

February 1979

BINARY COLLISION-INDUCED LIGHT SCATTERING BY MOLECULAR GASES

BY

DAVID PETER SHELTON

A dissertation submitted to the Faculty of Graduate Studies of the University of Manitoba in partial fulfillment of the requirements of the degree of

DOCTOR OF PHILOSOPHY

ACKNOWLEDGEMENT

Among many others:

To Peter and Kumar, without whom I would not be finished at this time,

And to George and Carol, without whom I would not be finished at all.

ABSTRACT

The spectrum of light scattered during binary molecular collisions, in gas samples at about one tenth the liquid density, has been studied both experimentally and theoretically. It is found that the molecular collision-induced scattering (CIS) spectrum can be accounted for by the sum of a component due to collision-induced translational Raman transitions and a component due to collision-induced rotational Raman transitions. The theory of the collision-induced rotational scattering (CIRS) spectrum has only recently been developed; the first quantitative comparison of theory and experiment for the CIRS spectrum is presented herein.

CONTENTS

LIST OF FIGURES

LIST OF TABLES

CHAPTER 1

INTRODUCTION

The present study is the outgrowth of the more-or-less unsecessful (from the narrow viewpoint of the following thesis) study of collision-induced light scattering from liquids.[1] The difficulty with the study of liquids is that the constituent molecules are densely packed, so that the scattered light spectrum depends on the details of the molecular motions as well as details of the mechanism by which light interacts with the molecules. The straightforward way out of the difficulty is to choose a system with a density low enough that only two molecules at a time need to be considered. Thus we have chosen to study the spectrum of light scattered from relatively low density gases.

Before discussing collision-induced light scattering (CIS), we will discuss the mechanism by which light is scattered by a single atom or molecule. We will adopt the classical picture of the interaction of light with matter because of its relative simplicity compared to the quantum mechanical description.

According to the classical picture, the oscillating electric field of the light wave induces an oscillating polarization in the atom with the same phase and frequency as the incident wave. The dipole induced in the atom follows the polarizing field essentially instantaneously -- even though the frequency of the light is large (6×10^{14} Hz for light of wavelength 5000 Å) the orbital frequency of even the outer shell electrons is usually 100 times larger, and to the electrons the variation of the applied electric field seems very slow indeed. The oscillating dipole induced in the atom is the source

of a radiated electromagnetic wave which is called the scattered wave and which has the same frequency, polarization and phase as the incident wave. If the atom is well removed from its neighbours, as in a dilute gas, then the relative phases of the waves scattered from neighbouring atoms will be random and the waves will add incoherently. The scattered light will have a very wide angular distribution about the direction of the incident light beam and is called "Rayleigh" scattered light.

Molecules, in addition, have internal vibrational and rotational degrees of freedom. The polarization induced in the molecule by the incident light wave is modulated at the vibrational or rotational frequency of the molecule. The scattered wave will now also contain the sum and difference of the vibrational (or rotational) frequency and the frequency of the incident light wave. The phase of the scattered wave depends on the phase of the molecular vibration (or rotation) and so the scattered, frequency shifted waves from neighbouring molecules will add incoherently. This is called "Raman" light scattering. In a dense medium, the total Raman scattered intensity is just the sum of the intensity scattered by each molecule, while for Rayleigh scattering we have to take into account the interference between waves scattered from individual molecules. In a perfect crystal the Rayleigh scattered waves will all cancel to give zero scattered intensity, but in real liquids and solids density fluctuations of the material will prevent this from occurring.[2]

In all the above discussion, the individual molecules are considered as being independent scattering sources - the resultant scattered wave is determined by superposing all the separately scattered waves

taking into account their phases and amplitudes. In the case of collision-induced light scattering, we can no longer consider the individual molecules as independent scattering sources, unaffected by their neighbours. Consider again the case of the dilute gas and in particular the light scattered by a pair of atoms when they are close enough to interact appreciably.

The dipole moment induced in the pair of atoms when they are close together is generally larger than the sum of the dipoles on the separated atoms placed in the same electric field, and the direction of the induced dipole need no longer be parallel to the incident electric field. As the atoms move past each other the amplitude of the scattered wave will be increased for a short time. The modulation of the scattered wave introduces new frequency components — the collision-induced scattered light is shifted in frequency from the incident and the Rayleigh scattered light. The faster the modulation, the larger the frequency shift. Molecular velocities are in the order of 5 Å/psec (500 m/sec) and the interaction between atoms occurs within about 2.5 Å of the closest approach distance so that the amplitude of the scattered wave is modulated for a period of about 1.0 psec each time a pair of atoms collide. The peak value of the modulation is about 10 percent of the amplitude of the wave scattered by the pair when the atoms are far apart. The period of the modulation is very long compared to the period of oscillation of the light wave, which is about 0.002 psec. (See Figure 1-1 a.)

We may note in passing that for Rayleigh scattering there is phase modulation of the scattered wave due to the translational motion of the atom. For a dilute gas the period of phase modulation is given by the

FIGURE 1 - 1

Modulation of the Scattered Light Amplitude by Molecular Collisions

Each diagram shows the envelope of the electric field of the scattered light wave and a schematic representation of the trajectories of the colliding molecules in the gas during the same time interval.

a) The gas density is about 0.2 mole/liter or less. Only isolated binary collisions are important since the time interval between collisions is about 25 psec (25×10^{-12} sec.), which is about 25 times the duration of the intermolecular interaction during a collision. The amplitude of the scattered wave has a constant value due to Rayleigh scattering when the molecules are far apart. When they are sufficiently close together the amplitude of the scattered wave is increased; the modulated wave has the form of a short pulse on a flat baseline.

b) The gas density is about 2.0 mole/liter and the average time between collisions is about 2.5 psec. Isolated binary collisions still account for a large fraction of all collisions, but triple collisions of the type where 1 hits 2 and 2 hits 3 in rapid succession are also common. The intensity scattered in this type of triple collision is less than if the two successive collisions were more widely separated in time, because of destructive interference between the waves scattered in the two collisions.

c) The density is about 20 mole/liter or more and the time between collisions is only 0.25 psec. It is no longer possible to talk about isolated binary collisions since the motion of each individual molecule depends on the motion of all the other molecules in the cluster. The scattered amplitude must take into account all the molecules in the cluster, and it takes the form of a "random" fluctuation around the mean amplitude.

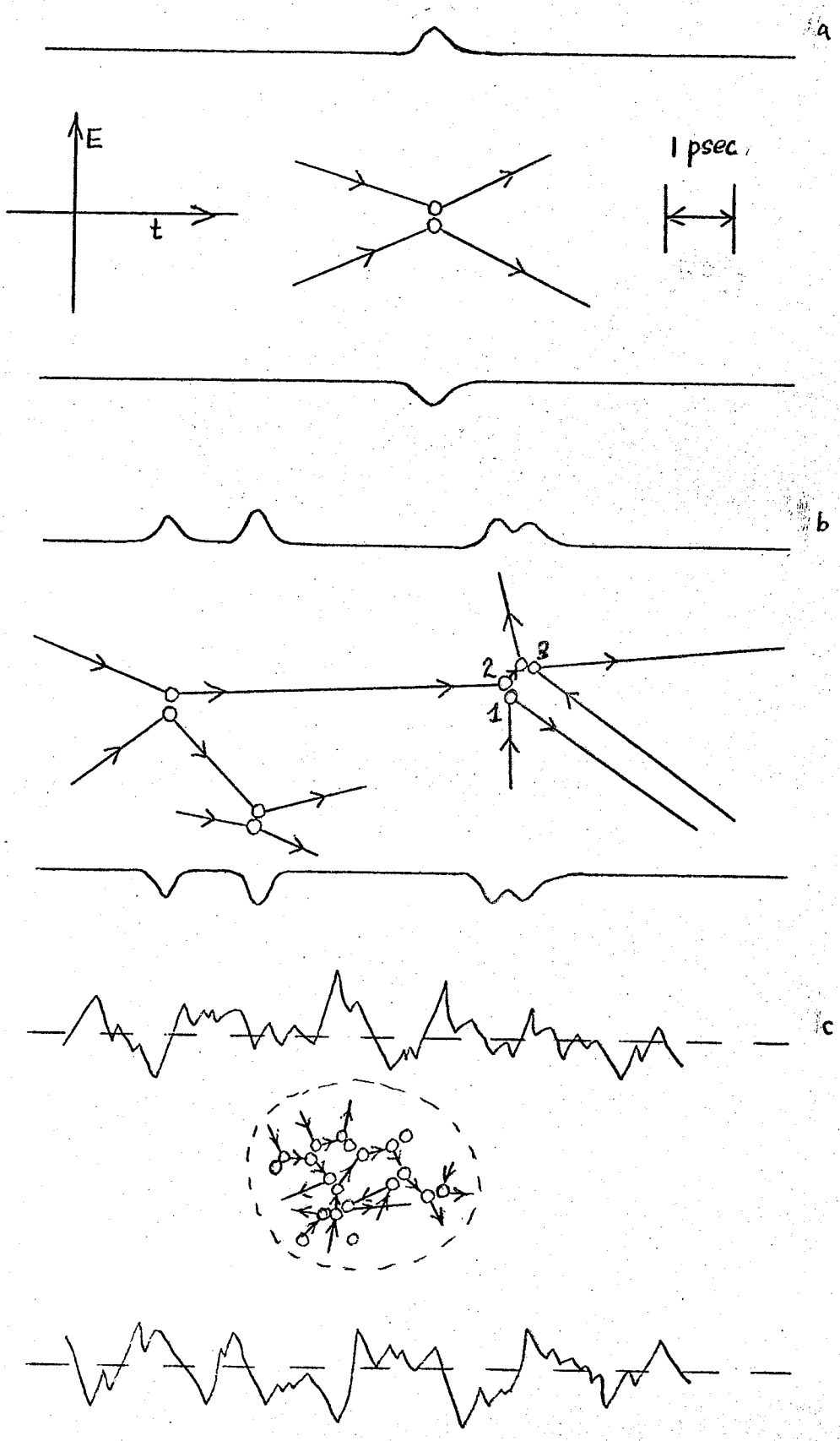
a
E
t
1 psec.
b
1
2
3
c

time an atom takes to travel one wavelength of light - about (5000 Å)/(5 Å/psec) = 1000 psec - which is a very long time compared with the duration of the events with which we will be dealing.

Collision-induced scattering from pairs of atoms or molecules becomes conveniently observable in gases at densities of the order of 1 mole/liter. (For comparision, a gas at NTP has a density of about 1/25 mole/liter while a liquid will have a density of about 25 mole/liter.) The time interval between successive collisions of a molecule will be about 5 psec at this density and there will seldom be more than two molecules participating in a collision. At these low densities the intensity of the CIS will increase as the square of the density since the density of pairs of molecules increases as the square of the density of molecules. At higher densities, collisions involving three molecules will become more frequent and the density-cubed term becomes significant in the expansion of the scattered light intensity as a power series in the sample density. The sign of the so-called three-body term is negative and the scattered light intensity increases more slowly than before because of it.[3] (See Figure 1-1 b.) When densities greater than 10 mole/liter are considered the clusters of interacting molecules are so large that our description, based on the model of independent binary collisions, becomes inadequate. The modulation of the scattered wave no longer looks like distinct pulses on a flat baseline but rather undergoes a continual random fluctuation. (See Figure 1-1 c.) Our experiments have been conducted in the density range of 0.5 - 5.0 mole/liter, where the CIS spectrum is conveniently observable and interpretation in terms of binary collisions is possible.

The defining features of collision-induced light scattering in

the chosen density range are:

1) The intensity behaves as $I = I^{(2)} \rho^2 - I^{(3)} \rho^3$, so that the contribution to the scattered light due to colliding pairs may be extracted from the data with little difficulty.

2) The CIS spectrum is "depolarized"; that is to say, light may be scattered with a polarization different from that of the incident light.

3) The spectral distribution is very broad compared to that of the Rayleigh scattered light.

The frequency shifts corresponding to vibrational Raman scattering are much larger than those corresponding to CIS, but the frequency shifts due to Raman scattering by rotating molecules lie in the same range as those due to CIS. Since the rotational Raman scattering by a molecule is usually much stronger than CIS by the same molecule, and is also depolarized and occurs at the same frequencies, we have been forced to observe only those molecules for which there is no rotational Raman spectrum. We may choose molecules of tetrahedral or higher symmetry or atoms, where the polarizability is invariant under rotations. The particular atoms and molecules chosen for this study were Ar, CH_4, CD_4, CF_4 and SF_6.

The object of this study is to compare the experimental and theoretical results for the intensity and spectral distribution of the light scattered by colliding pairs of optically isotropic atoms or molecules with the hope of elucidating the mechanisms involved. The thorough understanding of binary CIS is considered to be a necessary prerequisite for an understanding of the more complicated three-body and N-body CIS processes which occur in high density gases and liquids. Even in the two-body case the molecular dynamics of the collision and

the mechanism of light scattering are linked in describing the scattered spectrum. Both the intensity and the spectral distribution of the CIS spectrum must be studied since, very roughly, the collision dynamics governs the spectral width while the cluster polarizability governs the total intensity. In the following chapters we will develop the theory of collision-induced light scattering by pairs of molecules as an extension of the theory for Raman light scattering by a rotating diatomic molecule and the results of our model will be compared with the observed CIS spectrum.

NOTES AND REFERENCES

1. As an example of the earlier work in the area of CIS liquids, see:

G. C. Tabisz, W. R. Wall, D. P. Shelton, Chem.Phys. Lett. 15, 387 (1972) .

For a survey of the subject of CIS and an extensive list of references, we refer the reader to the review articles by Gelbart and by Tabisz. They cover the development and present state of the field.

W. M. Gelbart, Adv. Chem. Phys. 26, 1 (1974)

G. C. Tabisz, Specialist Periodical Reports 29, Molecular Spectroscopy Vol 6 (to be published 1979)

2. Rayleigh and Raman light scattering are discussed in:

J. D. Jackson, Classical Electrodynamics, Wiley,New York, 1975

B. J. Berne, R. Pecora, Dynamic Light Scattering, Wiley, New York, 1976.

G. W. King, Spectroscopy and Molecular Structure, Holt, Rinehart and Winston, New York, 1964

D. A. Long, Raman Spectroscopy, McGraw-Hill, New York, 1977

3. J. P. McTague, W. D. Ellenson, L. H. Hall, J. de Phys. (Paris) 33, C1-241 (1972)

CHAPTER 2

THE DIATOMIC ROTOR

This chapter will consist of a fairly detailed discussion of light scattering by a rotating diatomic molecule, both in terms of the classical theory and the quantum mechanical theory. The discussion of light scattering by a pair of colliding molecules in the next chapter will be an extension of the classical scattering theory developed for the rigid diatomic rotor. Likewise, the discussion of the quantum rotor will provide an introduction to the theory of collision-induced rotational scattering covered in Chapter 4.

Besides providing the background for discussion of collision-induced light scattering, the diatomic rotor is important in its own right. As a matter of experimental convenience (bordering on necessity) the intensity of the CIS Spectrum is measured by comparing it with the intensity of the rotational Raman lines of the hydrogen molecule. The intensity of these Raman lines may be calculated using the quantum mechanical theory of the diatomic rotor. Finally, since the theory of the diatomic rotor can be worked out in both the classical and the quantum cases, the comparison of the classical and quantum results for the diatomic rotor at least gives an indication of the accuracy and range of validity of the classical approximation as it is applied to light scattering.

2.1 The Classical Case

In the classical theory of light scattering,[1] the scattered wave is generated by the oscillating dipole moment induced in an atom by

the oscillating electric field of the incident light wave. The strength of the induced dipole moment is proportional to the strength of the applied electric field; the constant of proportionality is called the polarizability of the atom. However, the induced dipole will not in general lie along the direction of the applied electric field when we consider molecules rather than atoms. The scalar polarizability must be replaced by a second rank tensor called the polarizability tensor. The induced dipole moment is now given by the expression:

$$\vec{d} = \underset{\sim}{\alpha}\, \vec{E}$$

or in Cartesian tensor notation:

$$d_i = \alpha_{ij} E_j \quad .$$

For our purposes, the incident light wave is completely specified by its amplitude, wavevector and (linear) polarization vector. (In the quantum mechanical description this is called the random phase approximation.) The wavevector $\vec{k}$ is the vector in the direction of propagation with magnitude $|\vec{k}| = \omega/c$. The polarization vector $\vec{\lambda}$ is the vector orthogonal to $\vec{k}$ which lies in the direction of the electric field of the light wave. The electric field of the light wave specified by $\vec{k},\vec{\lambda}$ is:

$$\vec{E} = E_{\vec{k},\vec{\lambda}}\, \vec{\lambda} e^{i\omega t} \quad .$$

The elctric field of the light wave radiated by an induced dipole oscillating at the frequency ω_s is given by:

$$\vec{E}_s = \vec{k}_s \times (\vec{k}_s \times \vec{d}) \frac{1}{R}$$

where the subscript s denotes "scattered" and R is the distance from the scattering source to the observation position. The component

of the scattered field with polarization $\vec{\lambda}_s$ is given by:

$$\vec{\lambda}_s \cdot \vec{E}_s = \vec{\lambda}_s \cdot (\vec{k}_s \times (\vec{k}_s \times \underset{\sim}{\alpha} \vec{E})) \frac{1}{R}$$

where we have expressed the induced dipole in terms of the molecular polarizability and the applied field.

Rather than work directly with electric field amplitudes, it is usual to describe the light scattering in terms of the differential scattering cross section. The cross section is the ratio of the intensity of the light scattered with wavevector and polarization $\vec{k}_s$, $\vec{\lambda}_s$ into the solid angle $d\Omega$, to the intensity of the incident light wave:

$$\begin{aligned}
\frac{d\sigma}{d\Omega} &= \frac{|\vec{\lambda}_s \cdot \vec{E}_s|^2}{|\vec{E}|^2} = \left| \vec{\lambda}_s \cdot (\vec{k}_s \times (\vec{k}_s \times \underset{\sim}{\alpha} \vec{\lambda})) \right|^2 \\
&= \left| \vec{\lambda}_s \cdot \left[\underset{\sim}{\alpha} \vec{\lambda} (\vec{k}_s \cdot \vec{k}_s) - \vec{k}_s (\vec{k}_s \cdot \underset{\sim}{\alpha} \vec{\lambda}) \right] \right|^2 \\
&= \left| (\vec{\lambda}_s \cdot \underset{\sim}{\alpha} \vec{\lambda}) |\vec{k}_s|^2 - (\vec{\lambda}_s \cdot \vec{k}_s) (\vec{k}_s \cdot \underset{\sim}{\alpha} \vec{\lambda}) \right|^2 \\
&= \left(\frac{\omega_s}{c} \right)^4 \left| \vec{\lambda}_s \cdot \underset{\sim}{\alpha} \cdot \vec{\lambda} \right|^2
\end{aligned}$$

where the relation $\vec{\lambda}_s \cdot \vec{k}_s = \vec{\lambda} \cdot \vec{k} = 0$ has been used in the last step.

The expression for the scattering cross section just given pertains to a molecule of fixed orientation. For a freely rotating molecule, we must average this expression over all possible orientations of the molecule in order to obtain the observed cross section. The orientation dependence of the cross section arises from the orientation dependence of the components of the polarizability tensor. The scattering cross section for a freely rotating molecule will be:

$$\frac{d\sigma}{d\Omega} = \left(\frac{\omega}{c} \right)^4 \left\langle \left| \vec{\lambda}_s \cdot \alpha(\theta, \varphi) \cdot \vec{\lambda} \right|^2 \right\rangle$$

where the brackets $\langle \ldots \rangle$ denote an average over all orientations of the molecule. This expression gives the total scattered intensity but no information about the spectral distribution of intensity.

In order to calculate the spectral distribution of the scattered light, we will make use of the Wiener-Khintchine theorem which relates the power spectrum of a time varying quantity to its autocorrelation function.[2] The autocorrelation function of A(t) is defined as:

$$C(\tau) = \langle A(t)\ A(t+\tau) \rangle$$

where the brackets $\langle \ldots \rangle$ now denote the following time average:

$$\frac{1}{T} \int_0^T dt\ A(t)\ A(t+\tau) \quad .$$

The brackets are also used to denote an ensemble average, that is an average of the quantity $A(t)\ A(t+\tau)$ over all possible states of the system. Systems for which the time average and the ensemble average may be used interchangeably are termed "ergodic". The Wiener-Khintchine theorem states that:

$$I_A(\omega) = \frac{1}{2\pi} \int_{-\infty}^{\infty} dt\ e^{-i\omega\tau} \langle A(t)\ A(t+\tau) \rangle \quad .$$

The frequency spectral intensity distribution of $A(t)$ is just the Fourier transform of the time autocorrelation function of the variable $A(t)$. The inverse relation is:

$$\langle A(t)\ A(t+\tau) \rangle = \int_{-\infty}^{\infty} d\omega\ e^{i\omega\tau} I_A(\omega) \quad .$$

This is formally identical with our expression for the differential scattering cross section of a molecule. The correlation function from which we may calculate the spectral distribution of the scattered light is:

$$C(\tau) = \left(\frac{\omega}{c}\right)^4 \left\langle \left(\vec{\lambda}_s \cdot \underset{\sim}{\alpha}_w(t) \cdot \vec{\lambda}\right) \left(\vec{\lambda}_s \cdot \underset{\sim}{\alpha}_w(t+\tau) \cdot \vec{\lambda}\right) \right\rangle \quad .$$

Before proceeding with the discussion, we should mention a certain inconsistency in our notation. While the correlation function that we have just written down is essentially the same as:

$$C(\tau) = \frac{\left\langle \left(\vec{\lambda}_s \cdot \vec{E}_s(t)\right)\left(\vec{\lambda}_s \cdot \vec{E}_s(t+\tau)\right) \right\rangle}{\left|\vec{E}\right|^2} \quad ;$$

the two forms differ in that the factor $e^{i\omega_0 t}$ of $\vec{\lambda}_s \cdot \vec{E}_s(t) = \left(\vec{\lambda}_s \cdot \underset{\sim}{\alpha}_w(t) \cdot \vec{\lambda}\right) e^{i\omega_0 t}$ has been suppressed in the former expression. For this reason, the spectrum calculated from the first correlation function will have the frequency of the incident light as its origin and ω will represent the frequency shift of the scattered light rather than its actual frequency. However, the ω_s which appears in the factor $\left(\frac{\omega_s}{c}\right)^4$ still represents the actual fequency of the scattered light and not its frequency shift. Since we are interested in the time dependence arising from molecular motions we will usually mean frequency shift when we say frequency, but it should be clear from context whether frequency or frequency shift is intended.[3]

In order to apply our expression for $C(\tau)$ we must know the form of $\underset{\sim}{\alpha}_w(t)$. In the case of a diatomic molecule the polarizability tensor is completely specified in terms of the polarizabilities of the molecule for electric fields applied parallel to and perpendicular to the internuclear axis; these two polarizabilities are denoted $\alpha_{\parallel}$ and $\alpha_{\perp}$ respectively. When the molecule has its symmetry axis oriented along the space fixed z-axis, the polarizability tensor has diagonal form:

$$\underset{\sim}{\alpha}_w = \begin{pmatrix} \alpha_{\perp} & & \\ & \alpha_{\perp} & \\ & & \alpha_{\parallel} \end{pmatrix}$$

To determine the time dependence of $\underset{\sim}{\alpha}_{ww}(t)$ for the diatomic rotor we must first determine how $\underset{\sim}{\alpha}_{ww}$ transforms under rotations of the molecule.

Let the unit vector $\vec{u}$ specify the orientation of the internuclear axis of the molecule. The components of the electric field $\vec{E}$ parallel to and perpendicular to the molecular axis are:

$$\vec{E}_{\parallel} = \vec{u}(\vec{u}\cdot\vec{E}) \quad \text{and} \quad \vec{E}_{\perp} = \vec{E} - \vec{E}_{\parallel} = \vec{E} - \vec{u}(\vec{u}\cdot\vec{E}) \quad .$$

The Cartesian components of $\vec{d}$ and $\underset{\sim}{\alpha}_{ww}$ are thus:

$$\vec{d} = \underset{\sim}{\alpha}_{ww}\vec{E} = \alpha_{\parallel}\vec{E}_{\parallel} + \alpha_{\perp}\vec{E}_{\perp}$$

$$d_i = \alpha_{ij} E_j = \alpha_{\parallel} u_i u_j E_j + \alpha_{\perp}(\delta_{ij} E_j - u_i u_j E_j)$$

$$\alpha_{ij} = \bar{\alpha}\,\delta_{ij} + \beta(u_i u_j - \tfrac{1}{3}\delta_{ij}) = \bar{\alpha}\,\delta_{ij} + \beta_{ij}$$

where $\bar{\alpha} = \dfrac{\alpha_{\parallel} + 2\alpha_{\perp}}{3}$ and $\beta = \alpha_{\parallel} - \alpha_{\perp}$. The polarizability tensor of a diatomic molecule is the sum of an orientation independent part proportional to $\bar{\alpha}$, called the <u>isotropic</u> part of the polarizability, and an orientation dependent part proportional to β , called the <u>anisotropic</u> part of the polarizability.

Now that we know the form of $\underset{\sim}{\alpha}_{ww}$ for a diatomic molecule, we may attempt to compute $C(\tau)$. The correlation function is:

$$C(\tau) = \left(\frac{\omega_s}{c}\right)^4 \left\langle (\vec{\lambda}_s \cdot \underset{\sim}{\alpha}_{ww}(0)\cdot\vec{\lambda})(\vec{\lambda}_s \cdot \underset{\sim}{\alpha}_{ww}(\tau)\cdot\vec{\lambda}) \right\rangle$$

$$= \left(\frac{\omega_s}{c}\right)^4 \lambda_{s_i} \lambda_j \lambda_{s_k} \lambda_l \left\langle \alpha_{ij}(0)\alpha_{kl}(\tau) \right\rangle$$

where the first step involves the invariance of the correlation function under time translations and the second is possible because $\vec{\lambda}_s, \vec{\lambda}$ are space fixed and time independent. The bracket may be expanded to give

$$\left\langle \alpha_{ij}(0)\alpha_{kl}(\tau) \right\rangle = \bar{\alpha}^2 \delta_{ij}\delta_{kl} + \bar{\alpha}\,\delta_{ij}\langle\beta_{kl}\rangle + \bar{\alpha}\,\delta_{kl}\langle\beta_{ij}\rangle + \langle\beta_{ij}\beta_{kl}\rangle \quad .$$

The average $\langle \beta_{ij} \rangle$ may be written explicitly as:

$$\langle \beta_{ij} \rangle = \beta \langle u_i u_j - \frac{1}{3}\delta_{ij} \rangle$$

$$= \frac{\beta}{4\pi} \int_0^{\pi} \sin\theta \, d\theta \int_0^{2\pi} d\varphi \, (u_i u_j - \frac{1}{3}\delta_{ij}) \quad .$$

Recalling the $\vec{u}$ is the unit vector specifying the orientation of the internuclear axis with respect to the space fixed z-axis,

$$\vec{u} = \begin{pmatrix} \sin\theta \cos\varphi \\ \sin\theta \sin\varphi \\ \cos\theta \end{pmatrix}$$

we may easily show by direct substitution that $\langle \beta_{ij} \rangle = 0$.

Hence, our expression simplifies to:

$$\langle \alpha_{ij}(0) \alpha_{kl}(\tau) \rangle = \bar{\alpha}^2 \delta_{ij} \delta_{kl} + \langle \beta_{ij}(0) \beta_{kl}(\tau) \rangle$$

and we have only $\langle \beta_{ij} \beta_{kl} \rangle$ left to work out.

Since we are averaging over an ensemble representing an isotropic gas the tensor $\langle \beta_{ij} \beta_{kl} \rangle$ is isotropic, even though β_{ij} is not. The only isotropic fourth rank tensors are $\delta_{ij}\delta_{kl}$, $\delta_{ik}\delta_{jl}$ and $\delta_{il}\delta_{jk}$. The tensor $\langle \beta_{ij}\beta_{kl} \rangle$ is symmetric in the index pairs i,j and k,l because the tensor β_{ij} is symmetric. The most general fourth rank isotropic tensor of the required symmetry has the form:

$$\langle \beta_{ij}\beta_{kl} \rangle = A \, \delta_{ij} \delta_{kl} + B \, (\delta_{ik} \delta_{jl} + \delta_{il} \delta_{jk}) \quad .$$

The tensor β_{ij} is traceless, $\beta_{ii} = \text{trace}(\beta_{ij}) = 0$, so that $\langle \beta_{ii} \beta_{kl} \rangle = 0$ as well. This condition allows us to determine A, and the expression which results when the value of A is substituted is:

$$\langle \beta_{ij} \beta_{kl} \rangle = B \, (\delta_{ik} \delta_{jl} + \delta_{il} \delta_{jk} - \frac{2}{3} \delta_{ij} \delta_{kl}) \quad .$$

In order to fix the value of B we may set i=1, j=k in the above equation, which gives the result:

$$B = \frac{1}{10} \langle \beta_{ij}(0)\, \beta_{ji}(\tau) \rangle$$

$$= \frac{1}{10}\beta^2 \left\langle \left[u_i(0)\, u_j(0) - \frac{1}{3}\delta_{ij} \right] \left[u_j(\tau)\, u_i(\tau) - \frac{1}{3}\delta_{ji} \right] \right\rangle$$

$$= \frac{1}{10}\beta^2 \left\langle u_i(0)u_i(\tau)u_j(0)u_j(\tau) - \frac{1}{3}\delta_{ij}\left(u_i(0)u_j(0) + u_i(\tau)u_j(\tau) \right) + \frac{1}{9}\delta_{ij}\,\delta_{ij} \right\rangle$$

$$= \frac{1}{10}\beta^2 \left\langle \left[\vec{u}(0)\cdot\vec{u}(\tau) \right]^2 - \frac{1}{3}\left(\vec{u}(0)\cdot\vec{u}(0) + \vec{u}(\tau)\cdot\vec{u}(\tau) \right) + \frac{1}{3} \right\rangle$$

$$= \frac{1}{10}\beta^2 \left\langle \left[\vec{u}(0)\cdot\vec{u}(\tau) \right]^2 - \frac{1}{3} \right\rangle$$

$$= \frac{1}{15}\beta^2 \left\langle P_2\left(\vec{u}(0)\cdot\vec{u}(\tau) \right) \right\rangle$$

where $P_2(x) = \frac{1}{2}(3x^2 - 1)$ is the second Legendre polynomial, and $\vec{u}(0)\cdot\vec{u}(\tau)$ is the cosine of the angle through which the internuclear axis has rotated between $t=0$ and $t=\tau$. Having determined B, our expression for $\langle \alpha_{ij}(0)\,\alpha_{kl}(\tau) \rangle$ becomes:

$$\langle \alpha_{ij}(0)\alpha_{kl}(\tau) \rangle = \bar{\alpha}^2\,\delta_{ij}\,\delta_{kl} + \frac{\beta^2}{15} \left\langle P_2\left(\vec{u}(0)\cdot\vec{u}(\tau) \right) \right\rangle \cdot \left[\delta_{ik}\,\delta_{jl} + \delta_{il}\,\delta_{jk} - \frac{2}{3}\delta_{ij}\,\delta_{kl} \right] .$$

Finally we may write down the expression for the correlation function as:

$$C(\tau) = \left(\frac{\omega_s}{c}\right)^4 \lambda_{s_i}\,\lambda_j\,\lambda_{s_k}\,\lambda_l \left\langle \alpha_{ij}(0)\,\alpha_{kl}(\tau) \right\rangle$$

$$= \left(\frac{\omega_s}{c}\right)^4 \bar{\alpha}^2 (\vec{\lambda}_s\cdot\vec{\lambda})^2 + \left(\frac{\omega_s}{c}\right)^4 \frac{\beta^2}{15} \left\langle P_2\left(\vec{u}(0)\cdot\vec{u}(\tau) \right) \right\rangle \cdot \left[(\vec{\lambda}_s\cdot\vec{\lambda}_s)(\vec{\lambda}\cdot\vec{\lambda}) + (\vec{\lambda}_s\cdot\vec{\lambda})^2 - \frac{2}{3}(\vec{\lambda}_s\cdot\vec{\lambda})^2 \right]$$

$$= \left(\frac{\omega_s}{c}\right)^4 \bar{\alpha}^2 (\vec{\lambda}_s\cdot\vec{\lambda})^2 + \left(\frac{\omega_s}{c}\right)^4 \frac{\beta^2}{15} \left\langle P_2\left(\vec{u}(0)\cdot\vec{u}(\tau) \right) \right\rangle \cdot \left(1 + \frac{1}{3}(\vec{\lambda}_s\cdot\vec{\lambda})^2\right)$$

The choice of one of the four right angle scattering geometries described in Figure 2-1 allows a further slight simplification of the

FIGURE 2 - 1

Polarization Geometries

The incident beam travels in the y - direction and is either vertically (V) or horizontally (H) polarized with respect to the scattering (x, y) plane. The scattered light is observed in the x - direction and either the vertically (V) or horizontally (H) polarized component is selected. We may note that the spectral intensities of the light scattered in the VH, HV and HH geometries are all equal by symmetry for the gas samples which we will be considering.

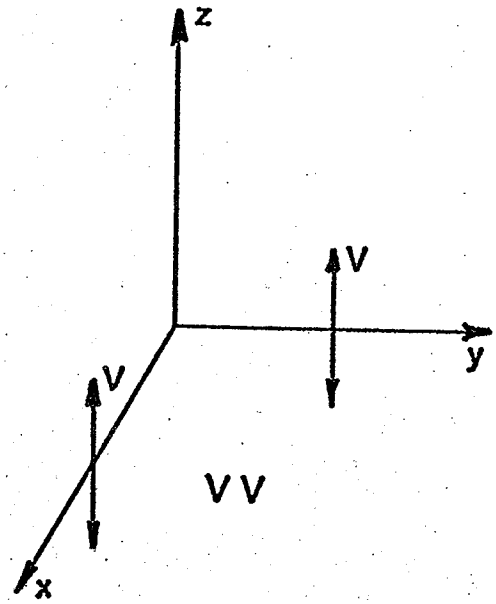
z
V
y
V
x
VV

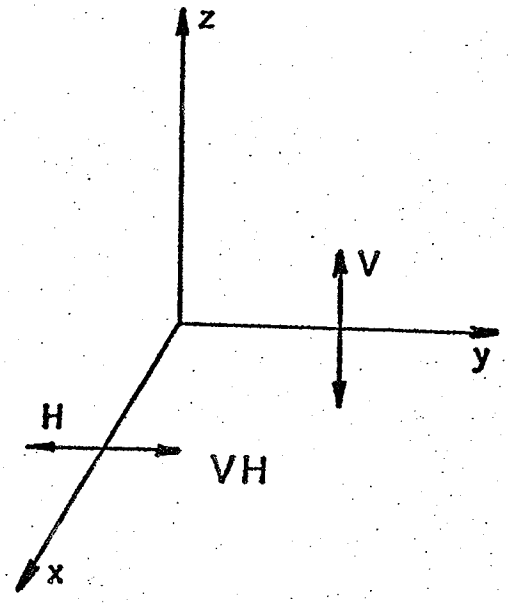
z
V
y
H
VH
x

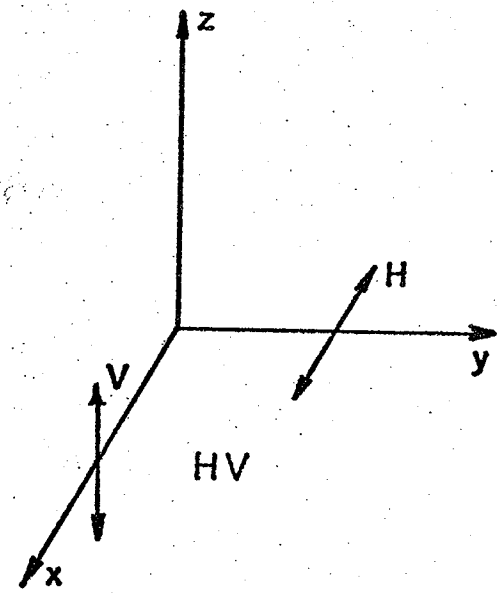
z
H
y
V
HV
x

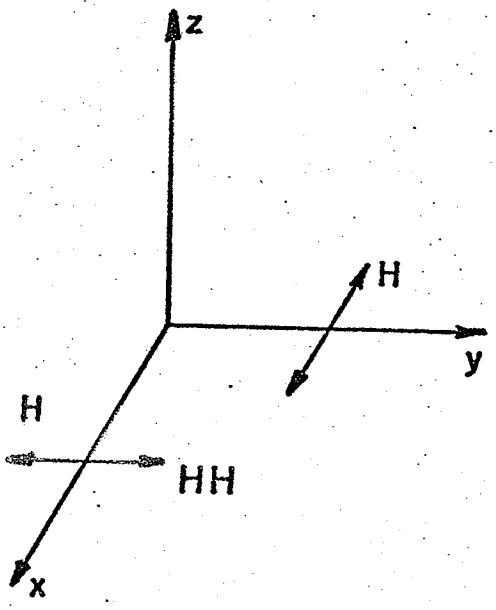
z
H
y
H
HH
x

expression for $C(\tau)$:

$$C(\tau)_{VH} = C(\tau)_{HV} = C(\tau)_{HH} = \left(\frac{\omega_s}{c}\right)^4 \frac{\beta^2}{15} \left\langle P_2\left(\vec{u}(0)\cdot\vec{u}(\tau)\right)\right\rangle$$

$$C(\tau)_{VV} = \left(\frac{\omega_s}{c}\right)^4 \bar{\alpha}^2 + \frac{4}{3} C(\tau)_{VH}$$

The contribution to $C(\tau)$ from the isotropic part of the polarizability is polarized parallel to the incident light and is unshifted in frequency -- this is the Rayleigh scattered light. The anisotropic part of the polarizability yields a contribution which is depolarized and which is shifted in frequency from the incident light frequency because of the time dependent factor $P_2\left(\vec{u}(0)\cdot\vec{u}(\tau)\right)$ -- this is the so-called Raman scattered light.[4]

We may now calculate the correlation function and hence the spectral distribution of light scattered by a diatomic rotor using the results we have obtained. For a free rotor, the normalized distribution function of molecular angular speeds at thermal equilibrium is just:

$$g(\omega_R) = \left(\frac{I\omega_R}{kT}\right) \exp\left(-\frac{\frac{1}{2}I\omega_R^2}{kT}\right)$$

Knowing the distribution function we proceed as follows:

$$\left\langle P_2\left(\vec{u}(0)\cdot\vec{u}(\tau)\right)\right\rangle = \left\langle P_2\left(\cos\omega_R\tau\right)\right\rangle$$

$$= \int_0^\infty d\omega_R \; g(\omega_R) \; P_2\left(\cos\omega_R\tau\right) = \frac{1}{4} + \frac{3}{4}\int_0^\infty d\omega_R \; g(\omega_R) \cos 2\omega_R\tau$$

$$\left(\frac{d^2\sigma}{d\Omega d\omega}\right)_{VH} = \left(\frac{\omega_s}{c}\right)^4 \frac{\beta^2}{15} \frac{1}{2\pi} \int_{-\infty}^{\infty} d\omega \, e^{-i\omega\tau} \left\langle P_2\left(\cos\omega_R\tau\right)\right\rangle$$

$$= \left(\frac{\omega_s}{c}\right)^4 \frac{\beta^2}{15} \left\{ \frac{1}{4} \frac{1}{2\pi} \int_{-\infty}^{\infty} d\omega \, e^{-i\omega\tau} + \frac{3}{4} \int_0^\infty d\omega_R \; g(\omega_R) \frac{1}{2\pi} \int_{-\infty}^{\infty} d\omega \, e^{-i\omega\tau} \cos 2\omega_R\tau \right\}$$

$$= \left(\frac{\omega_s}{c}\right)^4 \frac{\beta^2}{15} \left\{ \frac{1}{4}\delta(\omega) + \frac{3}{4} \int_0^\infty d\omega_R \; g(\omega_R) \left[\frac{\delta(2\omega_R - \omega) + \delta(2\omega_R + \omega)}{2} \right] \right\}$$

$$\left(\frac{d^2\sigma}{d\Omega\, d\omega}\right)_{VH} = \left(\frac{\omega_s}{c}\right)^4 \frac{\beta^2}{15} \left\{ \frac{1}{4}\delta(\omega) + \frac{3}{8}\,\frac{I}{kT}\left|\frac{\omega}{2}\right| \exp\left(\frac{-\frac{1}{2} I \left(\frac{\omega}{2}\right)^2}{kT}\right) \right\}$$

The angular frequencies ω_R, ω, ω_s are respectively the molecular rotation frequency, the frequency shift and absolute frequency of the scattered light. The quantity $\frac{1}{2\pi}\int_{-\infty}^{\infty} d\tau\ e^{-i\omega\tau} = \delta(\omega)$ is a representation of the Dirac delta function.

The spectrum as predicted by the classical theory has a sharp central component at zero frequency shift with a symmetric pair of broad peaks on either side of it. The above result is the scattering cross section per unit frequency interval and per unit solid angle for a single molecule.

2.2 The Quantum Case

The starting point of the quantum mechanical description of light scattering is very different from the classical picture. In the quantum mechanical case, the scattering process is represented by the following two diagrams.[5]

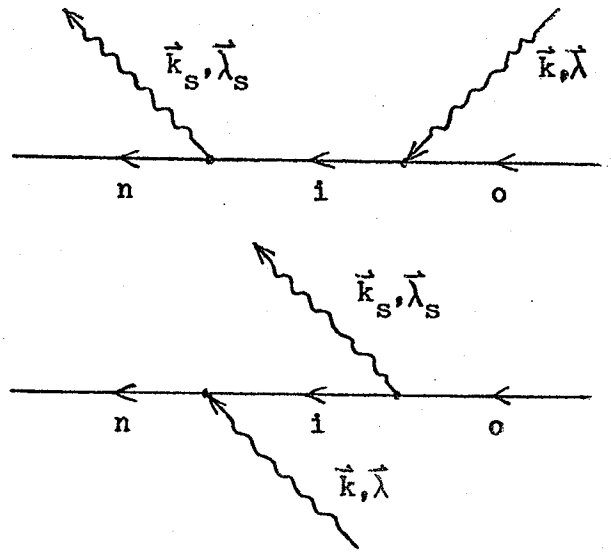

In the first diagram the original photon, specified by wavevector $\vec{k}$

and polarization vector $\vec{\lambda}$, is absorbed by the molecule, promoting it from the initial state $|o\rangle$ to an intermediate state $|i\rangle$. A short time later the molecule emits the scattered photon, specified by wavevector $\vec{k}_s$ and polarization vector $\vec{\lambda}_s$, and makes the transition to the final state $|n\rangle$. The second scattering diagram differs from the first only in the order of absorption and emission. The intermediate state $|i\rangle$ is called a "virtual" state. During the time when the molecule is "in" the intermediate state $|i\rangle$ the energy of the system is not conserved. The lifetime of such a virtual state is limited by the uncertainty principle. The process represented by the two diagrams is called Raman scattering. To determine the probability of the scattering event in which the photon $\vec{k},\vec{\lambda}$ is replaced by the photon $\vec{k}_s, \vec{\lambda}_s$ and the molecule goes from the state $|o\rangle$ to the state $|n\rangle$, we must sum the contribution of all possible processes connecting the initial and final states of the system. For each of the two diagrams the intermediate state must be allowed to range over all the states of the molecule and the transition amplitudes corresponding to the various $|i\rangle$ must be summed. (If the energy difference between the initial state $|o\rangle$ and an intermediate state $|i\rangle$ coincides with the photon energy, then the scattering changes and the process is called resonance Raman scattering or resonance fluorescence.)

Using second order perturbation theory we may write the expression for the transition rate in Raman scattering as:

$$\Gamma = \frac{2\pi}{\hbar^2}\left| \sum_i \left\langle N_{\vec{k}_s,\vec{\lambda}_s}+1 \, , \, N_{\vec{k},\vec{\lambda}}-1 \, , \, n \,\middle|\, \hat{H}_{int} \,\middle|\, N_{\vec{k}_s,\vec{\lambda}_s} \, , \, N_{\vec{k},\vec{\lambda}}-1 \, , \, i \right\rangle \right.$$

$$\left. \cdot \frac{\left\langle N_{\vec{k}_s,\vec{\lambda}_s} \, , \, N_{\vec{k},\vec{\lambda}}-1, \, i \,\middle|\, \hat{H}_{int} \,\middle|\, N_{\vec{k}_s,\vec{\lambda}_s} \, , \, N_{\vec{k},\vec{\lambda}} \, , \, o \right\rangle}{\mathcal{E}_o + \hbar\omega - \mathcal{E}_i} \right|$$

$$+ \quad \left\langle N_{\vec{k}_s,\vec{\lambda}_s}+1 \, , \, N_{\vec{k},\vec{\lambda}}-1 \, , \, n \left| \hat{H}_{int} \right| N_{\vec{k}_s,\vec{\lambda}_s}+1 \, , \, N_{\vec{k},\vec{\lambda}} \, , \, i \right\rangle$$

$$\cdot \left| \frac{\left\langle N_{\vec{k}_s,\vec{\lambda}_s}+1 \, , \, N_{\vec{k},\vec{\lambda}} \, , \, i \left| \hat{H}_{int} \right| N_{\vec{k}_s,\vec{\lambda}_s} \, , \, N_{\vec{k},\vec{\lambda}} \, , \, o \right\rangle}{\mathcal{E}_o - \hbar\omega_s - \mathcal{E}_i} \right|^2$$

$$\cdot \, \delta(\mathcal{E}_o + \hbar\omega - \mathcal{E}_n - \hbar\omega_s)$$

$N_{\vec{k},\vec{\lambda}}$ is the number of photons in the state specified by $\vec{k},\vec{\lambda}$. The ket $\left| N_{\vec{k}_s,\vec{\lambda}_s}+1 \, , \, N_{\vec{k},\vec{\lambda}}-1 \, , \, n \right\rangle$ is the state where the initial number of photons with wavevector and polarization $\vec{k}_s,\vec{\lambda}_s$ has been increased by one, the number of photons in the state $\vec{k},\vec{\lambda}$ has been reduced by one, and the molecule now resides in the state $|n\rangle$. The operator $\hat{H}_{int}$ is the part of the Hamiltonian of the system which describes the interaction between radiation and matter. In terms of the electromagnetic potentials, the Hamiltonian of the system will be of the form:

$$\hat{H} = \frac{1}{2m} \left(\vec{p} - \frac{e}{c}\vec{A} \right)^2 + e\varphi + V$$

and the interaction Hamiltonian will be:

$$\hat{H}_{int} = -\frac{e}{2mc} \left(\vec{p}\cdot\vec{A} + \vec{A}\cdot\vec{p} \right) + \frac{e}{2mc^2} \vec{A}\cdot\vec{A} + e\varphi \quad .$$

In the electric dipole approximation only the first term is retained. Introducing the creation and annihilation operators of the photon field and a Fourier representation of the current distribution, the matrix elements become, for example:

$$\left\langle N_{\vec{k},\vec{\lambda}}-1 \, , \, n \left| \hat{H}_{ED} \right| N_{\vec{k},\vec{\lambda}} \, , \, o \right\rangle$$

$$= \left(\frac{1}{Vc^2} \, \frac{2\pi\hbar c^2}{\omega} \right)^{\frac{1}{2}} \left(N_{\vec{k},\vec{\lambda}} \right)^{\frac{1}{2}} (-i\omega) \, \left\langle n \left| \vec{d}\cdot\vec{\lambda} \right| o \right\rangle$$

where $\vec{d} = e\sum_j \vec{r}_j$ is the dipole operator. Using this result, the

transition rate for Raman scattering becomes:

$$\Gamma = \frac{2\pi}{\hbar^2}\left(\frac{1}{Vc^2}\right)^2 \left(2\pi\hbar c^2\right)^2 \omega\omega_s \, N_{\vec{k},\vec{\lambda}} \left(N_{\vec{k}_s,\vec{\lambda}_s}+1\right)$$

$$\cdot \left| \sum_i \frac{\langle n|\vec{d}\cdot\vec{\lambda}_s|i\rangle\langle i|\vec{d}\cdot\vec{\lambda}|o\rangle}{\varepsilon_o+\hbar\omega-\varepsilon_i} + \frac{\langle n|\vec{d}\cdot\vec{\lambda}|i\rangle\langle i|\vec{d}\cdot\vec{\lambda}_s|o\rangle}{\varepsilon_o-\hbar\omega_s-\varepsilon_i} \right|^2$$

$$\cdot \delta(\varepsilon_o+\hbar\omega-\varepsilon_n-\hbar\omega_s)$$

The scattering cross section is the number of photons scattered into the solid angle $d\Omega$ per incident photon, and is given by:

$$\frac{d\sigma}{d\Omega} = \frac{V}{(2\pi)^3}\frac{\int k_s^2\, dk_s\, \Gamma}{N_{\vec{k},\vec{\lambda}}\frac{c}{V}} = \frac{V}{(2\pi c)^3}\frac{\int \omega_s^2\, d\omega_s\, \Gamma}{N_{\vec{k},\vec{\lambda}}\frac{c}{V}}$$

where the number of states within the solid angle $d\Omega$ and centered at $\vec{k}_s$ is $k_s^2\, d\Omega$ and where the incident flux of photons is $N_{\vec{k},\vec{\lambda}}\frac{c}{V}$. Substituting the expression for Γ, the scattering cross section becomes:

$$\frac{d\sigma}{d\Omega} = \left(\frac{\omega\omega_s^3}{c^4}\right)\left(N_{\vec{k}_s,\vec{\lambda}_s}+1\right)\left| \sum_i \frac{\langle n|\vec{d}\cdot\vec{\lambda}_s|i\rangle\langle i|\vec{d}\cdot\vec{\lambda}|o\rangle}{\varepsilon_o+\hbar\omega-\varepsilon_i} + \frac{\langle n|\vec{d}\cdot\vec{\lambda}|i\rangle\langle i|\vec{d}\cdot\vec{\lambda}_s|o\rangle}{\varepsilon_o-\hbar\omega_s-\varepsilon_i} \right|^2$$

In ordinary Raman scattering $N_{\vec{k}_s,\vec{\lambda}_s} << 1$ and we may use the approximation $\left(N_{\vec{k}_s,\vec{\lambda}_s}+1\right) \simeq 1$. (When the incident beam comes from a giant pulse laser, with a typical power of 10^8 W, then the number of scattered photons in a single state $\vec{k}_s,\vec{\lambda}_s$ may be very large.

Under these conditions the scattering is strongly enhanced and the effect is called the stimulated Raman effect.[6]

Now that we have obtained an expression for the Raman scattering cross section, we will apply it to the case of the diatomic rotor.[7] In order to compute the matrix elements, we make the assumption that the overall wavefunction of the molecule may be factored into an electronic part and a part describing the nuclear motion. This is called the Born-Oppenheimer approximation and fortunately it is usually a good approximation.[8] The dipole operator $\vec{d}$ only operates on the electronic wavefunction and the polarization vector $\vec{\lambda}$ only operates on the part involving the molecular orientation — the rotational wavefunction. Thus, we may factor the matrix elements to obtain the following expression for the rotational Raman scattering cross section:

$$\frac{d\sigma}{d\Omega} = \left(\frac{\omega\omega_s^3}{c^4}\right) \left| \sum_{\tau''} \sum_{\rho''} \frac{\langle\tau|d_j|\tau''\rangle\langle\tau''|d_i|\tau\rangle\langle\rho'|\lambda_{s_j}|\rho''\rangle\langle\rho''|\lambda_i|\rho\rangle}{\varepsilon_o + \hbar\omega - \varepsilon_i} + \frac{\langle\tau|d_i|\tau''\rangle\langle\tau''|d_j|\tau\rangle\langle\rho'|\lambda_i|\rho''\rangle\langle\rho''|\lambda_{s_j}|\rho\rangle}{\varepsilon_o - \hbar\omega_s - \varepsilon_i} \right|^2$$

The electronic and rotational states are denoted by τ and ρ respectively. It is assumed that the initial and final electronic states are the same. The scalar products $\vec{d}\cdot\vec{\lambda}$ have been expressed in terms of Cartesian components as $d_i\lambda_i$.

One further approximation must be made before the expression for the cross section can be cast in a useful form. We will assume that the energy denominators are essentially independent of the rotational state of the molecule. This is a good approximation as long as there are no electronic excitations near the incident frequency so that

$\mathcal{E}_o - \mathcal{E}_i >> (\hbar\omega, \hbar\omega_s) >> \hbar\omega_{rot}$ holds for all intermediate states $|i\rangle$.[9]

With this assumption, we may factor the rotational and electronic matrix elements once more:

$$\frac{d}{d} = \left(\frac{\omega\omega_s^3}{c^4}\right) \left| \left(\sum_{\tau''} \frac{\langle\tau|d_j|\tau''\rangle\langle\tau''|d_i|\tau\rangle}{\mathcal{E}_o + \hbar\omega - \mathcal{E}_i} \right) \sum_{\rho''} \langle\rho'|\lambda_{s_j}|\rho''\rangle\langle\rho''|\lambda_i|\rho\rangle \right.$$

$$\left. + \left(\sum_{\tau''} \frac{\langle\tau|d_i|\tau''\rangle\langle\tau''|d_j|\tau\rangle}{\mathcal{E}_o - \hbar\omega_s - \mathcal{E}_i} \right) \sum_{\rho''} \langle\rho'|\lambda_i|\rho''\rangle\langle\rho''|\lambda_{s_j}|\rho\rangle \right|^2 .$$

The sums over ρ'' yield $\langle\rho'|\lambda_{s_j}\lambda_i|\rho\rangle$ and $\langle\rho'|\lambda_i\lambda_{s_j}|\rho\rangle$. Since λ_{s_j} and λ_i commute, both matrix elements are the same. Thus:

$$\frac{d\sigma}{d\Omega} = \left(\frac{\omega\omega_s^3}{c^4}\right) \left| \sum_{\tau''} \left(\frac{\langle\tau|d_j|\tau''\rangle\langle\tau''|d_i|\tau\rangle}{\mathcal{E}_o + \hbar\omega - \mathcal{E}_i} + \frac{\langle\tau|d_i|\tau''\rangle\langle\tau''|d_j|\tau\rangle}{\mathcal{E}_o - \hbar\omega_s - \mathcal{E}_i} \right) \right.$$

$$\left. \cdot \langle\rho'|\lambda_{s_j}\lambda_i|\rho\rangle \right|^2$$

Identifying the quantity summed over τ'' as the polarizability tensor, the cross section assumes the following form:

$$\frac{d\sigma}{d\Omega} = \left(\frac{\omega\omega_s^3}{c^4}\right) \left| \langle\rho'|\lambda_i \alpha_{ij} \lambda_{s_j}|\rho\rangle \right|^2 = \left(\frac{\omega\omega_s^3}{c^4}\right) \left| \langle\rho'|\vec{\lambda}\cdot\underleftrightarrow{\alpha}\cdot\vec{\lambda}_s|\rho\rangle \right|^2 .$$

This has just the same form as the classical result for the scattering cross section. (The factor $\omega\omega_s^3$ rather than ω_s^4 in the quantum cross section arises because it is defined in terms of the number of scattered photons per incident photon instead of the scattered intensity per unit incident intensity.) In the classical description, one had

to average over all orientations of the molecule to obtain the observed intensity. In the quantum case this averaging occurs in evaluating the matrix element of $(\vec{\lambda} \cdot \underset{\sim}{\alpha} \cdot \vec{\lambda}_s)$ between the initial and final rotational states.

The diagonal form of the polarizability tensor for a diatomic molecule must be:

$$\underset{\sim}{\alpha}' = \begin{pmatrix} \alpha_\perp & & \\ & \alpha_\perp & \\ & & \alpha_\parallel \end{pmatrix}$$

When the internuclear axis of the diatomic molecule is oriented at angles θ, φ with respect to the space fixed coordinate axes, the diagonal form for $\underset{\sim}{\alpha}$ will be transformed to:

$$\underset{\sim}{\alpha} = R(\theta,\varphi)\, \underset{\sim}{\alpha}'\, R^{-1}(\theta,\varphi) = \alpha_\perp \underset{\sim}{I} + (\alpha_\parallel - \alpha_\perp)\, R(\theta,\varphi) \begin{pmatrix} 0 & & \\ & 0 & \\ & & 1 \end{pmatrix} R^{-1}(\theta,\varphi)$$

where $R(\theta,\varphi)$ is the matrix generating the rotation. By explicitly constructing $R(\theta,\varphi)$ we may evaluate $(\vec{\lambda} \cdot \underset{\sim}{\alpha} \cdot \vec{\lambda}_s)$ for the cases $\vec{\lambda} \cdot \vec{\lambda}_s = 0$ and $\vec{\lambda} \cdot \vec{\lambda}_s = 1$. The results are:

$$\vec{\lambda} \cdot \underset{\sim}{\alpha} \cdot \vec{\lambda}_s = \begin{cases} (\alpha_\parallel - \alpha_\perp) \cos\theta \sin\theta \cos\varphi & \vec{\lambda} \cdot \vec{\lambda}_s = 0 \\ \alpha_\perp + (\alpha_\parallel - \alpha_\perp) \cos^2\theta & \vec{\lambda} \cdot \vec{\lambda}_s = 1 \end{cases}$$

where the first case corresponds to the VH, HV or HH polarization geometries and the second case corresponds to the VV geometry.

The eigenfunctions of a rigid diatomic rotor are just the spherical harmonics:

$$|\rho\rangle = Y_J^M(\theta,\varphi) = |J,M\rangle \quad .$$

The energy levels for the diatomic rotor depend only on J and not M,

so that all transitions $J \rightarrow J'$ will have the same energy difference and hence give rise to scattered photons with the same frequency shift. The total cross section for scattering involving the transition $J \rightarrow J'$ will be:

$$\left(\frac{d\sigma}{d\Omega}\right)_{VH,\ J\rightarrow J'} = \left(\frac{\omega\omega_s^3}{c^4}\right)(\alpha_{\parallel}-\alpha_{\perp})^2 \frac{\sum_M \sum_{M'} \left|\langle J',M'|\cos\theta \sin\theta \cos\varphi|J,M\rangle\right|^2}{\sum_M (1)}$$

with a similar expression for the VV geometry. Since a molecule can start in any one of the $2J+1$ degenerate states $|J,M\rangle$, the cross section has been averaged over M. However, a molecule starting in a particular state $|J,M\rangle$ can make a transition to any of the states $|J',M'\rangle$ allowed by the selection rules, so that the cross section must be summed over the possible values of M'. Using the Legendre polynomial recursion relations we may evaluate the matrix elements.[10] The selection rules are:

$$\Delta J = J' - J = 0, \pm 2$$

$$\Delta M = M' - M = \pm 1$$

The total cross section for the $J \rightarrow J+2$ transition is:

$$\left(\frac{d\sigma}{d\Omega}\right)_{VH,\ J\rightarrow J+2} = \left(\frac{\omega\omega_s^3}{c^4}\right)(\alpha_{\parallel}-\alpha_{\perp})^2 \left(\frac{1}{2J+1}\right) \sum_{M=-J}^{J} \left\{ \frac{1}{4} \frac{(J+1)^2 - M^2}{(2J+1)(2J+3)^2(2J+5)} \right\}$$

$$\cdot \left\{ (J+2+M)(J+3+M) + (J+2-M)(J+3-M) \right\}$$

with similar expressions for the other cases. The above expression may be rearranged as:

$$\left(\frac{d\sigma}{d\Omega}\right)_{VH,\ J\rightarrow J+2} = \left(\frac{\omega\omega_s^3}{c^4}\right)(\alpha_{\parallel}-\alpha_{\perp})^2 \frac{1}{2} \left[(2J+1)^2(2J+3)^2(2J+5)\right]^{-1}$$

$$\cdot \sum_{M=-J}^{J} \left\{ (J+1)^2(J+2)(J+3) - M^2(2J+5) - M^4 \right\}$$

The sums $\sum_{M=-J}^{J} M^k$ may be evaluated using the Euler-Mauclarin integration formula.[11] The final result for the cross section is:

$$\left(\frac{d\sigma}{d\Omega}\right)_{VH,\ J\to J+2} = \left(\frac{\omega\omega_s^3}{c^4}\right)(\alpha_{\parallel}-\alpha_{\perp})^2 \frac{1}{10}\frac{(J+1)(J+2)}{(2J+1)(2J+3)}$$

The scattering cross sections for all the allowed transitions are:

$$\left(\frac{d\sigma}{d\Omega}\right)_{VH,\ J\to J+2} = \left(\frac{\omega\omega_s^3}{c^4}\right)\frac{\beta^2}{10}\quad\frac{(J+1)(J+2)}{(2J+1)(2J+3)}$$

$$\left(\frac{d\sigma}{d\Omega}\right)_{VH,\ J\to J} = \left(\frac{\omega}{c}\right)^4\quad\frac{\beta^2}{15}\quad\frac{J(J+1)}{(2J-1)(2J+3)}$$

$$\left(\frac{d\sigma}{d\Omega}\right)_{VH,\ J\to J-2} = \left(\frac{\omega\omega_s^3}{c^4}\right)\frac{\beta^2}{10}\quad\frac{J(J-1)}{(2J-1)(2J+1)}$$

$$\left(\frac{d\sigma}{d\Omega}\right)_{VV,\ J\to J+2} = \frac{4}{3}\left(\frac{d\sigma}{d\Omega}\right)_{VH,\ J\to J+2}$$

$$\left(\frac{d\sigma}{d\Omega}\right)_{VV,\ J\to J} = \left(\frac{\omega}{c}\right)^4\bar{\alpha}^2 + \frac{4}{3}\left(\frac{d\sigma}{d\Omega}\right)_{VH,\ J\to J}$$

$$\left(\frac{d\sigma}{d\Omega}\right)_{VV,\ J\to J-2} = \frac{4}{3}\left(\frac{d\sigma}{d\Omega}\right)_{VH,\ J\to J-2}$$

where $\bar{\alpha} = \frac{\alpha_{\parallel}+2\alpha_{\perp}}{3}$ and $\beta = \alpha_{\parallel}-\alpha_{\perp}$ are the mean polarizability and the polarizability anisotropy as previously defined.

The energy levels of a rigid rotor are $E(J) = J(J+1)\hbar B$ where the rotational constant B is defined as $B = \hbar/2I$ with I being the moment of inertia. The energy difference between the initial and final levels in the transition $J\to J+2$ is just $E = (4J+6)\hbar B$. Photons scattered during the transition $J\to J+2$ will give up energy to the molecule and be shifted in frequency by the amount $\Delta\omega = (4J+6)B$. The set of transitions $J\to J+2$ generates the so-called "S-branch"

of the spectrum. Similarily the $J \to J$ and $J \to J-2$ transitions produce the "Q-branch" and "O-branch" of the spectrum. In general, the downward frequency shifted side of the spectrum is called the "Stokes" side, while the upward shifted side of the spectrum is called the "anti-Stokes" side.

The spectrum of light scattered by a gas of diatomic rotors consists of a number of discrete lines with frequency shifts $\Delta\omega = 0, \pm(4J+6)\, B$. The scattering cross sections we have so far calculated pertain to a single molecule in the appropriate initial state. At thermal equilibrium, the probability of finding a molecule in the level J is given by normalized distribution function:

$$n(J) = \frac{(2J+1)\, \exp(-E(J)/kT)}{\sum_J (2J+1)\, \exp(-E(J)/kT)} \cdot$$

Thus the intensity of the spectral line corresponding to the transition $J \to J+2$ for a molecule in the gas will be:

$$\left(\frac{d\sigma}{d\Omega}\right)_{VH,\ J\to J+2} = \left(\frac{\omega\omega_s^3}{c^4}\right) \frac{\beta^2}{10} \frac{(J+1)(J+2)}{(2J+1)(2J+3)}\, n(J)$$

with analogous expressions for the other cross sections. If we sum over all the transitions for the O,Q and S-branches of the spectrum, we obtain the following results for the total cross section:

$$\left(\frac{d\sigma}{d\Omega}\right)_{VH} = \left(\frac{\omega}{c}\right)^4 \frac{\beta^2}{15}$$

$$\left(\frac{d}{d\Omega}\right)_{VV} = \left(\frac{\omega}{c}\right)^4 \left(\bar{\alpha}^2 + \frac{4}{3}\frac{\beta^2}{15}\right)$$

These expressions are precisely the same as the classical results previously obtained.[12] Next, we will compare the spectral distribution

for the classical and quantum calculations.

The obvious difference between the classical and the quantum spectra for the rigid rotor is that the classical spectrum is a continuous distribution while the quantum spectrum consists of discrete lines. The second major difference is that while the classical spectrum is symmetric about zero frequency shift, the quantum spectrum is asymmetric. The transitions $J \to J+2$ and $J+2 \to J$ have equal and opposite frequency shifts and the transition rates in the two directions are the same (when we count all the states in each level.) However, at thermal equilibrium the transitions starting from a higher energy level will tend to have a lower population in their initial state. (For rotational Raman transitions the degeneracy factor $2J+1$ for the level cancels with a similar factor in the scattering cross section.) For a given frequency shift ω, the intensity on the anti-Stokes side of the spectrum will tend to be lower than on the Stokes side by the Boltzmann factor $\exp(-\hbar\omega/kT)$. This result holds for any Raman scattering mechanism, not just that involving rotational transitions,[13] since the Boltzmann factor eventually dominates any competing population factors.

Despite these differences, the classical calculation correctly predicts the <u>envelope</u> of the spectrum obtained by the quantum calculation in the limit of large quantum numbers J and small rotational constant B. In this limit, the scattering cross section may be approximated as:

$$\left(\frac{d\sigma}{d\Omega}\right)_{VH,\ J\to J+2} = \left(\frac{\omega\omega_s^3}{c^4}\right)\frac{\beta^2}{10}\ \frac{(J+1)(J+2)}{(2J+1)(2J+3)}\ (2J+1)\ \exp\left(\frac{-J(J+1)\hbar B}{kT}\right)$$

$$\longrightarrow \left(\frac{\omega}{c}\right)^4 \frac{\beta^2}{10}\ \frac{J}{2}\ \exp\left(-\frac{J^2\hbar B}{kT}\right)$$

$$\left(\frac{d\sigma}{d\Omega}\right)_{VH,\ J\to J} \longrightarrow \left(\frac{\omega}{c}\right)^4 \frac{\beta^2}{15}\ \frac{J}{2}\ \exp\left(-\frac{J^2\hbar B}{kT}\right)$$

$$\left(\frac{d\sigma}{d\Omega}\right)_{VH,\ J\to J-2} \to \left(\frac{\omega}{c}\right)^4 \frac{\beta^2}{10} \frac{J}{2} \exp\left(-\frac{J^2 \hbar B}{kT}\right)$$

The O and S-branch lines appear at a frequency shift of $\omega = (4J+6)\,B \triangleq 4JB$. Substituting $B = \hbar/2I$ and $J = \omega/4B$ we have

$$\left(\frac{d\sigma}{d\Omega}\right)_{VH,\ J\to J+2} \simeq \left(\frac{\omega}{c}\right)^4 \frac{\beta^2}{10} \frac{\omega}{8B} \exp\left(-\frac{\omega^2}{16B^2} \frac{\hbar B}{kT}\right) \delta(\omega - 4JB)$$

$$= \left(\frac{\omega}{c}\right)^4 \frac{\beta^2}{15} \frac{1}{3}\left(\frac{\omega}{2}\right) \frac{I}{\hbar} \exp\left(-\frac{\frac{1}{2}I\left(\frac{\omega}{2}\right)^2}{kT}\right) \delta(\omega - 4JB)$$

Now we approximate the spectrum as continous distribution, introducing the normalization constant $\left(\frac{9}{16}\frac{\hbar}{kT}\right)$ to preserve the total intensity of the S-branch lines, with the result:

$$\left(\frac{d\sigma}{d\Omega}\right)_{VH,\ J\to J+2} \to \left(\frac{d^2\sigma}{d\Omega\, d\omega}\right)_{VH,\ S\text{-branch}} = \left(\frac{\omega}{c}\right)^4 \frac{\beta^2}{15} \left(\frac{\omega}{2}\right) \frac{I}{kT} \exp\left(-\frac{\frac{1}{2}I\left(\frac{\omega}{2}\right)^2}{kT}\right)$$

The O and Q-branches may be treated similarily with the final result:

$$\left(\frac{d^2\sigma}{d\Omega\, d\omega}\right)_{VH} = \left(\frac{\omega}{c}\right)^4 \frac{\beta^2}{15} \left\{ \frac{1}{4}\delta(\omega) + \frac{3}{8}\left|\frac{\omega}{2}\right| \frac{I}{kT} \exp\left(-\frac{\frac{1}{2}I(\omega/2)^2}{kT}\right) \right\} .$$

This is just the classical result for the diatomic rotor. The classical model of light scattering seems to be adequate in describing the gross features of the spectrum: the total intensity and the envelope of the spectral distribution.

Before leaving the quantum description of the diatomic rotor, we must consider several effects which appear when we consider real molecules: the nuclear statistical weights, centrifugal distortion and vibration-rotation coupling. The nuclear statistical weights, $g_{ns}(J)$,

cause the population of successive rotational levels of a homonuclear diatomic molecule to alternate. When the $g_{ns}(J)$ are included, the intensity of the S-branch lines (per molecule) becomes:

$$\left(\frac{d\sigma}{d\Omega}\right)_{VH,\ J\to J+2} = \left(\frac{\omega\omega_s^3}{c^4}\right)\frac{\beta^2}{10}\ \frac{(J+1)(J+2)}{(2J+1)(2J+3)}\ \frac{(2J+1)\ g_{ns}(J)\ \exp(-E(J)/kT)}{\sum_J (2J+1)\ g_{ns}(J)\ \exp(-E(J)/kT)}$$

The nuclear statistical weights are discussed in Appendix 2-A. A real diatomic molecule is not perfectly rigid, so that the average spacing of the nuclei will depend on both the rotational and vibrational quantum numbers. These effects are called centrifugal distortion and vibration-rotation coupling, and they chiefly result in shifts in the frequencies at which the rotational lines occur. Since the polarizability of the molecule also depends on the internuclear separation, these effects also change the intensities of the rotational lines. The effect of imperfect rigidity of the molecule may be treated as a perturbation and the results are sketched out in Appendix 2-B.

The scattered light spectrum depends not only on the molecular properties, but also to some extent on the environment of the molecules. The principal environmental effect is line broadening due to collisions between the molecules. When collisions become so frequent that the molecule no longer behaves as a free rotor, then the description in terms of free rotor wave functions $|J,M\rangle$ is no longer a "faithful" representation. The molecules reorient, not by an unhindered rotation, but by a series of large or small steps whose direction may also change with every step. The discrete line characteristic of the free rotor first broaden, then coalesce, and finally even the envelope of the band becomes distorted. At pressures low enough to preserve the appearance

of discrete lines, the pressure broadening coefficient is about 5×10^{-2} cm^{-1}/atm in simple non-polar gases such as N_2 or O_2, while for polar gases it is about 1 cm^{-1}/atm and more strongly J dependent. As a rough estimate we may consider that the molecules no longer exhibit free rotor behaviour when the time between collisions becomes shorter than the period of rotation. At a density of 1 mole/liter (about 40 atmospheres) the time between collisions is approximately 5 psec. Let us see how this compares with the period of rotation for various molecules.

The energy of the quantum mechanical rotor is $E(J)=J(J+1)\hbar B = J(J+1)\, hc\tilde{B}$ where $B=\hbar/2I$ and $I=\mu R^2$.[14] Comparing this with the classical expression, $E = \frac{1}{2} I \omega^2$, we find that $\omega = (\hbar J/I)$. The peak intensity of the rotational band occurs at approximately the value $J_{max} = (\frac{kT}{2hc\tilde{B}})^{\frac{1}{2}} - \frac{1}{2}$ (at room temperature, T=22°C, the value of $kT/hc = 205$ cm^{-1} .) The characteristic rotational periods for several rotors at room temperature are:

rotor	$\tilde{B}$ (cm^{-1})	J_{max}	T (psec) at J_{max}
H_2	59.32	1	0.28
N_2	2.00	7	1.18
CH_4	5.25	4	0.79
CF_4	0.186	23	3.85
dimers of CF_4	0.0116	94	15.11

Only the lightest molecules may be adequately described as free rotors

for the densities, in the range of 0.5 -- 5.0 mole/liter, at which our collision-induced scattering experiments are conducted. This must be borne in mind when considering the bound-dimer spectrum of Chapter 2 and the collision-induced rotational spectrum of Chapter 4, since the free rotor model has been assumed in the calculations. We must also keep in mind the limitations of the free rotor model in Chapter 5, since the experiment uses the S(1) rotational line of H_2 as an internal standard in determining the intensity of the spectrum being observed; fortunately H_2 behaves as a free rotor even at the highest densities that we will consider. The experiment also uses the computed rotational spectra of O_2 and N_2 with the lines suitably broadened, to subract out the contribution of these impurities to the observed spectrum; fortunately the intensity of the O_2 and N_2 rotational spectrum becomes relatively weaker compared with the overall spectrum at the same time as the deviations from free rotor behavior become large at higher densities.

The final task to be performed in this chapter is to work out the rotational Raman spectra for the molecules H_2, N_2 and O_2. We start with H_2. Taking into account vibration-rotation coupling and centrifugal distortion, the rotational energy levels for the H_2 molecule are:

$$\frac{E(J)}{hc} = J(J+1)\,\tilde{B}_o - J^2\,(J+1)^2\,\tilde{D}_e$$

where $\tilde{B}_o = 59.32\ cm^{-1}$ and $\tilde{D}_e = 4.7 \times 10^{-2}\ cm^{-1}$. The normalized distribution function $n(J)$ for the population of the rotational levels is:

$$n(J) = \frac{(2J+1)\ g_{ns}(J)\ \exp(-E(J)/kT)}{\sum_J (2J+1)\ g_{ns}(J)\ \exp(-E(J)/kT)}$$

where $g_{ns}(J) = \begin{cases} 1 & J=\text{even} \\ 3 & J=\text{odd} \end{cases}$.

The intensity of the S-branch ones is:

$$\left(\frac{d\sigma}{d\Omega}\right)_{\substack{VH \\ S(J)}} = \left(\frac{\omega\omega_s^3}{c^4}\right) \rho_{H_2} \frac{\beta_{H_2}^2}{10} \frac{(J+1)(J+2)}{(2J+1)(2J+3)}\ n(J)$$

Using the values $\beta_{H_2} = 0.314\ \text{Å}^3$, $\tilde{\omega} = \frac{1}{2\pi}\frac{\omega}{c} = 20492\ \text{cm}^{-1} = 2.0492 \times 10^{-4}\ \text{Å}^{-1}$

$\rho_{H_2} = 1$ mole/liter $= 6.02 \times 10^{-4}\ \text{Å}^{-3}$ and $T = 22^\circ\text{C}$ $\left(\frac{kT}{hc} = 205.1\ \text{cm}^{-1}\right)$

we may calculate the S-branch of the spectrum. The factor

$\left[\left(\frac{\omega}{c}\right)^4 \rho_{H_2} \frac{\beta_{H_2}^2}{10}\right]$ has the value $1.63 \times 10^{-17}\ \text{Å}^{-1}\ \text{sterad}^{-1} = 1.63 \times 10^{-7}\ \text{m}^{-1}\ \text{sterad}^{-1}$. The relative intensity of the S-branch lines is determined by the dimensionless factor:

$$\left[\left(\frac{\omega_s}{\omega}\right)^3 \frac{(J+1)(J+2)}{(2J+1)(2J+3)}\ n(J)\right].$$

The cross section is just the product of these two factors. Table 2-1 contains the results for H_2. The brightest line of the H_2 rotational spectrum by a large margin is the S(1) line; it is for this reason that the S(1) line is used as an intensity standard. (the Q-branch under the stated conditions will have $\left[\sum_J \frac{J\ (J+1)}{(2J-1)(2J+3)}\ n(J)\right] = 0.3218$, but since it occurs at zero frequency shift it is not useful as an intensity standard.)

In terms of the H_2 S(1) line intensity, we may express the spectral intensities for N_2 and O_2 in dimensionless form:

TABLE 2 - 1

The Rotational Spectrum of H_2

J	n(J)	measured n(J)	$\frac{(J+1)(J+2)}{(2J+1)(2J+3)}$	$\frac{E(J)}{hc}$ (cm^{-1})	$\Delta\omega_{S(J)}$ (cm^{-1})	$(\frac{\omega_S}{\omega})^3 \frac{(J+1)(J+2)}{(2J+1)(2J+3)} n(J)$
0	0.1305	0.1293 ± 0.6%	2/3	0	354.23	0.082566
1	0.6585	0.6628 ± 0.4%	2/5	118.45	586.62	0.241421
2	0.1150	0.1146 ± 1.0%	12/35	345.23	813.34	0.034917
3	0.0851	0.0799 ± 1.3%	20/63	705.07	1032.23	0.023136
4	0.0036	0.0030 ± 9 %	10/33	1167.60	1240.93	0.000904
5	0.0073	-	42/143	1737.30	1437.23	0.001724
6	0.000009	-	-	-	-	-

$$\frac{I_{S(J)}}{I_{H_2\ S(1)}} = \left(\frac{\omega_s}{\omega_{H_2\ S(1)}}\right)^3 \frac{\frac{(J+1)(J+2)}{(2J+1)(2J+3)}n(J)}{(2/5)\ (0.662)} \left(\frac{\beta^2}{\beta^2_{H_2}}\right)\left(\frac{\rho}{\rho_{H_2}}\right)$$

$$\frac{I_Q}{I_{H_2\ S(1)}} = \left(\frac{\omega}{\omega_{H_2\ S(1)}}\right)^3 \frac{\sum_J \frac{J\ (J+1)}{(2J-1)(2J+3)}n(J)}{(2/5)\ (0.662)} \left(\frac{\beta^2}{\beta^2_{H_2}}\right)\left(\frac{\rho/15}{\rho_{H_2}/10}\right)$$

For N_2 the value of n(J)(at T=22°C) is:

$$n(J) = \frac{(2J+1)\ g_{ns}(J)\ \exp(\ -J(J+1)/103.07\ )}{155.1051}$$

where $g_{ns}(J) = \begin{cases} 2 & J=\text{even} \\ 1 & J=\text{odd} \end{cases}$.

Similarily for O_2 the value of n(J) is:

$$n(J) = \frac{(2J+1)\ g_{ns}(J)\ \exp(\ -J(J+1)/142.67\ )}{71.5017}$$

where $g_{ns}(J) = \begin{cases} 0 & J=\text{even} \\ 1 & J=\text{odd} \end{cases}$.

The values of the sums $\sum_J \frac{J(J+1)}{(2J-1)(2J+3)}\ n(J)$ for N_2 and O_2 are 0.2012 and 0.2992 respectively while $\beta_{N_2}=0.69$ Å^3 and $\beta_{O_2}=1.09$ Å^3 . The rotational lines occur at frequency shifts given by $\Delta\tilde{\omega}=(4J+6)\ \tilde{B}_o$ where $\tilde{B}_o$ had the value 1.9902 cm^{-1} for N_2 and 1.4378 cm^{-1} for O_2. The rotational spectra computed for H_2, N_2 and O_2 presented in Figure 2-2.[15]

FIGURE 2 - 2

Rotational Spectra of H_2, N_2 and O_2.

The intensity scales are in units of the intensity of the H_2 S(1) rotational line, where all the gases are held at the same temperature ($22^{\circ}C$) and density. The frequency scale gives the downward shift in the frequency of the scattered photon (Stokes side of the spectrum) in units of cm^{-1}. Unless otherwise noted, spectral intensities will be given in units of the intensity of the H_2 S(1) rotational Raman line in H_2 gas at $22^{\circ}C$ and at unit (1 mole/liter) density. The origin of the frequency scale (0 cm^{-1} shift) will be at 20492 cm^{-1} (the incident photon wavelength is 4880 Å.)

a) The brightest line (which is usable for intensity calibration purposes) of the H_2 rotation spectrum is the S(1) line at a frequency shift of 587 cm^{-1}. The effect of the Boltzmann factor is very marked; the first line on the anti-Stokes side of the spectrum, O(2), has intensity about 10 times smaller than the corresponding transition, S(0), on the Stokes side.

b) The lines of the N_2 rotational spectrum alternate in intensity because of the nuclear statistical weights. The peak of the spectrum occurs at 60 cm^{-1} and the tail of the spectrum will be observable to 200 cm^{-1}.

c) Every second line of the O_2 rotational spectrum is missing because of the nuclear statistical weight factor. The peak of the spectrum occurs at 60 cm^{-1} and the tail of the spectrum will be observable to 200 cm^{-1}.

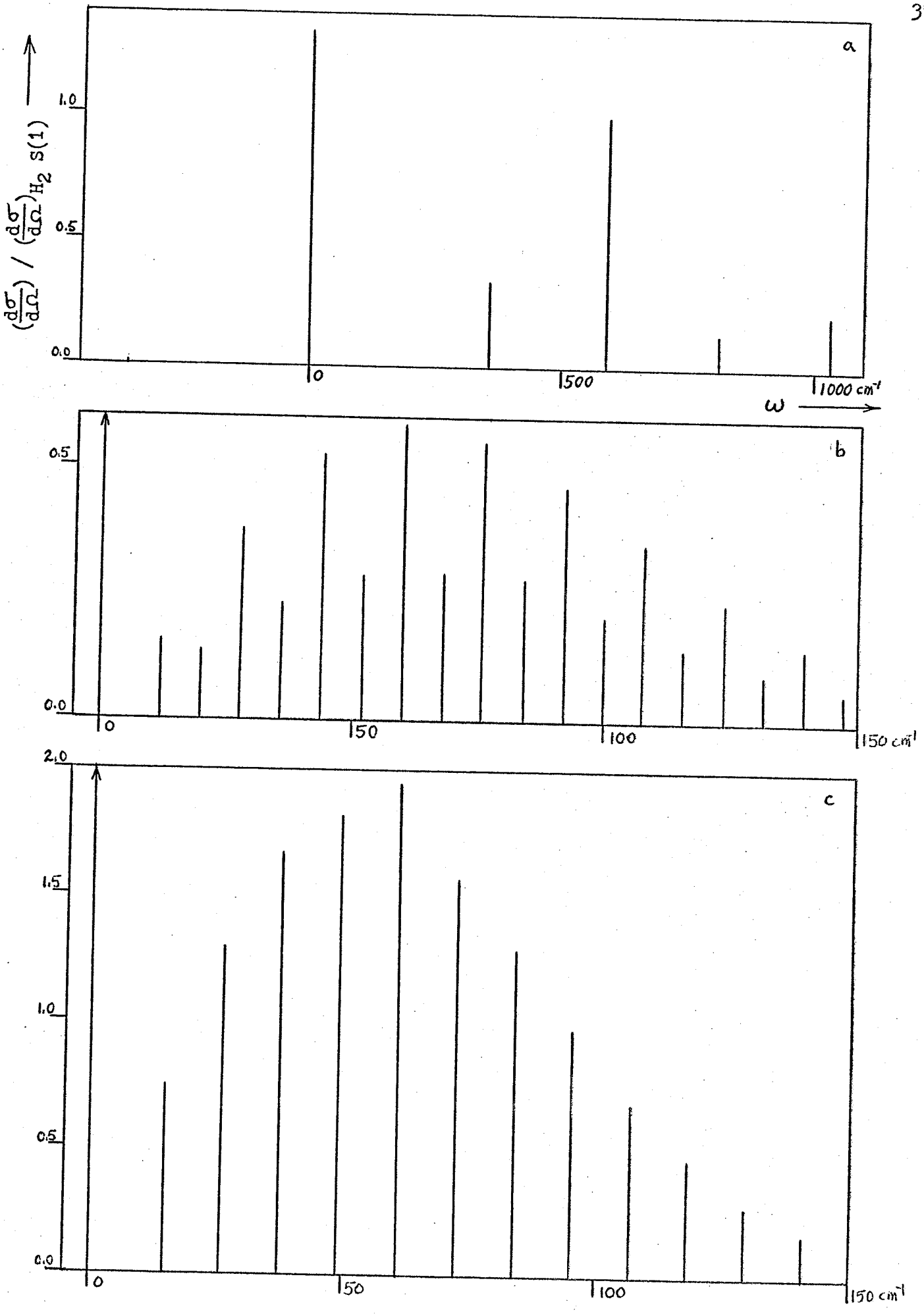
a
$(\frac{d\sigma}{d\Omega}) / (\frac{d\sigma}{d\Omega})_{H_2}$ S(1)
1.0
0.5
0.0
0
500
1000 cm⁻¹
ω
b
0.5
0.0
0
50
100
150 cm⁻¹
c
2.0
1.5
1.0
0.5
0.0
0
50
100
150 cm⁻¹

APPENDIX 2-A

Nuclear Statistical Weights[16]

For a homonuclear diatomic molecule the wavefunction must be symmetric or antisymmetric under exchange of the spatial and spin coordinates of the two identical nuclei according to whether they are bosons or fermions (integral or half-integral spin.) We may approximate the total wavefunction of the diatomic molecule by $\psi_{ttl} = \psi\psi_{ns} = \psi_{el}\psi_{vibr}\psi_{rot}\psi_{ns}$ where the factors are the electronic, vibrational, rotational and nuclear spin functions respectively. Under exchange of the nuclear spatial coordinates, ψ_{rot} and ψ_{vibr} have eigenvalues $(-1)^J$ and $(+1)$ respectively, where J is the rotational angular momentum quantum number. For the electronic states of a diatomic molecule the eigenvalues for exchange of the space fixed nuclear coordinates are:

$+1$ for Σ_g^+, Σ_u^-, Π_g^+, Π_u^-, ...

-1 for Σ_g^-, Σ_u^+, Π_g^-, Π_u^+, ...

where the symbols Σ, Π, ...represent electronic orbital angular momentum of 0,1, ... unit, the subscript g (or u) specifies that the electronic wavefunction is symmetric (or antisymmetric) under inversion of the molecule fixed coordinates, and the superscript + (or -) specifies that the electronic wavefunction is of even (or odd) parity under inversion of the space fixed coordinates of all particles in the molecule.

Let us denote a wavefunction symmetric (or antisymmetric) under exchange of the nuclei as ψ^s (or ψ^a.) If the nuclei are bosons (I = nuclear "spin" = integral) then only states $\psi^s_{ttl} = \psi^s \psi^s_{ns}$ or $\psi^a \psi^a_{ns}$ are allowed, similarily if the nuclei are fermions (I = half integral) then only states $\psi^a_{ttl} = \psi^a \psi^s_{ns}$ or $\psi^s \psi^a_{ns}$ are allowed. The states ψ^s are those for which:

J=even and $\psi_{el} = \sum_g^+ , \sum_u^- , \cdots$

J=odd and $\psi_{el} = \sum_g^- , \sum_u^+ , \cdots$

while the states ψ^a are those for which:

J=odd and $\psi_{el} = \sum_g^+ , \sum_u^- , \cdots$

J=even and $\psi_{el} = \sum_g^- , \sum_u^+ , \cdots$.

The number of degenerate states ψ_{ns} which are symmetric or antisymmetric under exchange of the nuclear spin coordinates is $(I+1)(2I+1)$ or $I(2I+1)$ respectively, where I is the total angular momentum quantum number of the nucleus (nuclear "spin") which results from adding the orbital and spin angular momenta of the nucleions. Since s and a rotational levels alternate, the nuclear statistical degneracy or weight $g_{ns}(J)$ and hence the population of the levels will alternate with the ratio $I/(I+1)$. The nuclear statistical weights for the three molecules of immediate interest to us are given below.

molecule	I	ψ_{el}	symmetry of J=even	symmetry of J=odd	g_{ns} (J) J=even	g_{ns} (J) J=odd	symmetry of ψ_{ttl}
H_2^1	$\frac{1}{2}$	$^1\sum_g^+$	s	a	1	3	a
N_2^{14}	1	$^1\sum_g^+$	s	a	2(3)	1(3)	s
O_2^{16}	0	$^3\sum_g^-$	a	s	0	1	s

(The left superscript of $^3\sum_g^-$ refers to the pair of electrons in O_2 which have unpaired spins, which makes the ground electronic state a triplet.)

APPENDIX 2-B

The Non-Rigid Diatomic Rotor[16]

The Schroedinger equation in the center of mass frame for a rotating diatomic molecule is:

$$\left[-\frac{\hbar^2}{2\mu}\nabla^2 + U(R)\right]\psi_N = E\,\psi_N$$

where μ is the reduced mass of the nuclei, R is their separation and ψ_N is the wavefunction for the relative motion of the nuclei. (The Born-Oppenheimer approximation has already been applied to separate the total wavefunction into factors describing the electronic motion and the nuclear motion.) If the wavefunction is assumed to have the form: $\psi_N = R\,G(R)\;Y_J^M(\theta_N,\varphi_N)$

the the Schroedinger equation becomes:

$$-\frac{\hbar^2}{2\mu}G''(R) + \left[\frac{J(J+1)\hbar^2}{2\mu R^2} + U(R) - E\right]G(R) = 0 \quad .$$

We proceed by Taylor expanding the potential energy function U(R) about the equilibrium separation R_e.

$$U(R) = U(R_e) + \frac{1}{2}U''(R_e)\,q^2 + \frac{1}{6}U'''(R_e)\,q^3 + \ldots$$

where $q=(R-R_e)$ and $U'(R)=0$ at $R=R_e$. Making the change of variable $S(q)\equiv G(R)$ and substituting the expansion for U(R) we have

$$-\frac{\hbar^2}{2\mu}S''(q) + \left[\frac{J(J+1)\hbar^2}{2\mu(R_e+q)^2} + U(R_e) + \frac{1}{2}U''(R_e)\,q^2 + \frac{1}{6}U'''(R_e)\,q^3 + \frac{1}{24}U^{iv}(R_e)\,q^4 + \ldots - E\right]S(q) = 0 \quad .$$

Keeping only the lowest order terms we have:

$$-\frac{\hbar^2}{2\mu}S''(q) + \left(\frac{1}{2}k_e\,q^2 - W\right)S(q) = 0$$

where $W = E - U(R_e) - \frac{J(J+1)\hbar^2}{2\mu R_e^2}$ and $k_e = U''(R_e)$.

Solving this equation one obtains the following wavefunctions and energies (for nuclear motion of the diatomic molecule):

$$\psi_N = \frac{S_v(q)}{R} \; Y_J^M(\theta_N, \varphi_N)$$

$$E = U(R_e) + (v+\tfrac{1}{2})\hbar\omega_e + J(J+1)\hbar B_e$$

where $S_v(q)$ is the v-th harmonic oscillator wavefunction and ω_e and B_e are the equilibrium vibrational and rotational constants, respectively. Thus $\omega_e = (\frac{k_e}{\mu})^{\frac{1}{2}}$ and $B_e = \frac{\hbar}{2I_e}$ where $I_e = \mu R_e^2$ is the equilibrium moment of inertia.

We may now include the previously neglected terms as perturbations in order to calculate corrections to the energies of the rotational and vibrational states. The perturbation is:

$$\hat{H} = aq + bq^2 + cq^3 + dq^4 \qquad \text{where}$$

$$a = \frac{2J(J+1)\hbar B_e}{R_e} \qquad b = -\frac{3J(J+1)\hbar B_e}{R_e^2}$$

$$c = \frac{1}{6}U'''(R_e) \qquad d = \frac{1}{24}U^{iv}(R_e) \quad .$$

The improved expression for the energy of the diatomic molecule is (using the unperturbed wavefunctions):

$$E = U(R_e) + \hbar\omega_e(v+\tfrac{1}{2}) + \hbar B_e J(J+1) - \hbar\omega_e x_e(v+\tfrac{1}{2})^2$$

$$- \hbar\alpha_e(v+\tfrac{1}{2})J(J+1) - \hbar D_e J^2(J+1)^2 + \hbar Y_{oo}$$

where the new constants are:

$$\omega_e x_e = \frac{B_e^2 R_e^4}{4\hbar\omega_e^2}\left[\frac{10 B_e R_e^2 (U'''(R_e))^2}{3h\,\omega_e^2} - U^{iv}(R_e)\right]$$

$$\alpha_e = \frac{-2B_e^2}{\omega_e}\left[\frac{2B_e R_e^2 U'''(R_e)}{\hbar\omega_e} + 3\right]$$

$$D_e = \frac{4B_e^3}{\omega_e^2}$$

$$Y_{oo} = \frac{B_e}{4} + \frac{\alpha_e\omega_e}{12B_e} + \frac{\alpha_e^2\omega_e^2}{144B_e^3} - \frac{\omega_e x_e}{4} \quad .$$

The constants $\omega_e x_e$, α_e and D_e are called the anharmonicity constant, the vibration-rotation coupling constant and the centrifugal-distortion constant respectively. To this approximation, we may express the rotational energy as:

$$E(J) = J(J+1)\hbar\,(B_e - \alpha_e(v+\tfrac{1}{2})) - J^2(J+1)^2\hbar D_e$$

$$= J(J+1)\hbar B_v - J^2(J+1)^2\hbar D_e$$

The spectroscopic constants for H_2, N_2 and O_2 are given in Table 2-2. The constants are given in units of (cm^{-1}) rather than (rad/sec) and this expressed by the tilde above the symbol. The conversion factor is $\omega(\text{rad/sec}) = 2\pi c\,\tilde{\omega}(cm^{-1})$.

The imperfect rigidity of the molecule will also perturb the radial nuclear wavefunction. Since the polarizability of the molecule depends on the internuclear separation, the polarizability will depend on the vibrational and rotational state of the molecule. The polarizability will depend on the vibrational and rotational state of the molecule. The polarizability of the H_2 molecule and the matrix

TABLE 2 - 2

Spectroscopic Constants for H_2, N_2 and O_2

molecule	R_e(Å)	k_e(mdyne/Å)	$\tilde{\omega}_e$(cm^{-1})	$\tilde{B}_e$(cm^{-1})	$\tilde{\alpha}_e$(cm^{-1})	$\tilde{B}_o$(cm^{-1})	$\tilde{D}_e$(cm^{-1})	$\tilde{\omega_e x_e}$(cm^{-1})
H_2	0.7416	5.751	4401.2	60.85	3.06	59.32	4.7×10^{-2}	121.3
N_2	1.0976	22.94	2358.1	1.987	0.017	1.9902	5.7×10^{-6}	14.19
O_2	1.2074	11.768	1580.4	1.4457	0.0158	1.4378	4.8×10^{-6}	12.07

from Levine, Quantum Chemistry Vol II: Molecular Spectroscopy, Ch. 3, p. 153, Allyn and Bacon, Boston, 1970.

elements for transitions between various states have been calculated by Kolos and Wolniewicz.[17] Their results show that the polarizability anisotropy β increases by about 1 percent for each successive rotational line in the pure rotation spectrum of H_2. (Their calculated value of β for the S(1) transition is 0.304 $\mathring{A}^3$, while the experimental value is 0.314 $\mathring{A}^3$.)[18] For molecules heavier than H_2 centrifugal distortion will be negligibly small and it should be a good approximation to use the same value of the polarizability anisotropy for all rotational transitions of a given molecule.

NOTES AND REFERENCES

1. J. D. Jackson, Classical Electrodynamics, Wiley, New York, 1975

2. R. K. Pathria, Statistical Mechanics, Pergamon, Oxford, 1972

3. We may also note at this point that the factor $(\omega_s/c)^4$ will usually be treated as if it were a constant. This is permissible because the relative spread of scattered light frequencies ω_s is usually very small compared to the average value of ω_s for the entire spectrum. Whether a particular value of ω_s or the average value of ω_s is intended in a given expression should be clear from context. The average value of ω_s will usually be equal to the incident frequency, which is just denoted as ω_o.

4. In fact the Rayleigh component has a finite frequency spread which arises because of the phase modulation due to translational motion, as mentioned in Chapter 1. The time dependence of the phase modulated signal is given by the correlation function: $F(\Delta\vec{k},\tau) = \left\langle \exp\left[-(\vec{k}_s-\vec{k})\cdot(r(\tau)-r(0))\right]\right\rangle$. The frequency spread of the Rayleigh signal is several orders of magnitude less than the spectral width of the other spectral features which we will consider. For an extensive treatment of the Rayleigh spectrum, see:

   B. J. Berne, R. Pecora, Dynamic Light Scattering, Wiley, New York, 1976 .

5. The next few pages will follow the discussion in Chapter 13 of:

   G. Baym, Lectures on Quantum Mechanics, Benjamin, London, 1973

6. See, for example, Chapter 8 of:

   D. A. Long, Raman Spectroscopy, McGraw-Hill, New York, 1977

7. The derivation of the rotational Raman cross section follows N. J. Bridge, A. D. Buckingham, Proc. Roy. Soc. A295, 334 (1968).

8. See Chapter 13 in:
I. N. Levine, Quantum Chemistry Vol I: Quantum Mechanics and Molecular Electronic Structure, Allyn and Bacon, Boston, 1970.

9. Molecules such as Br_2 and NO_2, for example, do not satisfy this condition for photons in the red end of the visible spectrum since they have electronic excitations at these energies — they will exhibit resonance Raman scattering.

10. G. Arfken, Mathematical Methods for Physicists, Academic Press, New York, 1970

11. See page 284 of Arfken.

12. We have used the approximation $\omega_o = \omega_s$, where ω_o is the incident light frequency. If this approximation is not used, the terms in β^2 will be multiplied by the factor $(1-18B/\omega+\ldots)$.

13. The ratio of the cross sections for the transitions $J+2 \rightarrow J$ and $J \rightarrow J+2$ is:

$$\frac{\left(\frac{d\sigma}{d\Omega}\right)_{VH,\ J+2\rightarrow J}}{\left(\frac{d\sigma}{d\Omega}\right)_{VH,\ J\rightarrow J+2}} = \left(\frac{\omega_o+\Delta\omega_s}{\omega_o-\Delta\omega_s}\right)^3 \exp\left(-\frac{E(J+2)-E(J)}{kT}\right)$$

$$= \left(1+\frac{6\Delta\omega_s}{\omega_o}\right) \exp\left(-\hbar\Delta\omega_s/kT\right) .$$

The transition rates do not look equal in the expressions we have written for the cross sections because the degeneracy factor $2J+1$ of the level has been incorporated in the population factor $n(J)$ and the expression for the O-branch has been written in terms of the transition $J \rightarrow J-2$ rather than

$J+2 \rightarrow J$. The equality of the rates $\Gamma_{o \rightarrow n} = \Gamma_{n \rightarrow o}$ for transitions between two states, o and n , of a system is generally true for radiative transitions.

14. The rotational constants B(rad/sec) and $\tilde{B}(cm^{-1})$ differ in their units. For theoretical calculations B is more convenient, while for experimental purposes it is convenient to reduce most quantities to units of cm^{-1} . Quantities expressed in wavenumber (cm^{-1}) units will be distinguished by a tilde, as in $\tilde{B}$.

15. The values of β are the experimental values from:
N. J. Bridge, A. D. Buckingham, Proc. Roy. Soc. A295, 334 (1968) .
The values of $\tilde{B}_o$ are from Chapter 3 of:
I. N. Levine, Quantum Chemistry Vol II; Molecular Spectroscopy, Allyn and Bacon, Boston, 1970 .

16. I. N. Levine, Quantum Chemistry Vol II: Molecular Spectroscopy, Allyn and Bacon, Boston, 1970 , Chapter 3
G. W. King, Spectroscopy and Molecular Structure, Holt, Rinehart and Winston, New York, 1964 , Chapter 5

17. W. Kolos, L. Wolniewicz, J. Chem. Phys. 46, 1426 (1967)

18. The experimental value is from
N. J. Bridge, A. D. Buckingham, Proc. Roy. Soc. A295, 334 (1968) .

CHAPTER 3

THE COLLISION-INDUCED SPECTRUM

Viewed from the center of mass frame of reference, a pair of colliding atoms will look just like a rotating diatomic molecule with a time-varying internuclear separation. This similarity will enable us to formulate the theory of binary collision-induced scattering as an extension of the classical theory of the diatomic rotor. For the rigid diatomic rotor, the time dependence of $\underset{\sim}{\alpha}(t)$ was due only to the change in the orientation of the molecule during rotation. In the case of CIS by a pair of atoms or molecules, the time dependence of $\underset{\sim}{\alpha}(t)$ will have a component due to the dependence of $\underset{\sim}{\alpha}$ on the intermolecular separation in addition to the component due to the dependence of $\underset{\sim}{\alpha}$ on the orientation of the intermolecular axis. As in the previous chapter, the first step in computing the spectrum will be to determine the form of $\underset{\sim}{\alpha}(r)$.

3.1 The Pair Polarizability

3.1.1 The Point Dipole-Induced Dipole Model

The polarizability tensor of an isolated closed shell atom is completely isotropic and is completely specified by the scalar polarizability α_0. The polarizability of a widely separated pair of these

atoms has the value $2\alpha_o$.[1] However, when the separation of the two is made small enough, the field of the dipole moment induced on one of the atoms by an externally applied electric field will change the value of the local field seen by the other atom. The interaction between the induced dipoles on the atoms causes the polarizability of the pair to differ from the sum of the isolated atom polarizabilities.[2] From symmetry considerations we know that the pair polarizability tensor can be specified completely in terms of the values $\alpha_{\parallel}$ and $\alpha_{\perp}$. Thus we will proceed by calculating the values of the pair polarizability for atomic pairs oriented parallel to and perpendicular to the applied field.

The components of the electric field due to a dipole moment $\vec{d}$ located at the origin and oriented along the z-axis, when the observation point lies in the x,z plane at a distance r from the origin, are:

$$E_z = \frac{d}{r^3}\,(3\cos^2\theta - 1)$$

$$E_x = \frac{d}{r^3}\,(3\sin\theta\cos\theta)$$

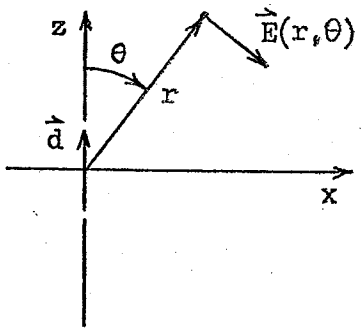

where θ is the angle measured from the z-axis. The dipole moment is produced by a uniform external field polarizing an atom sitting at the origin:

$$\vec{d} = \alpha_o E_o \vec{z} \quad .$$

If the second atom is placed at the observation point (r,θ), it will

see a local field which is the sum of the externally applied field and the dipole field of the first atom. We will choose the two values $\theta = 0$ (for α) and $\theta = \pi/2$ (for $\alpha_\perp$) as the direction of the second atom with respect to the first, and then use a perturbation iteration to calculate the total induced dipole in each of the two cases.

For $\theta = 0$ the calculation of the dipole on the second atom proceeds as follows:

$$d^{(1)} = \alpha_o E_o \qquad E_z^{(1)} = \frac{d^{(1)}}{r^3}\left(3\cos^2(0) - 1\right) = \frac{2\alpha_o}{r^3} E_o$$

$$d^{(2)} = \alpha_o E_z^{(1)} = \frac{2\alpha_o^2}{r^3} E_o \qquad E_z^{(2)} = \frac{d^{(2)}}{r^3}(2) = \frac{4\alpha_o^2}{r^6} E_o$$

$$d^{(3)} = \alpha_o E_z^{(2)} = \frac{4\alpha_o^3}{r^6} E_o \qquad E_z^{(3)} = \frac{d^{(3)}}{r^3}(2) = \frac{8\alpha_o^3}{r^9} E_o$$

$$d^{(4)} = \alpha_o E_z^{(3)} = \frac{8\alpha_o^4}{r^9} E_o \qquad \ldots .$$

$$\frac{d}{E_o} = \alpha_o + \frac{2\alpha_o^2}{r^3} + \frac{4\alpha_o^3}{r^6} + \frac{8\alpha_o^4}{r^9} + \cdots$$

Adding the contributions of both atoms we obtain:

$$\alpha_{\parallel} = 2\alpha_o + \frac{4\alpha_o^2}{r^3} + \frac{8\alpha_o^3}{r^6} + \frac{16\alpha_o^4}{r^9} + \cdots$$

In a similar fashion, the calculation for $\theta = \pi/2$ is :

$$d^{(1)} = \alpha_o E_o \qquad E_z^{(1)} = \frac{d^{(1)}}{r^3}\left(3\cos^2(\pi/2) - 1\right) = -\frac{\alpha_o}{r^3} E_o$$

$$d^{(2)} = \alpha_o E_z^{(1)} = \frac{-\alpha_o^2}{r^3} E_o \qquad E_z^{(2)} = \frac{d^{(2)}}{r^3}(-1) = \frac{+\alpha_o^2}{r^6} E_o$$

etc.

The result for the pair polarizability is:

$$\alpha_{\perp} = 2\alpha_o - \frac{2\alpha_o^2}{r^3} + \frac{2\alpha_o^3}{r^6} - \frac{2\alpha_o^4}{r^9} + \cdots$$

Having obtained the values of $\alpha_{\parallel}$ and $\alpha_{\perp}$, we may write down the isotropic and anisotropic parts of the pair polarizability tensor:

$$\bar{\alpha}(r) = \frac{\alpha_{\parallel}+2\alpha_{\perp}}{3} = 2\alpha_o + 0 + \frac{4\alpha_o^3}{r^6} + \frac{4\alpha_o^4}{r^9} + \cdots$$

$$\beta(r) = \alpha_{\parallel} - \alpha_{\perp} = 0 + \frac{6\alpha_o^2}{r^3} + \frac{6\alpha_o^2}{r^6} + \frac{18\alpha_o^4}{r^9} + \cdots$$

To lowest order, the pair polarizability tensor has the diagonal form:

$$\underset{\sim}{\alpha}(r) = 2\alpha_o \underset{\sim}{I} + \frac{2\alpha_o^2}{r^3} \begin{pmatrix} -1 & & \\ & -1 & \\ & & 2 \end{pmatrix} .$$

The leading contribution of the Dipole-Induced Dipole (DID) model, as far as CIS is concerned, comes from the totally anisotropic tensor $\underset{\sim}{\beta}(r)$. We will henceforth confine our discussion of the pair polarizability to consideration of the polarizability anisotropy $\beta(r)$. The CIS spectrum due to $\alpha(r)$ (where $\alpha(r) = \bar{\alpha}(r) - 2\alpha_o$) is much weaker than that due to $\beta(r)$, and since the spectrum due to $\alpha(r)$ is polarized, it is not observed in our experiments. The expressions for polarized CIS due to $\alpha(r)$ will be analogous to those involving $\beta(r)$.

3.1.2. Other Contributions to the Pair Polarizability of Atoms[3]

The point DID model yields a good first approximation to the atomic pair polarizability but its results are modified by serveral effects. These modifications arise from the effect of:

1) electron overlap,

2) electron density fluctuations, and

3) the non-uniformity of the local fields.

The effect of overlap of the electron clouds about the two colliding atoms, for small overlaps, is to reduce the polarizability of the pair below the DID value. For small overlaps, the electronic states of the colliding atoms will be essentially unchanged but the volume

occupied by the electrons will be slightly reduced. When the electrons are more tightly confined they move less in response to an applied field and hence the polarizability is reduced. The movement of the electrons away from the region of overlap also tends to reduce the anisotropy of the diatom. For collisions with very large overlap, the polarizability will not necessarily be reduced — for example, when two He atoms are made to overlap completely the electronic configuration changes to that of a Be atom and the polarizability is much greater than that of the separated atoms. Electron overlap is also responsible for the repulsive part of the interatomic potential, so it is expected that the dependence on interatomic separation of the electron overlap polarizability reduction will have the same form as the repulsive part of the interatomic potential.

The term in the atomic pair polarizability due to electron density fluctuations is analogous to the London dispersion term which accounts for the attractive part of the interatomic potential. The quantum mechanical result for the first order DID contribution is the same as the classical result, but the second and higher order DID terms will be affected. The London dispersion term arises because the electrons are not static within the atom; at any given moment the electron density distribution within the atom may differ from its time-averaged value, with the result that the net dipole moment of the atom fluctuates rapidly about zero. The instantaneous dipole moment on the atom tends

to induce a parallel dipole moment in any neighbouring atoms. Two parallel dipoles always attract and the time averaged effect of the correlated fluctuations is a net attraction between the charge distributions. The correction to the second order DID result arises in a similar fashion. The fluctuating dipole on one atom gives rise, at the site of its neighbouring atom, to a fluctuating field with mean value zero which is superimposed on the more slowly varying components of the local field. Because of the non-linear terms in the atomic polarizability (the so-called "hyperpolarizabilities"), the average value of the polarization due to the fluctuating field plus the local field is greater than it would be in the absence of the fluctuating field. The atom behaves as if its polarizability has been increased by the presence of its neighbour. Since the fluctuating dipole field falls off as r^{-3}, the polarizability enhancement also falls off as r^{-3}. When the polarizability enhancement is included in the DID calculation, the first term of $\beta(r)$ which is changed is the term in r^{-6}. The lowest order term introduced into $\alpha(r)$ by the electron density fluctuations is a "non-classical" term in r^{-4}; non-classical terms in r^{-8}, r^{-10}, ... are also introduced into the expression for $\beta(x)$.[4]

So far we have treated the atom as if it were a point polarizability. The point DID model takes the field at the atomic center as being representative of the field seen by the atom and uses the uniform field polarizability to compute the induced dipole. This approach gives the

correct asymptotic form of $\beta(r)$. However, when the interatomic separation is small, the field due to the dipole induced on one atom of the pair will be highly non-uniform over the volume of the other atom of the pair. In this case, the field at the atomic center is not even the average value of the field over the volume of the atom, and there is no reason to expect that the uniform field polarizability will correctly relate the applied non-uniform field to the induced dipole moment.[5]

3.1.3 Contributions to the Pair Polarizability of Molecules

All that has been said for atoms also applies in the case of molecules except that the situation is worse because molecules are usually larger and more complex than atoms. Since molecules lack the spherical symmetry of atoms, by virtue of containing more than one nucleus, there are additional internal degrees of freedom. We will consider two contributions to the pair polarizability which arise for molecules:

1) frame distortion, and

2) higher order molecular polarizabilities.

The second contribution will give rise to collision-induced rotational transitions and we will discuss it in the next chapter.

The frame distortion contribution to the molecular pair polarzability may be estimated by using vibrational frequencies to determine the bond stiffness, and the bond incremental polarizabilities

derived from intensity measurements of vibrational lines to determine the polarizability changes due to bond compression during a collision.

For an intermolecular potential of the Lennard-Jones 6-12 form, the intermolecular force is:

$$F(r) = -\frac{d\phi(r)}{dr} = -\frac{4\epsilon}{\sigma}\left(-12x^{-13} + 6x^{-7}\right)$$

where $x = r/\sigma$. The bond compression force is

$$F_v(\Delta r) = k_s \Delta r \quad .$$

Neglecting inertial effects:

$$F_v(\Delta r) = -F(r) \quad \text{and} \quad \Delta r = \frac{24\epsilon}{k_s \sigma}\left(2x^{-13} - x^{-7}\right) \quad .$$

The frame distortional polarizability change, counting both molecules, is just:

$$\Delta\alpha_{FD} = 2\left(\frac{d\alpha}{dr}\right)\left(\frac{24\epsilon}{k_s\sigma}\right)\left(2x^{-13} - x^{-7}\right)$$

while the DID polarizability change is:

$$\Delta\alpha_{DID} = \left(\frac{6\alpha_o^2}{\sigma^3}\right) x^{-3} \quad .$$

The frame distortion and DID contributions to the pair polarizability are compared in Table 3-1. The peak value of the frame distortion contribution is only about 1 percent of the peak DID contribution (at the turning point for thermal collisions.) The contribution to the total scattered light, denoted by $\phi^{(0)}$ the zeroth spectral moment, is only 0.1 percent of the DID value. Frame distortion provides a negligble correction to the DID result for the molecular pair polarizability.

TABLE 3 - 1

Frame Distortion Contribution to the Pair Polarizability

molecule	L.J. 6-12 parameters ϵ/k (°K)	σ(Å)	α_s(Å^3)	results for the "breathing" vibrational mode[a] ω(cm^{-1})	k_s(mdyne/Å)[b]	$\frac{d\alpha}{dr}$(Å^2)
CH_4	148.2	3.82	2.633 (at 5145Å)	2914	5.043	1.04
CF_4	152.5	4.70	2.85 (at 6328Å)	908	9.228	1.00
CCl_4	282	6.1	10.6 (at 5890Å)	459	4.401	2.17
SF_6	200.9	5.51	4.470 (at 6328Å)	775	6.723	1.23

molecule	$\left(\frac{24\epsilon}{k_s\sigma}\frac{d\alpha}{dr}\right)$(Å^3)	$\Delta\alpha_{FD}$(Å^3) / $\Delta\alpha_{DID}$(Å^3)[c]	$\phi^{(0)}_{FD}$(Å^9) / $\phi^{(0)}_{DID}$(Å^9)[d]
CH_4	2.65×10^{-3}	1.21×10^{-2} / -0.87	0.55 / 195
CF_4	1.16×10^{-3}	0.57×10^{-2} / 0.55	0.28 / 144
CCl_4	7.55×10^{-3}	3.72×10^{-2} / 3.46	25.58 / 12581
SF_6	2.21×10^{-3}	1.09×10^{-2} / 0.84	1.33 / 540

(a) from Murphy, Holzer, Bernstein, Appl. Spect. 23, 211 (1969), Gas Phase Raman Intensities: A Review of "Pre-Laser" Data.

(b) The typical "stiffness" of the intermolecular potential at the turning point for thermal collisions between these molecules is 0.1 mdyne/Å; 1 mdyne/Å = 100 Nt/m .

(c) $\Delta\alpha_{FD} = 2\left(\frac{d\alpha}{dr}\,\frac{24\epsilon}{k_s\sigma}\right)\left(2x^{-13} - x^{-7}\right)$; $\Delta\alpha_{DID} = \left(\frac{6\alpha_o^2}{\sigma^3}\right)x^{-3}$; $x = r/\sigma$

(d) $$\phi^{(0)} = 4\pi\int_0^\infty dr\, r^2\, g(r)\, \beta^2(r) \cong 4\pi\int_0^\infty dx\, x^2\, g(x)\, \sigma^3 \left[\left(\frac{6\alpha_o^2}{\sigma^3}\right)^2 x^{-6} + 4\left(\frac{6\alpha_o^2}{\sigma^3}\right)\left(\frac{24\epsilon}{k_s\sigma}\,\frac{d\alpha}{dr}\right)\left(2x^{-16} - x^{-10}\right)\right]$$

$$\cong 4\pi\,\frac{36\,\alpha_o^4}{\sigma^3}(0.50) + 4\pi\,(4)(6\alpha_o^2)\left(\frac{24\epsilon}{k_s\sigma}\,\frac{d\alpha}{dr}\right)(0.10) = \phi^{(0)}_{DID} + \phi^{(0)}_{FD}$$

The integrals were evaluated for $\frac{\epsilon}{kT} = 0.52$.

3.2 The Role of Molecular Dynamics in Collision-Induced Light Scattering

The correlation function which describes light scattering by pairs of atoms or molecules is a simple extension of the result obtained for the diatomic rotor:

$$C(t) = \left(\frac{\omega_s}{c}\right)^4 \left\langle \left(\vec{\lambda}_s \cdot \underset{\leftrightarrow}{\alpha}_w(0) \cdot \vec{\lambda}\right)\left(\vec{\lambda}_s \cdot \underset{\leftrightarrow}{\alpha}_w(t) \cdot \vec{\lambda}\right) \right\rangle$$

$$= \left(\frac{\omega_s}{c}\right)^4 \left(\vec{\lambda}_s \cdot \vec{\lambda}\right)^2 \left\langle \bar{\alpha}(0)\,\bar{\alpha}(t) \right\rangle$$

$$+ \left(\frac{\omega_s}{c}\right)^4 \frac{1}{15} \left(1 + \frac{1}{3}\left(\vec{\lambda}_s \cdot \vec{\lambda}\right)^2\right) \left\langle \beta(0)\,\beta(t)\; P_2\left(\vec{u}(0) \cdot \vec{u}(t)\right) \right\rangle$$

where $\bar{\alpha}(t) = \bar{\alpha}(r(t))$, $\beta(t) = \beta(r(t))$ and $\vec{u}(t)$ is the unit vector along the intermolecular axis at time t. The molecular dynamics of the collision enters the description through the determination of $r(t)$ and $\vec{u}(t)$ which in turn determine the time dependence of the quantities appearing in the correlation function. The correlation function itself involves an average over the Canonical ensemble to obtain the observable result. We shall now proceed to evaluate the correlation function which describes the depolarized CIS spectrum governed by $\beta(r)$.

The motion of two colliding molecules can be resolved into the motion of the center of mass and the relative motion of the two particles. The relative motion may in turn be expressed as the motion of a single particle of "reduced" mass $m = (m_1^{-1} + m_2^{-1})^{-1}$ interacting with

a fixed center of force described by the intermolecular potential energy function $\phi(r)$. The correlation function for the depolarized light scattering may be evaluated in terms of the following ensemble average:[6]

$$\langle \beta(t)\,\beta(t+\tau)\,P_2(\vec{u}(t)\cdot\vec{u}(t+\tau)) \rangle$$

$$= \frac{\int e^{-H/kT}\, dr\, d\theta\, d\varphi\, dp_r\, dp_\theta\, dp_\varphi\, \beta(r(t))\,\beta(r(t+\tau))\,P_2(\vec{u}(t)\cdot\vec{u}(t+\tau))}{\int e^{-H/kT}\, dr\, d\theta\, d\varphi\, dp_r\, dp_\theta\, dp_\varphi}$$

where H is the Hamiltonian of the system :

$$H = \left(p_r^2 + \frac{p_\theta^2}{r^2} + \frac{p_\varphi^2}{r^2 \sin^2\theta} \right) / 2m + \phi(r)$$

$$= \left(p_r^2 + \frac{L^2}{r^2} \right) / 2m + \phi(r) \quad .$$

(The Canonical momenta are $p_r = m\dot{r}$, $p_\theta = mr^2\dot{\theta}$ and $p_\varphi = mr^2\sin^2\theta\,\dot{\varphi}$.) We may change variables $(r,\theta,\varphi,p_r,p_\theta,p_\varphi) \longrightarrow (r,\theta,\varphi,E,L^2,p_\varphi/L)$ by multiplying the new volume element in phase space by the Jacobian of the transformation:

$$\frac{\partial(p_r,p_\theta,p_\varphi)}{\partial(E,L^2,p_\varphi/L)} = \begin{vmatrix} \frac{\partial E}{\partial p_r} & \frac{\partial E}{\partial p_\theta} & \frac{\partial E}{\partial p_\varphi} \\ \frac{\partial L^2}{\partial p_r} & \frac{\partial L^2}{\partial p_\theta} & \frac{\partial L^2}{\partial p_\varphi} \\ \frac{\partial p_\varphi/L}{\partial p_r} & \frac{\partial p_\varphi/L}{\partial p_\theta} & \frac{\partial p_\varphi/L}{\partial p_\varphi} \end{vmatrix}^{-1} = \frac{\sin\theta}{2\dot{r}} \left[\sin^2\theta - (p_\varphi/L)^2 \right]^{-\frac{1}{2}}$$

The quantities E and L are the total energy and the magnitude of the angular momentum of the system. When we consider the equations of motion for the system we will see that $r(t)$ and $\vec{u}(t)\cdot\vec{u}(t+\tau)$ are completely determined in terms of r, L^2 and E. This will enable us to integrate immediately over θ,φ and p_φ/L.

Because the interaction between the molecules can be expressed as a scalar central potential, the orbit of the single particle of the "reduced" problem lies in a single plane passing through the center of force and the total energy and angular momentum are constants of the motion. Specifying the position of the particle in the orbital plane by the polar coordinates (r,ψ), the energy and angular momentum may be expressed as:

$$E = \frac{1}{2} m v_o^2 = \frac{1}{2} m v^2 + \phi(r) = \frac{1}{2} m \dot{r}^2 + \frac{1}{2}\frac{L^2}{mr^2} + \phi(r)$$

$$L = mr^2\dot{\psi} \quad .$$

Introducing b, the impact parameter of the collision, these relations can be written as:

$$\left(\frac{\dot{r}}{v_o}\right) = \left[1 - \left(\frac{b}{r}\right)^2 - \frac{\phi(r)}{E}\right]^{\frac{1}{2}}$$

$$\dot{\psi} = \frac{bv_o}{r^2} \quad .$$

The turning point of the orbit, r_{min}, can be found by solving the following equation:

$$\left(\frac{\dot{r}}{v_0}\right)^2 = 0 = \left[1 - \left(\frac{b}{r_{min}}\right)^2 - \frac{\phi(r_{min})}{E}\right] .$$

Taking the values:

$$r(t=0) = r_{min}$$

$$\psi(t=0) = 0$$

as intial conditions, we may obtain $r(t)$ and $\psi(t)$ by integrating the equations for $\left(\frac{\dot{r}}{v_o}\right)$ and $\dot{\psi}$. The only parameters which appear in these equations are v_o^2 and b, which may be expressed in terms of E and L^2 as $v_o^2 = \frac{2}{m}E$ and $b = \frac{L}{mv_o}$.

The quantity $\vec{u}(t)\cdot\vec{u}(t+\tau)$ is the cosine of the angle through which the intermolecular axis has rotated between times t and $t+\tau$, which may be expressed in terms of $\psi(t)$ as:

$$\vec{u}(t)\cdot\vec{u}(t+\tau) = \cos(\psi(t) - \psi(t+\tau))$$

Thus, the function being averaged in the correlation function

$$f(t,t+\tau) = \beta(r(t))\,\beta(r(t+\tau))\,P_2(\cos(\psi(t)-\psi(t+\tau)))$$

has been expressed entirely in terms of $r(t)$ and $\psi(t)$, which in turn may be specified in terms of r, E and L^2.

We may now proceed by integrating over θ, φ and $P\varphi/L$ to obtain the following result:

$$\langle f(t,t+\tau)\rangle = \frac{4\pi^2 (2m)^{\frac{1}{2}} \int dr\, dE\, dL^2\, e^{-E/kT} \left(E-\phi(r) - \frac{L^2}{2mr^2}\right)^{-\frac{1}{2}} \bar{f}(t,t+\tau)}{V\,(2\pi mkT)^{3/2}}$$

Changing variable from (E,L^2) to $(E/kT,b)$ and rearranging, the expression becomes:

$$\langle f(t,t+\tau)\rangle = \frac{4\pi^2\, 2(2mkT)^{3/2}}{V\,(2\pi mkT)^{3/2}} \int_0^\infty d\left(\frac{E}{kT}\right) \left(\frac{E}{kT}\right)^{\frac{1}{2}} \int_0^\infty db \int_{r_{min}}^\infty dr$$

$$\cdot\, b \left[1 - \left(\frac{b}{r}\right)^2 - \frac{\phi(r)}{E}\right]^{-\frac{1}{2}} \bar{f}(t,t+\tau) \quad .$$

However, $\left[1 - \left(\frac{b}{r}\right)^2 - \frac{\phi(r)}{E}\right]^{-\frac{1}{2}} = \frac{v_o}{\dot{r}} = v_o \frac{dt}{dr}$, and by introducing this substitution and writing $\mathcal{E} = E/kT$ we get the final result:

$$\langle f(t,t+\tau)\rangle =$$

$$\frac{8\sqrt{\pi}}{V} \int_0^\infty d\mathcal{E}\; \mathcal{E}^{\frac{1}{2}}\, e^{-\mathcal{E}} \int_0^\infty b\, db \int_{-\infty}^\infty v_o\, dt\; \frac{f(t,t+\tau)}{2}$$

The integration limits for the r and t integrals require some explanation. A typical orbit will appear as follows:

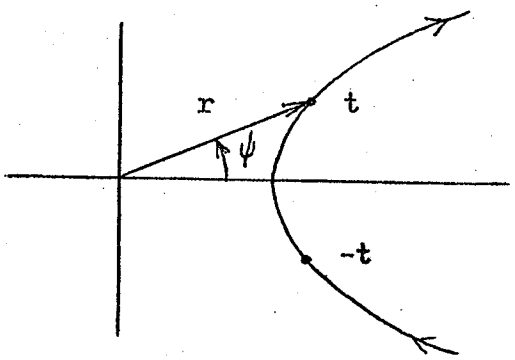

Since only r is specified, it is equally likely that the particle is on the ingoing or the outgoing trajectory, and the values of $r(t+\tau)$ and $\cos(\psi(t)-\psi(t+\tau))$ will depend on the direction chosen. In order to calculate the correct value of $\langle f(t,t+\tau)\rangle$ we must average over

ingoing and outgoing directions. Thus, the integrand of the r-integral becomes:

$$\bar{f}(t,t+\tau) = \frac{f(t,t+\tau) + f(-t,-t+\tau)}{2}$$

to account for the fact that the integration only extends over the outgoing branch of the orbit, $r = r_{min} \rightarrow \infty$. Since the orbit is symmetric about the apsidal direction (the direction of the turning point) we may express functions of $-t$ and $-t+\tau$ in terms of t and $t-\tau$ as follows:

$$r(-t) = r(t) \qquad \psi(-t) = -\psi(t)$$

$$r(-t+\tau) = r(t-\tau) \qquad \psi(-t+\tau) = -\psi(t-\tau) \quad ,$$

so that $\bar{f}(t,t+\tau)$ may be expressed entirely in terms of (r,ψ) along the outgoing branch of the orbit. By extending the t-integration limits to $t = -\infty \rightarrow +\infty$, we may write the integrand as $f(t,t+\tau)/2$. The factor of 1/2 is necessary because the original ensemble average correctly accounted for the time spent at a given r-value without distinguishing as to the direction of travel.

The Fourier transform of the correlation function

$$C(\tau) = \left(\frac{\omega_s}{c}\right)^4 \frac{1}{15} \left(1+(\vec{\lambda}_s \cdot \vec{\lambda})^2 \right) \langle f(t,t+\tau) \rangle$$

will give the depolarized scattering cross section per unit frequency interval and per unit solid angle due to a single pair of molecules

confined in the volume V. If the gas consists of N molecules, the number of pairs will be $N(N-1)/2 \simeq N^2/2$, and the density of pairs will be $N^2/2V$. When we multiply the above correlation function by the density of pairs in the gas, we get the more useful result:

$$C(\tau) = \left(\frac{\omega_s}{c}\right)^4 \frac{1}{15}\left(1+(\vec{\lambda}_s\cdot\vec{\lambda})^2\right) \frac{N^2}{2V} \frac{8\sqrt{\pi}}{V} \int_0^\infty d\varepsilon\, \varepsilon^{\frac{1}{2}} e^{-\varepsilon} \int_0^\infty b\, db \int_0^\infty v_o\, dt\, \bar{f}(t,t+\tau)$$

$$= \left(\frac{\omega_s}{c}\right)^4 \frac{1}{15}\left(1+(\vec{\lambda}_s\cdot\vec{\lambda})^2\right) \frac{\rho^2}{2} 8\sqrt{\pi} \int_0^\infty d\varepsilon\, \varepsilon^{\frac{1}{2}} e^{-\varepsilon} \int_0^\infty b\, db \int_0^\infty v_o\, dt\, \bar{f}(t,t+\tau)$$

where ρ is the number density of molecules in the gas. The Fourier transform of this correlation function is the depolarized scattering cross section per unit frequency interval and per unit solid angle and per unit volume of the gas with number density ρ.

The evaluation of the correlation function and of the scattered light spectrum can proceed from this point in two directions: in terms of the moments of the spectrum or in terms of the spectral distribution function. We will consider each of these methods in turn.

3.2.1 The Moments of the Spectrum [7]

There are several reasons for computing the moments of the spectrum rather than the complete spectral distribution. The chief reason is that the first few moments are far easier to compute theoretically than the entire spectral distribution. The second reason is that they present

the information about the spectral distribution in a compact and convenient form. The first two non-vanishing moments are essentially the total scattered intensity and the spectral width, so that the gross features of the spectrum are described by just two numbers. The experimental determination of the moments requires knowledge of the spectrum over an extended frequency range, which is sometimes difficult to manage. However, knowledge of the complete spectrum is usually necessary for proper interpretation in any case, so that this disadvantage is not unique to the analysis in terms of the moments.

The spectral intensity and the correlation function are Fourier transforms of each other:

$$I(\omega) = \frac{1}{2\pi} \int_{-\infty}^{\infty} d\tau \; e^{-i\omega\tau} C(\tau)$$

$$C(\tau) = \int_{-\infty}^{\infty} d\omega \; e^{i\omega\tau} I(\omega) \quad ,$$

but since the classical correlation function and spectral intensity are even functions of their arguments,

$$C(\tau) = C(-\tau) \qquad \text{and} \qquad I(\omega) = I(-\omega) \quad ,$$

the second relation may be written as:

$$C(\tau) = \int_{-\infty}^{\infty} d\omega \cos(\omega\tau) \; I(\omega) \quad .$$

Using the Taylor expansion of $\cos(\omega\tau)$ about $\tau = 0$ we have:

$$C(\tau) = \int_{-\infty}^{\infty} d\omega \, I(\omega) \sum_{m=0}^{\infty} (-1)^m \frac{(\omega\tau)^{2m}}{(2m)!}$$

$$C(\tau) = \sum_{m=0}^{\infty} \frac{(-1)^m \tau^{2m}}{(2m)!} \int_{-\infty}^{\infty} d\omega \; \omega^{2m} \; I(\omega) \quad .$$

Expanding $C(\tau)$ in a Taylor series about $\tau = 0$ and equating coefficients of equal degree in τ, we obtain the following result:

$$\phi^{(2m)} = (-1)^m \left. \frac{d^{2m} C(\tau)}{d\tau^{2m}} \right|_{\tau=0} = \int_{-\infty}^{\infty} d\omega \; \omega^{2m} \; I(\omega) \quad .$$

The derivatives of $C(\tau)$ evaluated at $\tau = 0$ are equal to the moments of the spectrum to within a + or - sign. The zeroth moment, $\phi^{(0)}$, is just the total intensity of the spectrum. We will compute the first two moments for the depolarized CIS spectrum using the correlation function:

$$C(\tau) = V \left\langle \beta(t) \, \beta(t+\tau) \, P_2(\vec{u}(t) \cdot \vec{u}(t+\tau)) \right\rangle \quad .$$

The expressions for moments higher than the second become quite cumbersome.[8] We will make use of the following property of the correlation function of the quantity $A(t)$:

$$\left\langle A(t) \, \ddot{A}(t+\tau) \right\rangle \Big|_{\tau=0} = \frac{d^2}{d\tau^2} \left\langle A(t) \, A(t+\tau) \right\rangle \Big|_{\tau=0}$$

$$= \frac{d}{d\tau} \left\langle A(t) \, \dot{A}(t+\tau) \right\rangle \Big|_{\tau=0} = \frac{d}{d\tau} \left\langle A(t-\tau) \, \dot{A}(t) \right\rangle \Big|_{\tau=0}$$

$$= - \left\langle \dot{A}(t-\tau) \, \dot{A}(t) \right\rangle \Big|_{\tau=0} = - \left\langle \dot{A}(t) \, \dot{A}(t+\tau) \right\rangle \Big|_{\tau=0}$$

The invariance of the correlation function under the time translation $t \rightarrow t - \tau$ has been used.

The first two moments are:

$$\phi^{(0)} = C(\tau)\Big|_{\tau=0} = V\langle \beta^2(t) \rangle$$

$$\phi^{(2)} = -\frac{d^2}{d\tau^2} C(\tau)\Big|_{\tau=0} = -\frac{d^2}{d\tau^2} V\langle \beta(t)\, \beta(t+\tau)\, P_2(\cos\theta)\rangle\Big|_{\tau=0}$$

where $\cos\theta = \vec{u}(t)\cdot\vec{u}(t+\tau)$.

Continuing, we have:

$$\phi^{(2)} = - V\Big\langle \beta(t)\Big[\ddot{\beta}(t+\tau)\, P_2(\cos\theta) + 2\,\dot{\beta}(t+\tau)\,\dot{P}_2(\cos\theta) + \beta(t+\tau)\,\ddot{P}_2(\cos\theta)\Big]\Big\rangle\Big|_{\tau=0}$$

With the results:

$$P_2(\cos\theta)\Big|_{\theta=0} = 1$$

$$\dot{P}_2(\cos\theta)\Big|_{\theta=0} = 0$$

$$\ddot{P}_2(\cos\theta)\Big|_{\theta=0} = -3\,\dot{\theta}^2$$

the expression for $\phi^{(2)}$ reduces to:

$$\phi^{(2)} = - V\langle \beta(t)\,\ddot{\beta}(t) - 3\,\beta^2(t)\,\dot{\theta}^2(t)\rangle \quad .$$

Applying the relation $\langle A(t)\,\ddot{A}(t)\rangle = -\langle \dot{A}^2(t)\rangle$ we obtain:

$$\phi^{(2)} = V\langle \dot{\beta}^2(t) + 3\,\beta^2(t)\,\dot{\theta}^2(t)\rangle$$

$$= V\left\langle \left(\frac{d\beta}{dr}\right)^2 \dot{r}^2 + 3\beta^2\,\dot{\theta}^2 \right\rangle \quad .$$

From the equations of motion we know that

$$\dot{r}^2 = \frac{2}{m}\left(E - \phi(r) - \frac{L^2}{2mr^2}\right) \quad \text{and} \quad \dot{\theta}^2 = \left(\frac{L}{mr^2}\right)^2$$

so that we may compute the moments using the ensemble average:

$$\langle A(t) \rangle = \frac{4\pi^2 (2m)^{\frac{1}{2}} \int dr\, dE\, dL^2\, e^{-E/kT} \left(E-\phi(r) - \frac{L^2}{2mr^2} \right)^{-\frac{1}{2}} A(t)}{V (2\pi mkT)^{3/2}}$$

In order to integrate over all phase space, the integration limits will be:

$$\int_0^{\infty} dr \int_{\phi(r)}^{\infty} dE \int_0^{2mr^2(E-\phi(r))} dL^2$$

and the results of the integrations are:

$$\phi^{(0)} = 4\pi \int_0^{\infty} dr\, r^2\, e^{-\phi(r)/kT}\, \beta^2(r)$$

$$\phi^{(2)} = 4\pi \frac{kT}{m} \int_0^{\infty} dr\, r^2\, e^{-\phi(r)/kT} \left(\left(\frac{d\beta}{dr}\right)^2 + 6\frac{\beta^2}{r^2} \right) .$$

These results show very clearly the manner in which the dynamics of the collison, determined by the intermolecular potential function $\phi(r)$, and the form of the pair polarizability function $\beta(r)$, which depends on the scattering mechanism, both enter into the determination of the scattered light spectrum — it is not possible to separate their respective contributions to the integrals they appear in. We have put our emphasis on the polarizability in our discussion of light scattering because the intermolecular potential is discussed extensively elsewhere.[9]

By altering the integration limits it is possible to restrict the average involved in calculating the spectral moments to only a portion of the phase space accessible to the system.[10] To understand the value

of this division of phase space we must consider the nature of the orbits of the colliding molecules. The particle of the "reduced" collision problem moves under the influence of the "effective" potential:

$$\phi_{eff}(r) = \phi(r) + \frac{L^2}{2mr^2} \quad .$$

A schematic $\phi_{eff}(r)$ for a particular value of L^2 is drawn below:

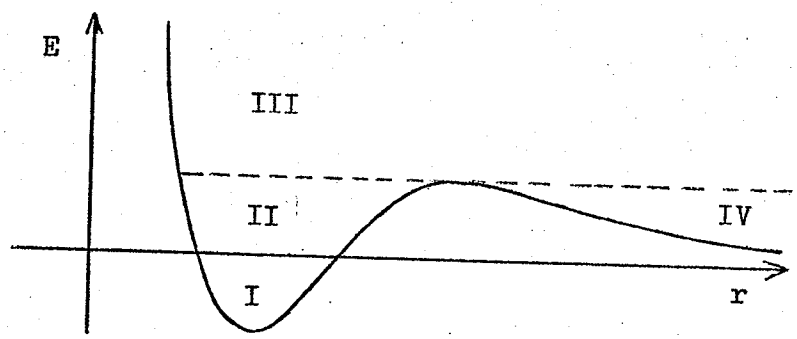

Particles in region I, with total energy $E<0$ will be bound. Particles in region II, with total energy less than the local maximum, will remain bound so long as L^2 is left unchanged — they may be called metastably bound. Particles in region IV have the same energy as particles in region II, but started to the right of the local maximum — we may call them low energy free particles. The remainder, region III, is composed of high energy free particles.

While the distinction between the various regions is not important insofar as calculation of the moments of the spectrum is concerned, when it comes to calculating the spectral distribution from the correlation function we must compute the actual orbits, and the orbits of bound and free particles are very different. However, when we calculate the

contribution of the bound and free particles to the scattered intensity, that is the zeroth moment $\phi^{(0)}$, we find that the free particles typically account for 85 percent of the total intensity at room temperature for the molecules we have studied. The free particle contribution increases for higher moments and for higher temperatures. For Ar at room temperature the contributions from the different regions of phase space to the first two moments are:[10]

	$\phi^{(0)}$	$\phi^{(2)}$
high energy free	79%	95%
low energy free	11%	3%
bound	7%	1%
metastable bound	3%	1%

From this we see that the spectrum, except perhaps at small frequency shifts, is dominated by the free particle contribution. Therefore it is a good first approximation to calculate the spectrum ignoring the scattering from bound dimers.

As a last illustration of the spectral moments, let us consider the spectrum of scattered light using the lowest order DID model for the pair polarizability:

$$\beta(r) = \frac{6\alpha_o^2}{r^3} \quad .$$

Substituting $\beta(r)$ into the expression for $\phi^{(0)}$ we obtain:

TABLE 3 - 2

The DID CIS Spectral Parameters for Several Atoms and Molecules (at 22°C)

molecule	L.J. 6-12 potential parameters $\epsilon/k(^\circ K)$	$\sigma(\AA)$	$\alpha(\AA^3)$	$\phi^{(0)}_{(DID)}(\AA^9)$	measured[d] $\phi^{(0)}(\AA^9)$	M(amu)	$v_{rms}(\AA/psec)$	$\tilde{\omega}_{rms}(cm^{-1})= \frac{1}{2\pi c}(\frac{15}{2})^{\frac{1}{2}} v_{rms}$	measured[e] $\tilde{\omega}_{rms}(cm^{-1})= \frac{1}{2\pi c}(\frac{\phi^{(2)}}{\phi^{(0)}})^{\frac{1}{2}}$
He	10.8	2.57	0.2051	0.040	-	4	15.65	88.6	-
H_2	31.3	2.92	0.8056	3.69	3.87	2	22.14	110.2	64.8
Ar[a]	142.1	3.76	1.642	42.7	51.5	40	4.95	19.1	15.6
CH_4[b]	217	3.559	2.633	192	296.2	16	7.83	32.0	28.6
CD_4[c]	212	3.551	2.597	183	282.3	20	7.00	28.7	25.6
CF_4	152.5	4.70	2.85	142	277	88	3.34	10.3	12.9
SF_6	200.9	5.51	4.470	574	1212	146	2.59	6.8	5.3

(a) The parameters are given for the Ar potential of the form $\phi(x) = \epsilon(\frac{6}{n-6} x^{-n} - \frac{n}{n-6} x^{-6})$ where $n = 4 + 9x$ and $x = r/r_m$; $r_m = 3.76\text{Å}$ and $\epsilon/k = 142.1^\circ K$.

See Smith, Physica 73, 211 (1974) .

(b) The parameters of the Lennard-Jones 6-20 potential suggested by Matthews, Smith, Mol. Phys. 32, 719 (1976) are given.

(c) The parameters for CD_4 are related to those for CH_4 as follows:

$$\frac{\alpha_{CH_4}}{\alpha_{CD_4}} = 1.014 , \qquad \frac{\epsilon_{CH_4}}{\epsilon_{CD_4}} = 1.022 , \qquad \frac{\sigma_{CH_4}}{\sigma_{CD_4}} = (1.0022)^{-1} .$$

See Thomaes, Steenwinkel, Mol. Phys. 5, 307 (1962) .

(d) The uncertainly of the measurements is expected to be in the range of ± 5 - 15 percent, increasing down the table. The accuracy is of the results is difficult to evaluate because of the possibility of unaccounted for systematic errors.

(e) The uncertainty in the experimental results is in the range of ± 5 - 10 percent. In comparing these figures with the calculated values of $\tilde{\omega}_{rms}$ recall that we have used the approximation:

$$\frac{\int_0^\infty dx\, g(x)\, x^{-6}}{\int_0^\infty dx\, g(x)\, x^{-4}} \doteq 1 .$$

$$\phi^{(0)}_{DID} = 4\pi \int_0^\infty dr\ r^2\ g(r)\ \left(\frac{6\alpha_o^2}{r^3}\right)^2$$

$$= 4\pi \left(\frac{36\alpha_o^4}{r_o^3}\right) \int_0^\infty dx\ g(x)\ x^{-4}$$

where $x = r/r_o$ and $g(x) = \exp(-\phi(x)/kT)$. Similary for $\phi^{(2)}$ we have:

$$\phi^{(2)}_{DID} = 4\pi\ \frac{kT}{m} \int_0^\infty dr\ r^2\ g(r)\ \left[\left(-3\ \frac{6\alpha_o^2}{r^4}\right)^2 + 6\left(\frac{6\alpha_o^2}{r^4}\right)^2\right]$$

$$= 4\pi \left(\frac{36\alpha_o^4}{r_o^3}\right) \frac{15\ kT}{r_o^2 m} \int_0^\infty dx\ g(x)\ x^{-6} \quad .$$

when the unit of length r_o is chosen as the molecular diameter (for example $r_o = \sigma$, where σ is the radius parameter in the Lennard-Jones 6-n potential function) then both integrals are approximately equal to $\frac{1}{2}$. An estimate of the frequency spread of the spectrum is then given by:

$$\omega_{rms} = \left(\frac{\phi^{(2)}}{\phi^{(0)}}\right)^{\frac{1}{2}} = \left(\frac{15\ kT}{\sigma^2 m}\right)^{\frac{1}{2}} = \left(\frac{15}{2}\right)^{\frac{1}{2}} \frac{v_{rms}}{\sigma} = \frac{2\pi}{T} \quad .$$

T is roughly the time it takes a molecule to travel one molecular diameter at the mean thermal velocity, $v_{rms} = \left(\frac{2}{m}\ kT\right)^{\frac{1}{2}}$. The spectral width, in cm^{-1} units is given by $\tilde{\omega}_{rms}(cm^{-1}) = \omega_{rms}(rad/sec)/\ 2\pi c$, and is typically 20 cm^{-1}. The depolarized scattering cross section (per unit solid angle and per unit volume) may be expressed in terms of the zeroth moment as:

$$\left(\frac{d\sigma}{d\Omega}\right)_{VH} = \left(\frac{\omega_s}{c}\right)^4 \frac{1}{15}\ \frac{\rho^2}{2}\ \phi^{(0)} \quad .$$

In Table 3-2 are presented the values of $\phi^{(0)}_{DID}$ and $\tilde{\omega}_{rms}$ for several molecules as well as the experimental values of $\phi^{(0)}$ and $\left(\frac{\phi^{(2)}}{\phi^{(0)}}\right)^{\frac{1}{2}}$ for comparison. The simple DID model predicts the intensity to within a factor of two for all the molecules in the table and does much better for the spectral width which depends chiefly on the molecular velocity.[11]

3.2.2. Calculation of the Spectral Distribution[12]

The spectral distribution of the scattered light is computed as the Fourier transform of the previously derived correlation function:

$$C(\tau) = 8\sqrt{\pi} \int_0^\infty d\varepsilon\ \varepsilon^{\frac{1}{2}}\ e^{-\varepsilon} \int_0^\infty b\ db \int_0^\infty v_o\ dt\ \bar{f}(t,t+\tau)$$

The computation of $C(\tau)$ involves two steps. The first step is to compute the orbits of the colliding molecules for the required values of energy and impact parameter, $\varepsilon = E/kT$ and b, neglecting the effect of the incident light. The second step is to evaluate $f(t,t+\tau)$ for each orbit and value of τ, and then compute the integrals over t, b and ε to obtain the correlation function $C(\tau)$.

This method is not wholly satisfactory. Let us consider the energy and momentum changes when a photon is scattered during a molecular collision. The incident photon has an energy about 100 times the mean thermal energy kT at room temperature. The energy change of a photon scattered with a frequency shift of 205 cm^{-1} will be equal to kT. The

largest possible momentum change for this photon as a result of a collision is only about 10^{-3} of the total momentum of a pair of molecules. Thus we are probably justified in ignoring the recoil of the molecules. However, a photon scattered with a frequency shift of 200 cm^{-1} on the Stokes side of the spectrum has given up enough energy to have doubled the energy of the pair of molecules it was scattered by. In the quantum mechanical description, the change of translational state is explicitly taken into account in calculating the scattering cross section, but this is not so for the classical calculation. For the diatomic rotor, the quantum results agree with the classical results in the limiting case that the initial and final rotational states are very close together. Similarily, the classical calculation for the CIS spectrum may be expected to agree with the quantum calculation so long as the intial and final translational states lie very close together in energy. At very large frequency shifts ($kT \sim 205$ cm^{-1}), our calculation may not be able to account for the observed scattering at all. Since the energy of the molecules changes during the collision, the symmetry of the orbit about the turning point is removed along with the symmetry of the correlation function and spectrum about $\tau = 0$ and $\omega = 0$, respectively.

Fortunately for our calculation, most of the scattered photons suffer frequency shifts of about 10 cm^{-1} or less ($\lesssim 1/20$ kT) .

so that the actual velocities of the molecules during a collision will differ by only a few percent from the values calculated ignoring the interaction with the light. Our simple mode of calculation should be adequate to account for the most intense part of the spectrum and it is only at large frequency shifts that the results must be viewed with suspicion.

Let us return to the calculation of the correlation function and the spectral distribution. The organization of the subroutines in the program for calculating the spectrum is given in Figure 3-1; the program listing appears in Appendix 3-A. We will discuss the design of the program below.

The first consideration is to rewrite the expression for $C(\tau)$ in a form appropriate for computation. As a unit of length we choose the molecular diameter σ (in fact this will be the length parameter in what-ever potential function $\phi(r)$ is chosen.) The time taken to travel the distance σ at the velocity $v_o = \sqrt{\frac{2}{m} E}$ is taken as the unit of time. The velocity v_o may be expressed in terms of the root mean square velocity, $v_{rms} = \sqrt{\frac{2}{m} kT}$, as $v_o = v_{rms} \sqrt{E/kT} = v_{rms}\ \varepsilon^{\frac{1}{2}}$. With these changes, $C(\tau)$ becomes:

$$C(\tau) = 8\sqrt{\pi}\,\sigma^3 \int_o^\infty d\varepsilon\ \varepsilon^{\frac{1}{2}}\ e^{-\varepsilon} \int_o^\infty d\left(\frac{b}{\sigma}\right)\left(\frac{b}{\sigma}\right) \int_o^\infty d\left(\frac{v_{rms}\,\varepsilon^{\frac{1}{2}}}{\sigma} t\right)\ \bar{f}(t, t+\tau)$$

$$= 8\sqrt{\pi}\,\sigma^3 \int_o^\infty d\varepsilon\ \varepsilon^{\frac{1}{2}}\ e^{-\varepsilon} \int_o^\infty dBE\ BE \int_o^\infty dTE\ \bar{f}(t, t+\tau)$$

FIGURE 3 - 1

The Organization of the Correlation Function Computation.

Information is passed between subroutines connected by lines, in the direction of the arrows. A line also represents a subroutine call, except in the case of ORBIT and COORD, where the information is passed through labeled common block storage.

The input data read by CORREL are:

CONST = $\frac{144\sqrt{\pi}\,\alpha^4}{\sigma^3}$ ($\mathring{A}^9$)

TSTEP = $\Delta\tau$ (psec)

EPSKT = ϵ/kT (—)

SIGVEE = σ/v_{rms} (psec)

and EKT(5), WEKT(5) (the abscissae and weights of a five-point Gauss-Laguerre quadrature. In the case of Ar, the parameter of the Lennard-Jones potential is replaced by r_m of the Smith potential.)

The output from CORREL and OUTCOR consists of listings and graphs of $C(\mathcal{E},\tau)$, for each of the five values of $\mathcal{E}$ in the energy integral, and of the final correlation function $C(\tau)$. The function values of $C(\tau)$ are given in units of $\mathring{A}^9$. The output of OUTFFT consists of a listing of the Fourier transform of $C(\tau)$ and graphs of the first 1/8, 1/4 and 1/2 of the transform, and listings of the spectrum interpolated every 1 cm^{-1}.

i) before "normalizing",

ii) after"normalizing", and

iii) after "normalizing" and correcting for the Boltzmann asymmetry of the spectrum.

The "normalization" involves scaling the spectrum so that the spectral intensity is given in units of the H_2 S(1) rotation line intensity per unit frequency interval (1 cm^{-1}) when all gases have a density of 1 mole/liter.

The correlation function program for Ar is presented in Appendix 3 - A. The first page of output, where the input parameters are tabulated, is included in the listing. The computation uses the parameter values given in Table 3 - 2.

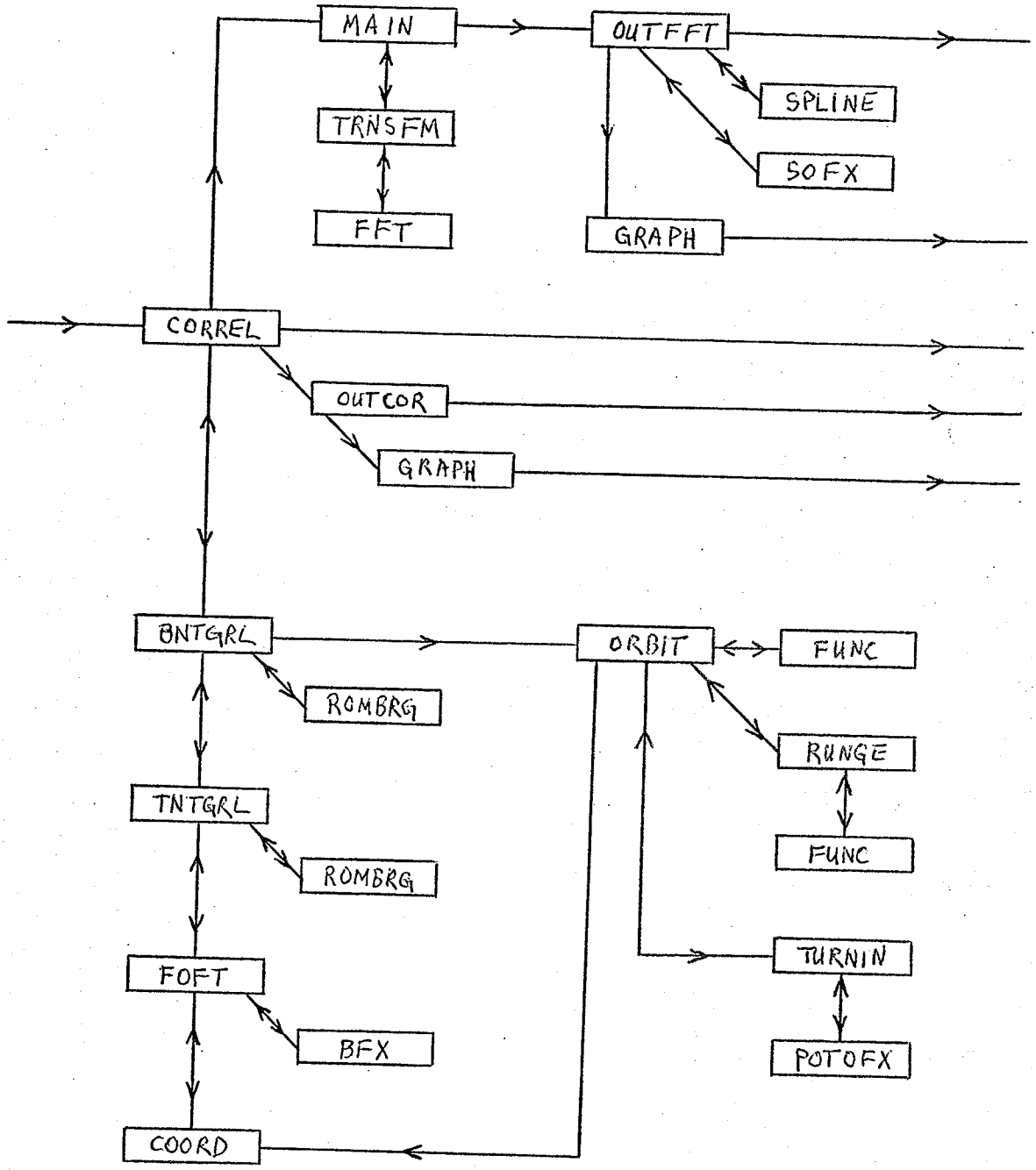
MAIN
TRNSFM
FFT
OUTFFT
SPLINE
SOFX
GRAPH
CORREL
OUTCOR
GRAPH
BNTGRL
ROMBRG
TNTGRL
ROMBRG
FOFT
BFX
COORD
ORBIT
FUNC
RUNGE
FUNC
TURNIN
POTOFX

where $BE = b/\sigma$ and $TE = \frac{v_o}{\sigma} t = \frac{v_{rms}}{\sigma} \varepsilon^{\frac{1}{2}} t$. Next we factor the polarizability anisotropy function,

$$\beta(r) = \frac{6\alpha_o^2}{\sigma^3} \beta(x) \quad ,$$

so that for the simple DID model $\beta(x) = x^{-3}$, where $x = r/\sigma$. Making this substitution, the expression becomes:

$$C(\tau) = \left(\frac{144\sqrt{\pi}\alpha_o^4}{\sigma^3}\right) \int_0^\infty d\varepsilon \; \varepsilon^{\frac{1}{2}} \; e^{-\varepsilon} \int_0^\infty dBE \; BE \int_0^\infty dTE \quad \hat{h}(t, t+\tau)$$

where

$$\hat{h}(t, t+\tau) = h(t, t+\tau) + h(-t, -t+\tau)$$

and

$$h(t, t+\tau) = \beta(x(t)) \; \beta(x(t+\tau)) \; P_2(\cos(\psi(t) - \psi(t+\tau))) \quad .$$

The calculation begins with the computation of the orbit for given values of BE and ε by numerically integrating the equations of motion starting from the turning point of the motion. The intermolecular separation at the turning point, x_{min}, is the largest solution to the equation

$$1 = \left(\frac{BE^2}{x_{min}}\right) + EE \; \phi(x_{min}) = \phi_{eff}(x_{min})$$

where $EE = \epsilon/E = (\epsilon/kT)/\varepsilon$, $\phi(x) = \frac{\phi(r/\sigma)}{\epsilon}$ and ϵ is the well depth of the intermolecular potential.[13] In Figure 3-2 the function $\phi_{eff}(x)$ for Argon is plotted for several values of the parameter $A = \left(\frac{BE^2}{EE}\right)$ which determines the shape of the effective potential. As the value of A increases, the positions of the local minimum and the local maximum of $\phi_{eff}(x)$ move closer together, until when $A = A_{crit}$

FIGURE 3 - 2

The Interatomic Effective Potential for Argon

The interatomic potential function assumed for Ar has the form:

$$\phi(x) = \left(\frac{6}{n-6} x^{-n} - \frac{n}{n-6} x^{-6} \right)$$

where $n = 4 + 9x$, $x = r/r_m$ and $r_m = 3.76$ Å is the radius of the minimum of the interatomic potential. The "effective" potential, including "centrifugal repulsion", is

$$\phi_{eff}(x) = EE\ \phi(x) + \left(\frac{BE}{x}\right)^2$$

where $EE = \epsilon/E$ and $BE = b/r_m$; ϵ is the well depth of the potential, E is the total energy (of relative motion) of the colliding atoms and b is the impact parameter of the collision. The effective potential, $\phi_{eff}(x)$, is plotted versus x for the parameter values EE = 1.0 and BE = 0.0, 1.0, 1.2, 1.4, 1.5, 1.6 and 2.0 .

The turning point in the collision between two unbound atoms will be at the largest value of x which satisfies the equation $\phi_{eff}(x) = 1$. The shape of the effective potential $\phi_{eff}(x)$ is specified by the parameter $A = \frac{BE^2}{EE}$. As the value of A increases, the local minimim of $_{eff}(x)$ moves outward from x = 1 and the local maximum moves inward from $x = \infty$. Eventually the local minimum and maximum merge at a horizontal inflection point, and for larger values of A, $\phi_{eff}(x)$ is monotonic. The value of A at which the $\phi_{eff}(x)$ becomes monotonic is called ACRIT, and it is the largest value of A for which there is a solution to the equation $A = \frac{1}{2} x^3 \phi(x)$ (this is derived from $\phi_{eff}(x) = 0$.) For the Ar-Ar potential which we have chosen, ACRIT = 2.1133325 . In the diagram this corresponds to BE $\doteq$ 1.45 .

For non-monotonic $\phi_{eff}(x)$, the peak value at the local maximum will always be smaller than the height of the horizontal inflection point obtained by increasing BE, with EE held constant, until A = ACRIT. The height of the inflection point is

FIGURE 3 - 2 (continued)

$$\phi_{eff}(x_{crit}) = \left(\frac{A_{crit}}{x_{crit}^2} + \phi(x_{crit}) \right)/EE \quad ,$$

and EE_{crit} = ECRIT is defined by

$$\phi_{eff}(XCRIT) = 1 = \left(\frac{ACRIT}{XCRIT^2} + \phi(XCRIT) \right)/ECRIT \quad .$$

For all EE < ECRIT the colliding atoms will have enough energy to surmount the local maximum of $\phi_{eff}(x)$, and there will be only one solution to the equation $\phi_{eff}(x) = 1$. For our Ar-Ar potential, ECRIT = 0.46086516 and XCRIT = 1.15278 . When A < ACRIT and EE $\geq$ ECRIT there may be two or three solutions of $\phi_{eff}(x) = 1$, and it is possible to have bound states of the interacting Ar atoms.

For potentials of the Lennard-Jones 6 - n form, $\phi(x) = C\,(x^{-n} - x^{-6})$ where $x = r/\sigma$, the critical values of A, x and EE are:

n	C	ACRIT	XCRIT	ECRIT
6	4.0	2.4623653	1.30766	1.25000000
20	2.3932763	2.5759863	1.213405	0.70707961

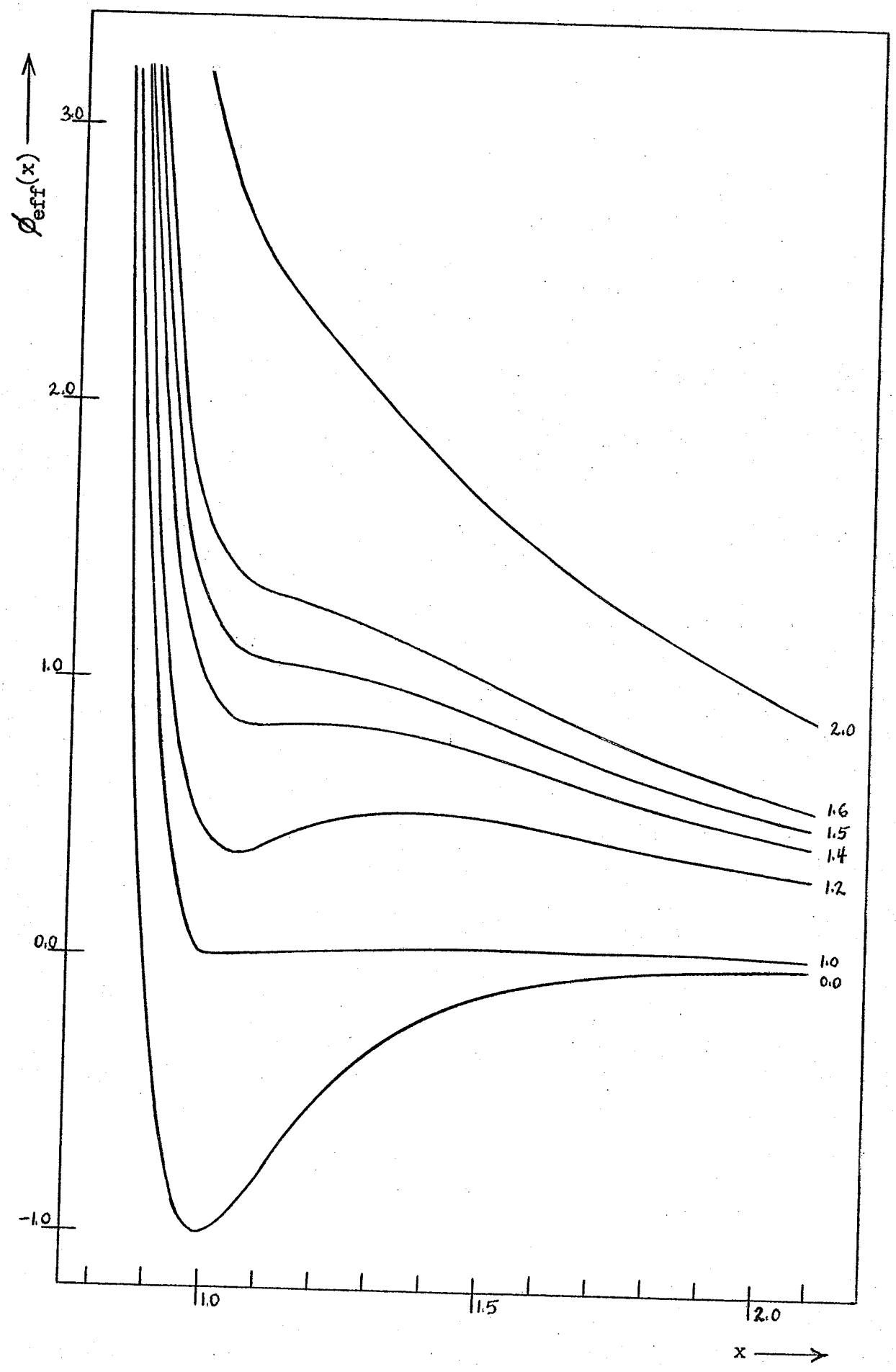
$\phi_{eff}(x)$
3.0
2.0
1.0
0.0
-1.0
1.0
1.5
2.0
x
2.0
1.6
1.5
1.4
1.2
1.0
0.0

they merge to give a horizontal inflection point at the position x_{crit}. For larger values of A the effective potential is monotonic. Similarily, for values of EE less than E_{crit}, given by:

$$EE_{crit} = \left[A_{crit} X^{-2}_{crit} + \phi(x_{crit}) \right]^{-1} ,$$

only one root of the equation $1 = \phi_{eff}(x)$ exists. For other values of A and EE there may be one, two or three roots to this equation. The largest root, corresponding to the turning point, was obtained by solving the equation by Newton's method.[14] The other solutions $\phi_{eff}(x) = 1$ correspond to turning points in the orbits of molecules bound by the local minimum of the effective potential and are ignored in this calculation.

Having obtained the position of the turning point, the orbit is computed by numerically integrating the equations of motion:

$$\frac{dx}{dTE} = \dot{x} = \left(1 - \left(\frac{BE}{x}\right)^2 - EE\,\phi(x) \right)^{\frac{1}{2}}$$

$$\frac{d\psi}{dTE} = \dot{\psi} = \frac{BE}{x^2}$$

using the lowest order Runge-Kutta method. When the orbit reaches the asymptotic region, where $EE\,\phi(x) \ll 1$, the parameters specifying the asymptote are computed. The angle φ, between the asymptote and the apsidal direction $\psi = 0$, is given by $\varphi = \psi_1 + |\theta_1|$ where:

$$\cos\theta_1 = \frac{\dot{x}_1}{v_1} = \left[\frac{1 - EE\,\phi(x_1) - (BE/x_1)^2}{1 - EE\,\phi(x_1)} \right]^{\frac{1}{2}} ,$$

and the point (x_1, ψ_1) lies in the asymptotic region. The results of

the orbit calculation are passed to the subroutine COORD which will compute the position (x,ψ) of the particle at any value of t required by the TE-integral.

The correlation function $C(\tau)$ is to be computed for 100 values of τ in steps of TSTEP. The TE-integral is evaluated for every value of τ each time it is called, since each pair of values $(\mathcal{E},BE)$ requires the computation of a new orbit. The energy integral is evaluated using a five point Gauss-Laguerre quadrature. The abscissae and weights of the quadrature are read in at the beginning of the computation as the arrays EKT and WEKT.[15] For the BE and TE-integrals, the following substitutions are made to reduce the domain of integration to the unit interval:

$$\int_0^\infty dBE \;\; BE \;\; f(EE,BE,\tau)$$

$$\longrightarrow \int_0^1 a^2 \;\; z^{-3} \;\; (1-z) \;\; dz \;\; f(EE,BE,\tau)$$

where $BE = a\,(z^{-1}-1)$ and $a \simeq 1$; and

$$\int_0^\infty dTE \;\; f(EE,BE,TE,\tau)$$

$$\longrightarrow \int_0^1 a \;\; z^{-2} \;\; dz \;\; f(EE,BE,TE,\tau)$$

where $TE = a\,(z^{-1}-1)$ and $a \simeq 1$.

The integrals were evaluated using Simpson's rule, with 64 and 16 intervals respectively, and three steps of Romberg's method. The small interval size in the BE-integral is required because there is a discontinuity in the integrand for low energy collisions. As the

impact parameter BE increases, for a fixed value of $\mathcal{E}$, the centrifugal barrier of ϕ_{eff} will eventually become high enough to reflect the particle and prevent it from reaching the repulsive core of the potential. When this happens, the turning point of the orbit will switch from a small radius to a larger one; since the pair polarizability function varies rapidly with intermolecular separation, this results in a large reduction in the peak value of the pair polarizability when the value of BE becomes large enough to cause the switch. This behavior is illustrated in Figure 3-3.

After obtaining $C(\tau)$, the Fourier transform is applied and the resulting spectrum is interpolated at intervals of 1 cm^{-1}. Finally, the spectrum is normalized so that the CIS intensity is expressed in units of the H_2 S(1) rotation line scattering cross section per unit (1 cm^{-1}) frequency interval, when both gases are maintained at unit (1 mole/liter) density. The spectrum is "corrected" for the Boltzmann asymmetry by multiplying the Stokes side by $\exp(+\frac{\tilde{\omega}(cm^{-1})}{2(205\ cm^{-1})})$ where $kT/hc = 205\ cm^{-1}$ at room temperature. The correction on the anti-Stokes side would be the inverse of this factor. The total scattering cross section for the spectrum is given by the value of $C(\tau=0)=\phi(0)$.

The computation of a single spectrum requires about 25 minutes on an IBM 370. The final results are expected to be accurate to about one percent and the execution time could be reduced by several factors

FIGURE 3 - 3

Discontinuity in the Integrand of the BE-Integral for Low Energy Collisions

a) The BE-integral sums the contribution to the correlation function of collisions with different impact parameters but a fixed energy. In the example we are presenting, $EE = \epsilon/E = 1.1575281$, $\tau = 0$ in $C(\tau)$, $\beta(x) = x^{-3}$ and the substitution $BE = 0.9\,(z^{-1} - 1)$ has been used to map the range $0 \to \infty$ of BE onto the unit interval, $z = 0 \to 1$. The discontinuity in the integrand of the BE-integral, plotted as a function of z, occurs at $z \triangleq 0.37$ $(BE \triangleq 1.52$.)

b) The discontinuity in a) occurs when the turning point jumps abruptly from $x \triangleq 1.07$ to $x \triangleq 1.18$ as BE increases through the value $BE = 1.52$. (The turning point of the motion is the point where the effective potential $\phi_{eff}(x)$ crosses the horizontal line $f(x) = 1$.) The discontinuity in a) is very pronounced in this case because the $\phi_{eff}(x)$ is almost flat in the region around the turning point for $B = 1.52$. For $BE < 1.52$, the particle has a very small velocity over a wide region approaching the turning point. It stays at small x values for a disproportionately long time, and since $\beta(x) = x^{-3}$ is strongly dependent on x, the contirbution to the BE-interal is also large. When $BE > 1.52$, the turning point moves to a larger x value, and the velocity of the particle as it approaches the turning point remains high. The particle spends less time near the turning point and the turning point is at a larger separation, so the contribution to the BE-integral is much smaller. A discontinuity in the BE-integrand can occur whenever the local maximum of $\phi_{eff}(x)$ lies near the horizontal line $f(x) = 1$.

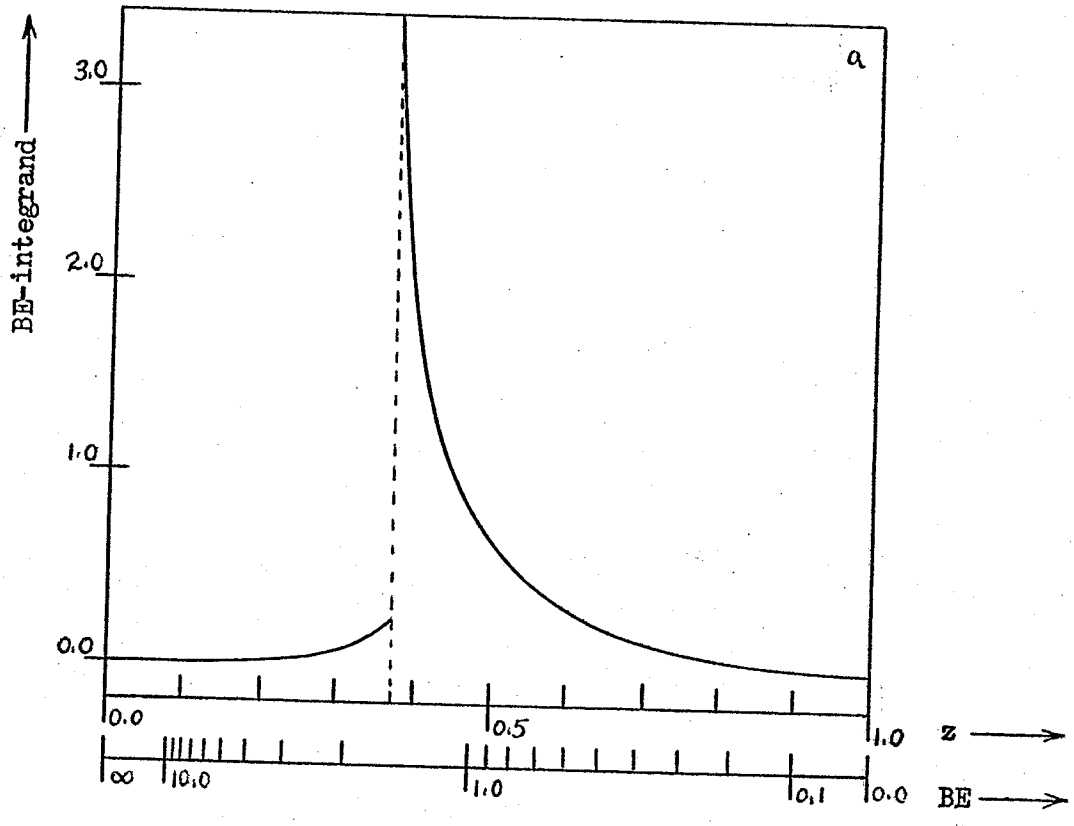
a
BE-integrand
3.0
2.0
1.0
0.0
0.0
0.5
1.0
z
∞
10.0
1.0
0.1
0.0
BE

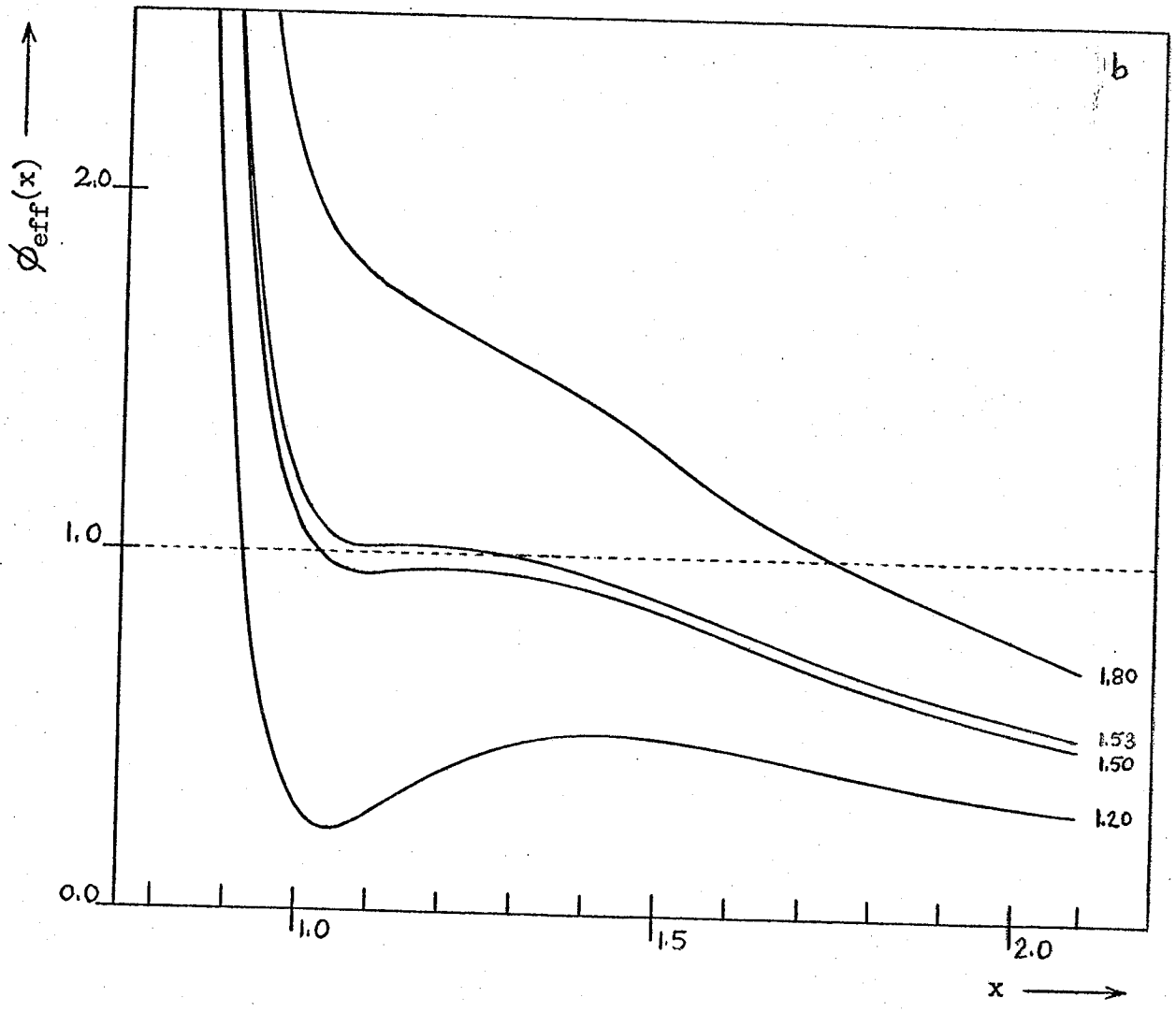
b
$\phi_{eff}(x)$
2.0
1.0
0.0
1.80
1.53
1.50
1.20
1.0
1.5
2.0
x

of two by eliminating all calculations which are unnecessary for achieving the required accuracy in the final result. This however would require a more flexible and more complicated program.

A typical calculated correlation function, for Ar, is presented in Figure 3-4 and the corresponding spectrum is given in Figure 3-5.

As was mentioned before, collisions involving free particles are not the only ones possible. But since the scattering from bound dimers is responsible for only about 10 percent of the total intensity and this contribution is confined to the region at small frequency shifts, we will be satisfied with a very rough approximation to the bound dimer spectrum. We will consider the bound dimer spectrum as being due to rigid, freely rotating pairs with the intermolecular separation fixed at the minimum of the intermolecular potential. The rotational constants are then $\tilde{B}$ = 0.060, 0.140, 0.105, 0.0116 and 0.0051 cm^{-1} for dimers of Ar, CH_4, CD_4, CF_4 and SF_6, respectively. In fact, the bound dimers are not rigid rotors but are only weakly bound, particularily the ones we classed as metastable bound dimers. Vibrations will have large amplitudes and the vibrational Raman spectrum (to the extent that we may talk about separate vibration and rotation spectra in this strongly coupled case) will lie in the same frequency range as the rotational spectrum and have a comparable intensity. Furthermore, the vibration and rotation frequencies will be lower than the

FIGURE 3 - 4

The Calculated Correlation Function For Unbound Dimers of Ar

The correlation function $C(\tau)$, in units of $\mathring{A}^9$, is plotted versus τ in the range of 0 to 10 psec. The DID model, $\beta(x) = x^{-3}$, was used in the calculation, along with the parameters in Table 3 - 2 and the program listed in Appendix 3 - A. The zeroth moment due to free dimers is $C(\tau = 0) = \phi^{(0)}_{free} = 37.5\ \mathring{A}^9$ while the zeroth moment due to all contributions is $\phi^{(0)}_{ttl} = 42.7\ \mathring{A}^9$, so that our calculation which ignores bound dimers, accounts for 88 percent of the total scattered intensity.

The correlation function $C(\tau)$ is calculated using five values of the total energy of the colliding pair of atoms. Past τ = 1.0 psec, $C(\tau)$ is almost completely determined by the lowest energy collisions $E \triangleq 0.26$ kT, except the higher energy collisions deepen the dip at τ = 3.0 psec by a factor of two. For $\tau < 1.0$ psec, the next two energies, $E \triangleq 1.4$ kT and $E \triangleq 3.6$ kT account for about 1/2 and 1/6, respectively, of the value of $C(\tau)$. The next two values of E (7.1 kT and 12.5 kT) are completely negligible except for $\tau \lesssim 0.1$ psec.

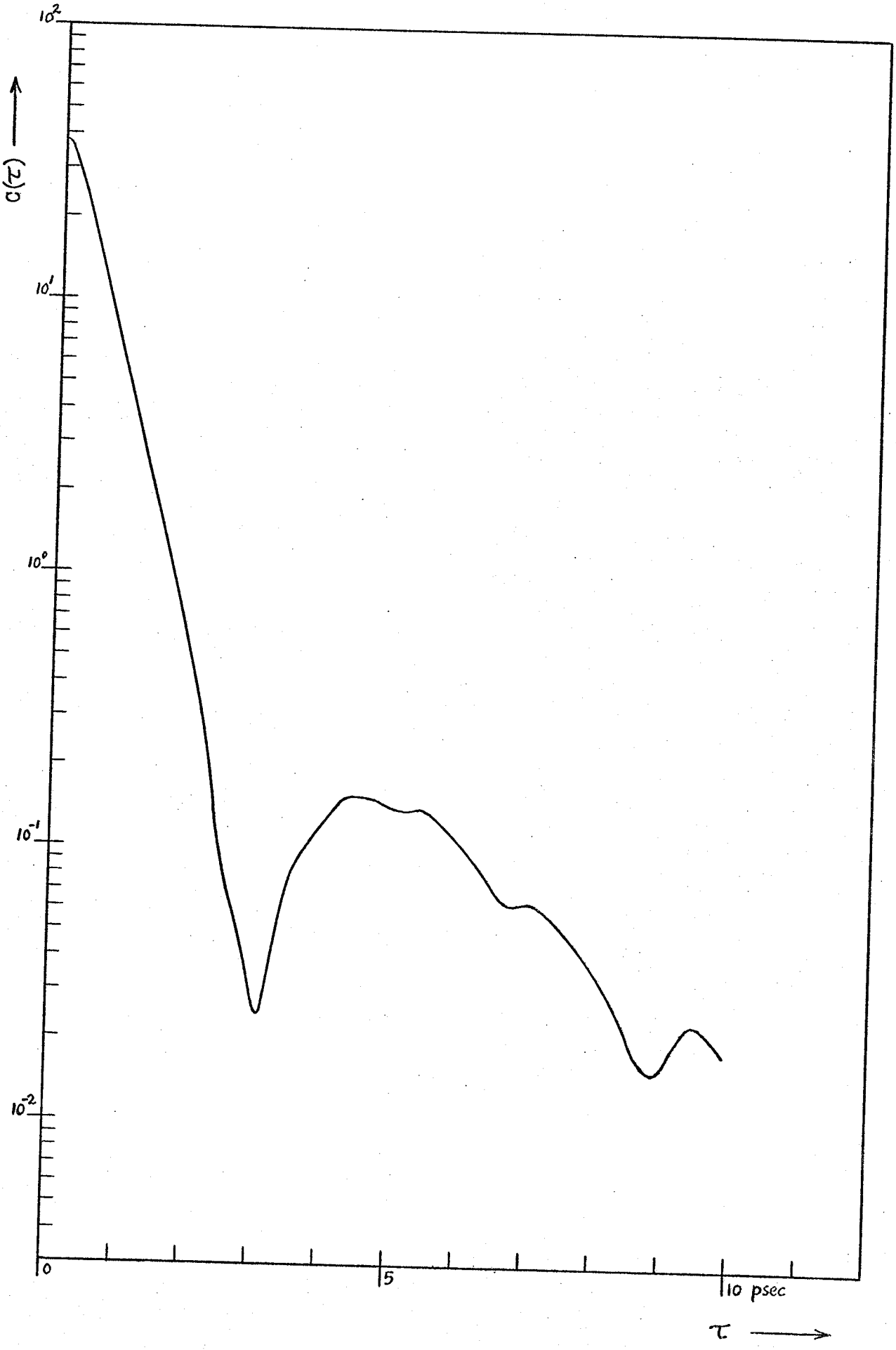
10^2
10^1
10^0
10^{-1}
10^{-2}
$G(\tau)$
0
5
10 psec
τ

FIGURE 3 - 5

The Calculated CIS Spectrum for Ar

The spectral intensity of CIS from Ar, obtained by Fourier transforming the $C(\tau)$ of Figure 3 - 4, is plotted as a function of frequency shift in cm^{-1}. The spectrum due only to unbound dimers of Ar is given by the dashed line, while the spectrum including the approximate bound dimer contribution is given by the solid line. The contribution to the spectral intensity due to bound dimers is significant out to about 8 cm^{-1}. The overall spectrum decreases roughly exponentially with frequency shift: $I(\omega) \stackrel{\circ}{=} A \exp(-\omega/\omega_o)$.

The spectral intensity scale is in units of the spectral intensity per unit frequency interval (1 cm^{-1}) divided by the intensity of the H_2 S(1) rotational Raman line when both gases (H_2 and Ar) are at unit (1 mole/liter) density.

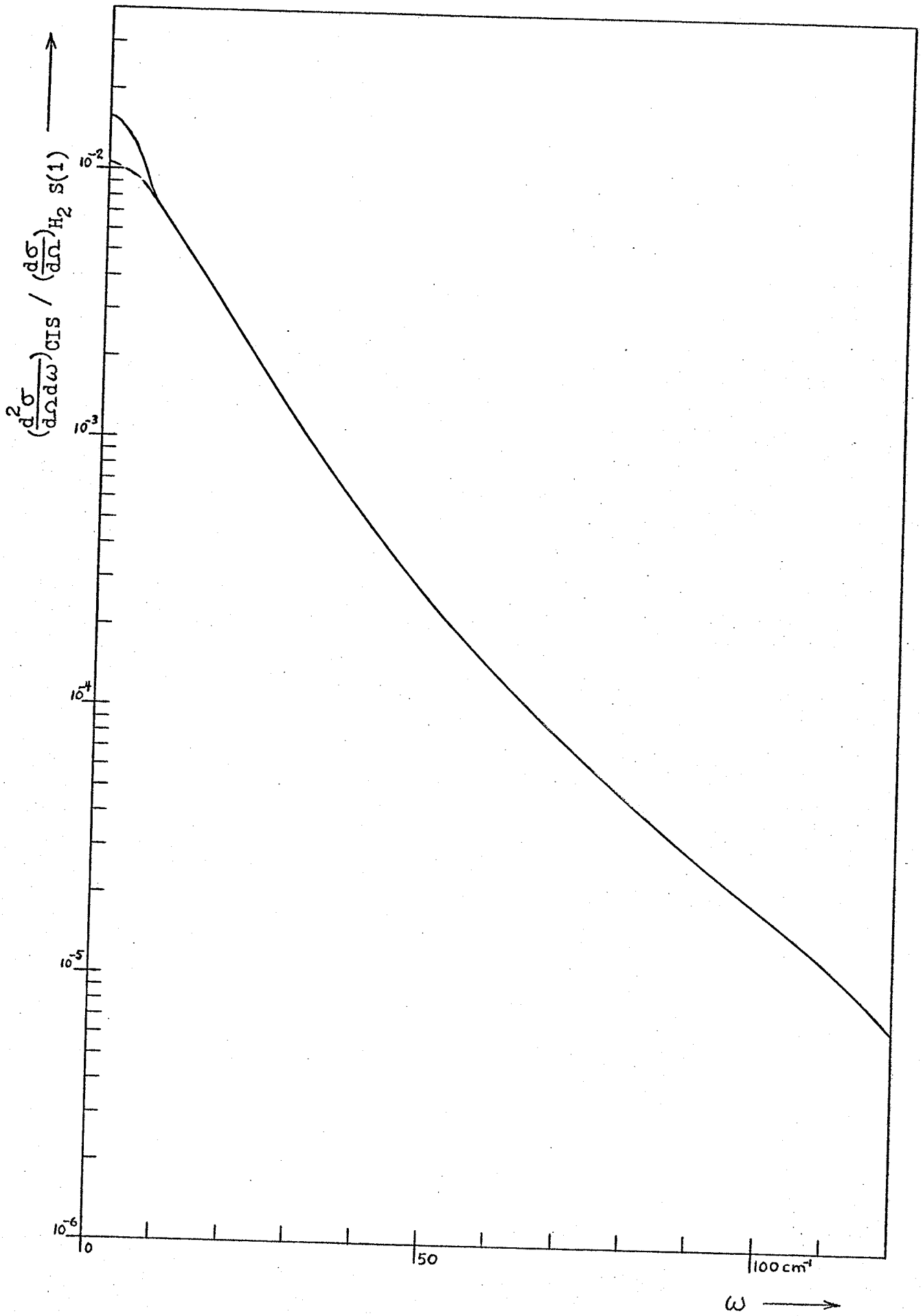
$(\frac{d^2\sigma}{d\Omega d\omega})_{CIS} / (\frac{d\sigma}{d\Omega})_{H_2\ S(1)}$
10^{-2}
10^{-3}
10^{-4}
10^{-5}
10^{-6}
0
50
100 cm^{-1}
ω

collision frequency at moderate densities, which makes even the assumption of free rotor behavior a poor approximation. Since it is difficult to proceed otherwise, we will take the shape of the bound dimer spectrum as given by rigid rotor calculation (with the Q-branch broadened to give a smooth spectral profile) and adjust its intensity to match the difference between the total scattered intensity and the free (unbound) dimer contribution. The result of this simple and crude approximation for the bound dimer spectrum is shown for Ar, along with the free dimer spectrum, in Figure 3-5.[16]

NOTES AND REFERENCES

1. When the separation of the atoms becomes comparable to the wavelength of the incident light, the phases of the scattered waves from the two atoms will not be the same. But, in the context of CIS, very large distances are about 40 atomic radii or about 0.02 wavelength of light. So, for our intents and purposes, the asymptotic value of the pair polarizability is just $2\alpha_o$.

2. L. Silberstein, Phil. Mag. 33, 521 (1917)
The results for two interacting point dipoles polarizabilities are;

$$\bar{\alpha}(r) = \frac{4\alpha_o^3}{r^6}\left(1 - \frac{\alpha_o}{r^3} - \frac{2\alpha_o^2}{r^6}\right)^{-1}$$

$$\beta(r) = \frac{6\alpha_o^2}{r^6}\left(1 - \frac{\alpha_o}{r^3} - \frac{2\alpha_o^2}{r^6}\right)^{-1}$$

3. The present state of the theory of the pair polarizability of atoms is indicated in:
K. Clarke, P. A. Madden, A. D. Buckingham, Mol. Phys. 36, 301 (1978).

4. A. D. Buckingham, R. S. Watts, Mol. Phys. 26, 7 (1973)

5. K. Clarke, P. A. Madden, A. D. Buckingham, Mol. Phys. 36, 301 (1978)

6. Goldstein, Classical Mechanics, Addison-Wesley, Reading, 1950
Pathria, Statistical Mechanics, Pergamon, Oxford, 1972
Child, Molecular Collision Theory, Academic Press, London, 1974

7. P. Lallemand, Compte Rendu Acad. Sc. Paris 273B, 89 (1971)
H. E. Levine, J. Chem. Phys. 56, 2455 (1972)
D. P. Shelton, G. C. Tabisz, Phys. Rev. All, 1571 (1975).

8. The expressions for the 0, 2, 4 and 6 th moments are given in the papers cited in Reference 6, above.

9. For example:

T. M. Reed, K. E. Gubbins, Applied Statistical Mechanics, McGraw-Hill Kogakusha, Tokyo, 1973 .

10. H. E. Levine, J. Chem. Phys. 56, 2455 (1972)

11. The experimental values of the spectral moments may be used, along with the theoretical expressions for the moments, to determine the parameter values in empirical models for the function $\beta(x)$. See for example:

H. E. Levine, G. Birnbaum, J. Chem. Phys. 55, 2914 (1971)

F. Barocchi, M. Zoppi, D. P. Shelton, G. C. Tabisz, Can. J. Phys. 55, 1962 (1977)

12. The classical calculation of the spectrum has been given in:

P. Lallemand, J. de Phys. (Paris) 32, 119 (1971)

The quantum mechanical calculation of the spectrum has been given in:

L. Frommhold, K. H. Hong, M. H. Proffitt, Mol. Phys. 35, 665 (1978)

13. The potential functions used were usually of the Lennard-Jones 6-n type:

$$\epsilon \phi(x) = C\,(x^{-n} - x^{-6})$$

where $C = 4$ for $n = 12$ and $C = 2.393276$ for $n = 20$.

For Ar, a potential of the form

$$\epsilon \phi(x) = \left(\frac{6}{n-6}\, x^{-n} - \frac{n}{n-6}\, x^{-6}\right)$$

was used, where $n = 4 + 9x$, $x = r/r_m$ and r_m = the radius of the minimum in the intermolecular potential.

14. For the techniques of numerical analysis see:
G. Dahlquist, A. Bjork, Numerical Methods, Prentice-Hall, Englewood Cliffs, 1974 .

15. M. Abramowitz, I. Stegun, Handbook of Mathematical Functions, Dover, New York, 1965

16. The results of a (quantum mechanical) calculation of the CIS spectrum for Ar which correctly accounts for the bound dimer spectrum is presented in:
L. Frommhold, M. H. Proffitt, Mol. Phys. 35, 681 (1978) .

APPENDIX 3 - A

Listing of the Program for the Correlation Function Calculation

The subroutines in the listing are:

MAIN

OUTFFT (COFT, TSTEP, A)

OUTCOR (CT)

GRAPH (PLOT, NPTS)

SPLINE (A, Y, N)

\+ SOFX (A, XO, Xl, N)

FFT (M, A, CK, CS, N)

CORREL (COFT, TSTEP)

BNTGRL (CT, EE, TSTEP, N)

\+ TNTGRL (TAU, BE)

ROMBRG (FVAL, RESULT, NM)

\+ FOFT (TE, TAU, BE)

\+ BFX (X)

COORD (T, BE, CX, CPSI)

ORBIT (BE, EE)

RUNGE (TX, TSI, BE, EE, H)

\+ FUNC (EX, BE, EE)

TURNIN (BE, EE, XMIN)

POTOFX (X, POT, POTD, POTDD)

The subroutines marked with a + are functions. See Figure 3-1 for the organization of the calculation.

```
0001                IMPLICIT REAL*8(A-H,O-Z)
0002                REAL*8 COFT(100)
0003                COMPLEX*16 A(1024)
                C
                C BOTH PROGRAM STEPS AND INPUT DATA MUST BE CHANGED WHEN MOLECULAR PARAMETERS
                C ARE CHANGED .
                C CHANGES IN THE POLARIZABILITY FUNCTION ARE INCORPORATED DIRECTLY IN 'BFX(X)' .
                C CHANGES IN THE INTERMOLECULAR POTENTIAL RESULTS IN CHANGES TO THE PARAMETERS
                C 'ACRIT','ECRIT','XCRIT' AND 'C' IN 'TURNIN(BE,EE,XMIN)' AND REQUIRES THAT
                C SEGMENTS OF 'FUNC(EX,BE,EE)' AND 'POTOFX(X,POT,POTD,POTDD)' BE REWRITTEN .
                C FROM THE FIRST CARD AND 'EKT(5)' AND 'WEKT(5)' FROM THE NEXT TWO CARDS .
                C THE NUMBERS 'EKT(5)' AND 'WEKT(5)' ARE THE ABSCISSAE AND WEIGHTS OF A FIVE
                C POINT GAUSS-LAGUERRE QUADRATURE .
                C THE VARIABLE SEGMENTS OF THE PROGRAM ARE DENOTED BY STARS AS FOLLOWS
                C ******
                C
                C VARIABLE SEGMENT
                C
                C ******
                C
0004                CALL CORREL(COFT,TSTEP)
0005                CALL TRNSFM(COFT,A)
0006                CALL OUTFFT(COFT,TSTEP,A)
0007                STOP
0008                END
```

```
0001            SUBROUTINE OUTFFT(COFI,TSTEP,A)
0002            IMPLICIT REAL*8(A-H,O-Z)
0003            COMPLEX*16 A(1024)
0004            REAL*8 TEMP(1024)
0005            REAL*4 PLOT(128)
0006            REAL*8 COFT(100)
0007            REAL*8 B(1027),Y(1027),C(400)
0008            NPTS=128
0009            DO 100 J=1,1024
0010          100 TEMP(J)=CDABS(A(J))
0011            WRITE(6,295)
0012            WRITE(6,296) (TEMP(J),J=1,1024)
0013          295 FORMAT('1'/'0')
0014          296 FORMAT('0',5D16.6)
0015            DO 110 J=1,1024
0016            IF(TEMP(J).EQ.0.D0) TEMP(J)=1.D0
0017          110 TEMP(J)=DLOG(TEMP(J))
0018            DO 120 J=1,128
0019          120 PLOT(J)=TEMP(J)
0020            CALL GRAPH(PLOT,NPTS)
0021            DO 130 J=1,128
0022          130 PLOT(J)=TEMP(2*J-1)
0023            CALL GRAPH(PLOT,NPTS)
0024            DO 140 J=1,128
0025          140 PLOT(J)=TEMP(4*J-3)
0026            CALL GRAPH(PLOT,NPTS)
0027            Y(514)=CDABS(A(1))
0028            DO 150 J=1,512
0029            Y(514+J)=CDABS(A(J+1))
0030          150 Y(514-J)=Y(514+J)
0031            N=1027
0032            CALL SPLINE(B,Y,N)
0033            X0=-16.678230D0/TSTEP
0034            X1=-X0
```

```
0035            NMAX=X1
0036            DO 155 J=1,NMAX
0037            X=J-1
0038        155 C(J)=SOFX(X,B,X0,X1,N)
0039            WRITE(6,300)
0040            WRITE(6,301)
0041            WRITE(6,305) (C(J),J=1,NMAX)
0042        300 FORMAT('1'/'0')
0043        301 FORMAT(' ',5X,'SPECTRUM EVERY 1 CM-1 BEFORE SCALING')
0044        305 FORMAT('0',5D16.6)
0045            TTL=C(1)
0046            DO 160 J=2,NMAX
0047        160 TTL=TTL+2*C(J)
0048            COFT1=COFT(1)
0049            CONST=8.389668D-3*COFT1
0050            FACTOR=CONST/TTL
0051            DO 165 J=1,NMAX
0052        165 C(J)=C(J)*FACTOR
0053            WRITE(6,300)
0054            WRITE(6,302)
0055            WRITE(6,305) (C(J),J=1,NMAX)
0056        302 FORMAT(' ',5X,'SPECTRUM EVERY 1 CM-1 AFTER SCALING ')
0057            DO 170 J=1,NMAX
0058            X=J-1
0059        170 C(J)=C(J)*DEXP(X/410.19D0)
0060            WRITE(6,300)
0061            WRITE(6,303)
0062            WRITE(6,305) (C(J),J=1,NMAX)
0063        303 FORMAT(' ',5X,'SPECTRUM EVERY 1 CM-1 AFTER SCALING AND BOLTZMANN'
              C ,' CORRECTION')
0064            RETURN
0065            END
```

FORTRAN IV G

OUTCOR

```
0001                  SUBROUTINE OUTCOR(CT)
0002                  IMPLICIT REAL*8(A-H,O-Z)
0003                  REAL*8 CT(100),CC(100)
0004                  REAL*4 PLOT(128)
0005                  WRITE(6,300)(CT(J),J=1,100)
0006            300   FORMAT('0',5D16.6)
0007                  DO 100 J=1,100
0008                  CC(J)=DABS(CT(J))
0009                  IF(CC(J).EQ.0.D0) CC(J)=1.D0
0010                  CC(J)=DLOG(CC(J))
0011            100   PLOT(J)=CC(J)
0012                  NPTS=100
0013                  CALL GRAPH(PLOT,NPTS)
0014                  RETURN
0015                  END
```

```
0001            SUBROUTINE GRAPH(PLOT,NPTS)
                C
                C INPUT IS A REAL*4 VECTOR PLOT(128)
                C NPTS MAY BE 100 OR 128 POINTS
                C
0002            REAL*4 PLOT(128)
0003            REAL*4 MAX,MIN
0004            INTEGER*4 IPLOT(128,2)
0005            LOGICAL*1 LINE(128)/128*' '/
0006            LOGICAL*1 BLANK/' '/,STAR/'*'/
                C
                C FIND MAX AND MIN
                C
0007            MAX=PLOT(1)
0008            MIN=PLOT(1)
0009            DO 100 I=1,NPTS
0010            IF(PLOT(I).GT.MAX) MAX=PLOT(I)
0011          100 IF(PLOT(I).LT.MIN) MIN=PLOT(I)
                C
                C SCALE AND ROUND TO NEAREST INTEGER
                C
0012            IF(MAX.EQ.MIN)GO TO 121
0013            SCALE=50./(MAX-MIN)
0014            GO TO 122
0015          121 SCALE=0.
0016          122 IBSLN=-SCALE*MIN
0017            DO 120 I=1,NPTS
0018            PLOT(I)=PLOT(I)*SCALE+IBSLN
0019            IPLOT(I,1)=PLOT(I)
0020            IF((IPLOT(I,1)+1.-PLOT(I)).LT.0.5)IPLOT(I,1)=IPLOT(I,1)+1
0021          120 IPLOT(I,2)=I
```

```
C
C SORT
C
  142 ISORT=0
      N=NPTS-1
      DC 140 I=1,N
      IF(IPLOT(I,1).LT.IPLCT(I+1,1))GO TO 141
      GO TO 140
  141 ITEMP1=IPLOT(I,1)
      ITEMP2=IPLOT(I,2)
      IPLOT(I,1)=IPLOT(I+1,1)
      IPLOT(I,2)=IPLOT(I+1,2)
      IPLOT(I+1,1)=ITEMP1
      IPLOT(I+1,2)=ITEMP2
      ISORT=1
  140 CONTINUE
      IF(ISORT.EQ.1)GO TO 142
C
C PLOT
C
      WRITE(6,200)
      IF(NPTS.EQ.100)WRITE(6,205)
      IF(NPTS.EQ.128)WRITE(6,206)
      L=1
      DO 180 K=1,52
      M=0
      DO 181 I=L,NPTS
      IF(I.GT.NPTS)GO TO 182
      IF(IPLOT(I,1).EQ.(52-K))GO TO 183
  182 GO TO 184
  183 J=IPLOT(I,2)
      LINE(J)=STAR
```

```
0048          181 M=M+1
0049          184 IF(NPTS.EQ.100) WRITE(6,210) (LINE(J),J=1,100)
0050              IF(NPTS.EQ.128) WRITE(6,211) (LINE(J),J=1,128)
0051              IF(NPTS.EQ.100.AND.IBSLN.EQ.(52-K)) WRITE(6,215)
0052              IF(NPTS.EQ.128.AND.IBSLN.EQ.(52-K)) WRITE(6,216)
0053              DO 185 N=1,NPTS
0054          185 LINE(N)=BLANK
0055          180 L=L+M
0056              IF(NPTS.EQ.100) WRITE(6,205)
0057              IF(NPTS.EQ.128) WRITE(6,206)
0058              WRITE(6,220) MAX,MIN
0059          200 FORMAT('1'/'0')
0060          205 FORMAT(' ',18X,10('+---------'),'+-')
0061          206 FORMAT(' ',2X,13('+---------'))
0062          210 FORMAT(' ',18X,'|',100A1,'|')
0063          211 FORMAT(' ',2X,'|',128A1,'|')
0064          215 FORMAT('+',18X,10('+---------'),'+-')
0065          216 FORMAT('+',2X,13('+---------'))
0066          220 FORMAT('0',30X,'MAXIMUM VALUE=',E14.7,5X,'MINIMUM VALUE=',
                C E14.7/'0')
0067              RETURN
0068              END
```

```
0001            SUBROUTINE SPLINE(A,Y,N)
              C FIND THE COEFFICIENTS OF THE BELL-SHAPED BASIS FOR THE CUBIC SPLINE PASSING
              C THROUGH N-2 EQUIDISTANT POINTS WITH ZERO CURVATURE AT THE END POINTS.
              C THE N-2 FUNCTION VALUES ARE ENTERED IN Y(2) TO Y(N-1).
0002          C THE GAUSS-SEIDEL METHOD IS USED TO FIND THE COEFFICIENTS RETURNED IN A(N).
0003            IMPLICIT REAL*8(A-H,O-Z)
0004            REAL*8 A(N),Y(N)
0005            EPS=1.D-10
0006            Y(1)=0.D0
0007            Y(N)=0.D0
0008            DO 100 J=1,N
0009          100 A(J)=Y(J)
0010          150 AOLD=A(N/2)
0011            A(1)=2*A(2)-A(3)+Y(1)
0012            NN=N-1
0013            DO 155 J=2,NN
0014          155 A(J)=-A(J-1)/4-A(J+1)/4+3*Y(J)/2
0015            A(N)=-A(N-2)+2*A(N-1)+Y(N)
0016            IF(DABS((A(N/2)-AOLD)/A(N/2)).GT.EPS) GO TO 150
0017            RETURN
                END
```

SOFX

```
0001                  DOUBLE PRECISION FUNCTION SOFX(X,A,X0,X1,N)
                    C THE COEFFICIENTS OF THE BELL-SHAPED BASIS FOR THE CUBIC SPLINE PASSING
                    C THROUGH N-2 EQUIDISTANT POINTS BETWEEN X0 AND X1 WITH ZERO CURVATURE AT THE
                    C END POINTS ARE GIVEN IN A(N).
                    C THE VALUE OF THE SPLINE AT THE POINT X BETWEEN X0 AND X1 IS CALCULATED.
0002                  IMPLICIT REAL*8(A-H,O-Z)
0003                  REAL*8 A(N)
0004                  H=(X1-X0)/(N-3)
0005                  JAY=(X-X0)/H
0006                  J=JAY+2
0007                  XJ=X0+JAY*H
0008                  DXJ=(X-XJ)/H
0009                  DXJP=(XJ+H-X)/H
0010                  IF(J.EQ.N-1) GO TO 100
0011                  SOFX=A(J-1)*DXJP**3/6+A(J)*(DXJ**3/2-DXJ**2+2.D0/3)
                     C  +A(J+1)*(DXJP**3/2-DXJP**2+2.D0/3)+A(J+2)*DXJ**3/6
0012                  GO TO 105
0013                100 SOFX=A(J-1)/6+A(J)*2/3+A(J+1)*(DXJP**3/2-DXJP**2+2.D0/3)
0014                105 CONTINUE
0015                  RETURN
0016                  END
```

```
0001            SUBROUTINE TRNSFM(COFT,A)
              C FOURIER TRANSFORM THE CORRELATION FUNCTION. USE ZERO FILLING.
0002            IMPLICIT REAL*8(A-H,O-Z)
0003            REAL*8 COFT(100)
0004            INTEGER*4 CK
0005            REAL*8 CS(1024)
0006            COMPLEX*16 A(1024),CMPLX
0007            CK=1
0008            M=10
0009            N=1024
0010            DO 100 J=1,1024
0011         100 A(J)=(0.D0,0.D0)
0012            DO 102 J=2,100
0013            A(J+511)=COFT(J)
0014         102 A(513-J)=A(J+511)
0015            A(512)=COFT(1)
0016            CALL FFT(M,A,CK,CS,N)
0017            RETURN
0018            END
```

```
0001          SUBROUTINE FFT(M,A,CK,CS,N)
              C
              C
              C       CK=0   GENERATE TABLE OF CS(I) ONLY
              C         =1,-1 GEN. TABLE AND TRANSFORM(1),INVERSE(-1)
0002          INTEGER*4 CK
              C         =2,-2 ASSUME TABLE EXISTS, GEN. TRAN.(2),INV.(-2)
0003          REAL*8 DFLOAT,DCOS
0004          REAL*8 FNM,FNMT,PION,FI,THT,WI,WR
0005          REAL*8 PI/3.1415926535898D0/,CS(N)
0006          COMPLEX*16 A(N),W,T,DCMPLX,DCONJG
0007          IC=CK
0008          IF(IABS(IC).GT.1)GO TO 20
              C     GENERATE TABLE OF COSINES, ETC.
0009          IF(M.LE.0)STOP
0010          MOLD=M
0011          NM=2**M
0012          FNM = DFLOAT(NM)
0013          NMT=NM/2
0014          NMTP1=NMT+1
0015          NMF=NMT/2
0016          NMFP1=NMF+1
0017          FNMT = DFLOAT(NMT)
0018          PION=PI/FNMT
0019          DO 10 I=1,NMFP1
0020          FI = DFLOAT(I-1)
0021          THT=FI*PION
0022       10 CS(I) = DCOS(THT)
0023          IF(IC.EQ.0)GO TO 140
0024       20 IF(M.NE.MOLD)STOP
0025          IF(IC.GT.0)GO TO 40
              C       INVERSE=(TRANSFORM(A*)/N)*, THUS, CONJUGATE
0026          DO 30 I=1,NM
0027       30 A(I) = DCONJG(A(I))
```

```
C          TRANSFORM
0028    40 DO 100 L=1,M
0029       LP1=L+1
0030       MML=M-L
0031       NSTEP=2**MML
0032       NS2=2*NSTEP
0033       ITER=NM/NS2
0034       DO 90 J=1,ITER
C             THE LAST BIT SHOULD ALWAYS BE ZERO FOR IR
0035       IR=(J-1)*2
0036       IBR=0
0037       DO 50 IL=1,L
0038       K=MOD(IR,2)
0039       IBR=2*IBR+K
0040       IR=IR/2
0041    50 CONTINUE
0042       IBR=IBR*NSTEP
0043       IBI=IABS(NMF-IBR)+1
0044       WI=CS(IBI)
0045       IF(IBR.GT.NMF)GO TO 60
0046       WR=CS(IBR+1)
0047       GO TO 70
0048    60 WR=-CS(NMTP1-IBR)
0049    70 W = DCMPLX(WR,WI)
0050       NB=(J-1)*NS2
0051       DO 80 I=1,NSTEP
0052       N=NB+I
0053       N1=N+NSTEP
0054       T=A(N1)*W
0055       A(N1)=A(N)-T
```

```
0056                A(N)=A(N)+T
0057             80 CONTINUE
0058             90 CONTINUE
0059            100 CONTINUE
                C
                C       THE FOURIER SUMS ARE COMPLETE, BUT THEIR
                C       ADDRESSES ARE BIT-REVERSED. THE FOLLOWING
                C       CODING PUTS THEM IN ORDER.
0060                DO 120 I=1,NM
0061                IR=I-1
0062                IBR=0
0063                DO 110 J=1,M
0064                K=MOD(IR,2)
0065                IBR=2*IBR+K
0066                IR=IR/2
0067            110 CONTINUE
                C       IBR IS THE BIT REVERSED VALUE OF I-1
0068                IBR=IBR+1
0069                IF(IBR.LE.I) GO TO 120
0070                T=A(I)
0071                A(I)=A(IBR)
0072                A(IBR)=T
0073            120 CONTINUE
                C       BIT REVERSAL IS COMPLETE
0074                IF(IC.GT.0) GO TO 140
                C       CONJUGATE AND DIVIDE BY N
0075                DO 130 I=1,NM
0076            130 A(I) = DCONJG(A(I))/FNM
0077            140 RETURN
0078                END
```

```
0001                  SUBROUTINE CORREL(COFT,TSTEP)
0002                  IMPLICIT REAL*8(A-H,O-Z)
0003                  REAL*8 COFT(100),CT(100),CE(100,5)
0004                  REAL*8 EKT(5),WEKT(5)
0005                  REAL*8 EEI(5),WT(5),ALPHA(5)
                    C 'EKT' AND 'WEKT' ARE THE ABSCISSAE AND WEIGHTS FOR A FIVE POINT
                    C GAUSS-LAGUERRE QUADRATURE .
0006                  N=100
0007                  READ(5,200)CONST,TSTEP,EPSKT,SIGVEE
0008                  READ(5,200) (EKT(J),J=1,5)
0009                  READ(5,200) (WEKT(J),J=1,5)
0010                200 FORMAT(5D16.8)
0011                  WRITE(6,293)
0012                293 FORMAT('1'/'0',5X,'CONST= ',11X,'TSTEP= ',11X,'EPSKT= ',11X,
                       C 'SIGVEE= ')
0013                  WRITE(6,294)CONST,TSTEP,EPSKT,SIGVEE
0014                294 FORMAT('0',4D18.8)
0015                  WRITE(6,295)
0016                295 FORMAT('0'/'0',5X,'J= ',5X,'EKT= ',12X,'WEKT= ')
0017                  DO 100 J=1,5
0018                100 WRITE(6,296)J,EKT(J),WEKT(J)
0019                296 FORMAT('0',5X,I3,2D18.8)
0020                  DO 101 J=1,5
0021                  EEI(J)=EPSKT/EKT(J)
0022                  WT(J)=WEKT(J)*DSQRT(EKT(J))
0023                101 ALPHA(J)=SIGVEE/DSQRT(EKT(J))
0024                  WRITE(6,300)
0025                300 FORMAT('0'/'0',5X,'J= ',8X,'EEI(J)= ',10X,'WT(J) = ',11X,
                       C 'ALPHA(J)= ')
0026                  DO 102 J=1,5
0027                102 WRITE(6,305)J,EEI(J),WT(J),ALPHA(J)
0028                305 FORMAT('0',5X,I3,3X,4D18.8)
0029                  DO 110 J=1,5
0030                  STEP=TSTEP/ALPHA(J)
```

```
0031            EE=EEI(J)
0032            CALL BNTGRL(CT,EE,STEP,N)
0033            DO 115 K=1,N
0034          115 CT(K)=CT(K)*CONST
0035            WRITE(6,298)
0036          298 FORMAT('1')
0037            WRITE(6,300)
0038            WRITE(6,305) J,EEI(J),WT(J),ALPHA(J),CT(1)
0039            WRITE(6,299)
0040          299 FORMAT('0')
0041            CALL CUTCOR(CT)
0042            DO 110 K=1,N
0043          110 CE(K,J)=CT(K)
0044            DO 120 K=1,N
0045          120 COFT(K)=CE(K,1)*WT(1)
0046            DO 130 K=1,N
0047            DO 130 J=2,5
0048          130 COFT(K)=COFT(K)+CE(K,J)*WT(J)
0049            WRITE(7,330) (COFT(J),J=1,N)
0050          330 FORMAT(5D16.6)
0051            WRITE(6,310)
0052            WRITE(6,315) TSTEP
0053          310 FORMAT('1'/'0','CORRELTATION FUNCTION IN STEPS OF       PSEC')
0054          315 FORMAT('+',33X,F6.3/'0')
0055            CALL CUTCOR(COFT)
0056            RETURN
0057            END
```

```
0001            SUBROUTINE BNTGRL(CT,EE,STEP,N)
0002            IMPLICIT REAL*8(A-H,O-Z)
0003            REAL*8 CT(100),TEMP(129,100),FVAL(129)
0004            NM=6
0005            NPT=2**(NM+1)+1
0006            RNPT=NPT-1
0007            DO 100 K=1,N
0008            TEMP(NPT,K)=0.D0
0009        100 TEMP(1,K)=0.D0
0010            JJ=NPT-2
0011            DO 105 J=1,JJ
0012            Z=J/RNPT
0013            A=0.9D0
0014            BE=(1/Z-1)*A
0015            CALL ORBIT(BE,EE)
0016            CONST=(A**2)*(Z**(-3))*(1-Z)
0017            DO 105 K=1,N
0018            TAU=STEP*(K-1)
0019        105 TEMP(J+1,K)=TNTGRL(TAU,EE)*CONST
0020            DO 110 K=1,N
0021            DO 115 J=1,NPT
0022        115 FVAL(J)=TEMP(J,K)
0023            CALL ROMBRG(FVAL,RESULT,NM)
0024        110 CT(K)=RESULT
0025            RETURN
0026            END
```

```
0001                DOUBLE PRECISION FUNCTION TNTGRL(TAU,BE)
0002                IMPLICIT REAL*8(A-H,O-Z)
0003                REAL*8 FVAL(129)
0004                NM=4
0005                NPT=2**(NM+1)+1
0006                RNPT=NPT-1
0007                FVAL(1)=0.D0
0008                JJ=NPT-1
0009                DO 100 J=1,JJ
0010                Z=J/RNPT
0011                A=(BE+0.9D0)
0012                TE=(1/Z-1)*A
0013                TEM=-TE
0014                CONST=A*Z**(-2)
0015          100   FVAL(J+1)=( FOFT(TE,TAU,BE)+FOFT(TEM,TAU,BE) )*CONST
0016                CALL RCMBRG(FVAL,RESULT,NM)
0017                TNTGRL=RESULT
0018                RETURN
0019                END
```

```
0001                  SUBROUTINE ROMBRG(FVAL,RESULT,NM)
0002                  IMPLICIT REAL*8(A-H,O-Z)
0003                  REAL*8 FVAL(129),FHAT(3)
                C THE INTEGAL OF F(X) ON THE INTERVAL (0,1) IS COMPUTED USING SIMPSON'S
                C RULE AND TWO STEPS OF ROMBERG'S METHOD. THE VALUES OF F(X) AT 2**(NM+1)+1
                C EQUALLY SPACED POINTS, INCLUDING X=0 AND X=1 , ARE TO BE CONTAINED IN 'FVAL'.
                C THE VALUE OF THE INTEGRAL IS RETURNED IN 'RESULT'. THE QUADRATURE IS
                C EXACT FOR SEVENTH ORDER POLYNOMIALS.
                C NM.GE.3 IS REQUIRED .
                C
                C THREE APPROXIMATIONS TO THE INTEGRAL ARE COMPUTED USING SIMPSON'S RULE,
                C THE STEP SIZE BEING HALVED FOR EACH SUCCESSIVE APPROXIMATION.
                C
0004                  NPT=2**(NM+1)+1
0005                  DO 100 M=1,3
0006                  MM=M+NM-3
0007                  N=2**MM
0008                  H=1.D0/(2*N)
0009                  NN=N-1
0010                  JJ=(NPT-1)*H
0011                  FHAT(M)=FVAL(1)
0012                  DO 110 J=1,NN
0013              110 FHAT(M)=FHAT(M)+4*FVAL(1+(2*J-1)*JJ)+ 2*FVAL(1+(2*J)*JJ)
0014                  FHAT(M)=FHAT(M)+4*FVAL(NPT-JJ)+FVAL(NPT)
0015              100 FHAT(M)=(H/3)*FHAT(M)
                C
                C NOW APPLY TWO STEPS OF ROMBERG'S METHOD.
                C
0016                  FHAT(1)=FHAT(2)+(FHAT(2)-FHAT(1))/15
0017                  FHAT(2)=FHAT(3)+(FHAT(3)-FHAT(2))/15
0018                  FHAT(1)=FHAT(2)+(FHAT(2)-FHAT(1))/63
0019                  RESULT=FHAT(1)
0020                  RETURN
0021                  END
```

FORTRAN IV G

FCFT

```
0001                DOUBLE PRECISION FUNCTION FOFT(TE,TAU,BE)
0002                IMPLICIT REAL*8(A-H,O-Z)
0003                T1=TE
0004                T2=TE+TAU
0005                CALL COORD(T1,BE,CX,CPSI)
0006                X1=CX
0007                PSI1=CPSI
0008                CALL COORD(T2,BE,CX,CPSI)
0009                X2=CX
0010                PSI2=CPSI
0011                P2=( 3*DCOS(PSI2-PSI1)**2-1 )/2
0012                FOFT=BFX(X1)*BFX(X2)*P2
0013                RETURN
0014                END
```

FORTRAN IV G

BFX

```
0001                DOUBLE PRECISION FUNCTION BFX(X)
0002                IMPLICIT REAL*8(A-H,O-Z)
                C ******
                C
0003                BFX=X**(-3)
                C
                C ******
0004                RETURN
0005                END
```

```
0001                  SUBROUTINE COORD(T,BE,CX,CPSI)
0002                  IMPLICIT REAL*8(A-H,O-Z)
0003                  REAL*8 X(101),PSI(101)
0004                  COMMON /AREA1/ X,PSI,INOT,PHI
0005                  TSIGN=1.D0
0006                  IF( T.NE.DABS(T) ) TSIGN=-1.D0
0007                  T=TSIGN*T
0008                  IF(T.GE.5.D0) GO TO 100
0009                  FN=20*T+1
0010                  N=FN
                C QUADRATIC INTERPOLATION, FIRST FOR X(T) .
0011                  Y2=X(N)
0012                  Y3=X(N+1)
0013                  IF(N.EQ.1) GO TO 115
0014                  Y1=X(N-1)
0015                  GO TO 116
0016                115 Y1=X(N+1)
0017                116 CONTINUE
0018                  A=(Y3+Y1)/2-Y2
0019                  B=(Y3-Y1)/2
0020                  C=Y2
0021                  XH=FN-N
0022                  CX=A*XH**2+ B*XH+ C
              C NOW INTERPOLATE FOR PSI(T)
0023                  Y2=PSI(N)
0024                  Y3=PSI(N+1)
0025                  IF(N.EQ.1)GO TO 117
0026                  Y1=PSI(N-1)
0027                  GO TO 118
0028                117 Y1=PSI(N+1)
0029                118 CONTINUE
```

```
0030                A=(Y3+Y1)/2-Y2
0031                B=(Y3-Y1)/2
0032                C=Y2
0033                CPSI=A*XH**2+ B*XH+ C
0034                GO TO 150
                C ASYMPTOTIC RESULT
0035              100 CX=DSQRT( (T-TNOT)**2+BE**2 )
0036                  CPSI=PHI-DARSIN(BE/CX)
0037              150 CCNTINUE
0038                  CPSI=TSIGN*CPSI
0039                  RETURN
0040                  END
```

```
0001                  SUBROUTINE ORBIT(BE,EE)
0002                  IMPLICIT REAL*8(A-H,C-Z)
0003                  REAL*8 X(101),PSI(101)
0004                  COMMON /AREA1/ X,PSI,TNOT,PHI
                    C FIRST INTEGRATE THE ORBIT OUT TO T=5 . STORE THE RESULTS IN STEPS OF 0.05 .
0005                  CALL TURNIN(BE,EE,XMIN)
0006                  X(1)=XMIN+2.D-8
0007                  PSI(1)=0.D0
0008                  TX=X(1)
0009                  TSI=PSI(1)
0010                  H=1.D-2
0011                  DO 100 K=2,21
0012                  DO 105 J=1,5
0013                105 CALL RUNGE(TX,TSI,BE,EE,H)
0014                  X(K)=TX
0015                100 PSI(K)=TSI
0016                  H=2.5D-2
0017                  DO 110 K=22,41
0018                  DO 115 J=1,2
0019                115 CALL RUNGE(TX,TSI,BE,EE,H)
0020                  X(K)=TX
0021                110 PSI(K)=TSI
0022                  H=5.D-2
0023                  DO 120 K=42,101
0024                  CALL RUNGE(TX,TSI,BE,EE,H)
0025                  X(K)=TX
0026                120 PSI(K)=TSI
                    C NOW COMPUTE THE PARAMETERS FOR THE ASYMPTOTIC REGION OF THE ORBIT.
0027                  TNOT=5.D0-DSQRT( X(101)**2-BE**2 )
0028                  EX=X(101)
0029                  XDOT=FUNC(EX,BE,EE)
0030                  VE=DSQRT( XDOT**2+(BE/EX)**2 )
0031                  THETA=DARCOS(XDOT/VE)
0032                  PHI=PSI(101)+THETA
0033                  RETURN
0034                  END
```

FORTRAN IV G

RUNGE

```
0001                  SUBROUTINE RUNGE(TX,TSI,BE,EE,H)
0002                  IMPLICIT REAL*8(A-H,O-Z)
0003                  EX=TX
0004                  XKAY1=H*FUNC(EX,BE,EE)
0005                  PKAY1=H*BE/EX**2
0006                  EX=TX+XKAY1/2
0007                  XKAY2=H*FUNC(EX,BE,EE)
0008                  PKAY2=H*BE/EX**2
0009                  EX=TX+XKAY2/2
0010                  XKAY3=H*FUNC(EX,BE,EE)
0011                  PKAY3=H*BE/EX**2
0012                  EX=TX+XKAY3
0013                  XKAY4=H*FUNC(EX,BE,EE)
0014                  PKAY4=H*BE/EX**2
0015                  TX =TX +(XKAY1+2*XKAY2+2*XKAY3+XKAY4)/6
0016                  TSI=TSI+(PKAY1+2*PKAY2+2*PKAY3+PKAY4)/6
0017                  RETURN
0018                  END
```

```
0001                  DOUBLE PRECISION FUNCTION FUNC(EX,BE,EE)
0002                  IMPLICIT REAL*8(A-H,O-Z)
                C THE SEGMENT BETWEEN THE STARS COMPUTES THE VALUE OF THE INTERMOLECULAR
                C POTENTIAL AT THE POSITION 'EX' .
                C ******
                C
0003                  EN=4+9*EX
0004                  IF(EX.GT.7.D0) GO TO 100
0005                  A=(6/(EN-6))*EX**(-EN)
0006                  GO TO 105
0007                100 A=0.D0
0008                105 B=(6/(EN-6))*EX**(-6)
0009                  POT=A-(EN/6)*B
                C
                C ******
0010                  FUNC=DSQRT(1-(BE/EX)**2-EE*POT)
0011                  RETURN
0012                  END
```

```
0001                  SUBROUTINE TURNIN(BE,EE,XMIN)
0002                  IMPLICIT REAL*8(A-H,O-Z)
                    C FIND THE LARGEST ROOT OF THE EQUATION  (1/EE)-ALPHA*X**(-2)-POT=0 .
                    C THE EFFECTIVE POTENTIAL IS MONOTONIC FOR ALPHA.GT.ACRIT .
                    C WHEN ALPHA.LT.ACRIT , BUT EE.LT.ECRIT , THERE IS ONLY ONE ROOT EVEN THOUGH THE
                    C EFFECTIVE POTENTIAL IS NOT MONOTONIC .
                    C OTHERWISE THERE WILL BE ONE, TWO OR THREE ROOTS DEPENDING ON THE HEIGHT OF
                    C THE LOCAL MAXIMUM OF THE EFFECTIVE POTENTIAL .
0003                  EPS=1.D-8
                    C THE VALUES OF THE FOUR PARAMETERS BETWEEN THE STARS DEPEND ON THE FORM OF
                    C THE INTERMOLECULAR POTENTIAL .
                    C ******
                    C
0004                  ACRIT=2.1133325D0
0005                  ECRIT=0.46086516D0
0006                  XCRIT=1.15278D0
0007                  C=1.D0
                    C
                    C ******
0008                  BESQ=BE**2
0009                  ALPHA=BESQ/EE
                    C
0010                  IF( ALPHA.GE.ACRIT ) GO TO 130
0011                   IF( (ALPHA.LT.ACRIT).AND.(EE.LE.ECRIT) ) GO TO 135
0012                  IF( ALPHA.LT.ACRIT ) GO TO 110
                    C WHEN ALPHA.LT.ACRIT AND EE.GT.ECRIT THE POSITION AND HEIGHT OF THE LOCAL
                    C MAXIMUM OF THE EFFECTIVE POTENTIAL MUST BE CALCULATED TO DECIDE ON THE NUMBER
                    C OF POSSIBLE ROOTS .
0013                110 IF( ALPHA.EQ.0.D0 ) GO TO 135
0014                  XMAX=( 3*C/ALPHA )**(0.25)
0015                  IF( XMAX.LT.XCRIT ) XMAX=XCRIT
0016                115 IF( XMAX.GT.5.D0 ) GO TO 120
```

```
0017          116 X=XMAX
0018              CALL POTOFX(X,POT,POTD,POTDD)
0019              STEP=( POTD-2*ALPHA/X**3 )/( POTDD+6*ALPHA/X**4 )
0020              IF( DABS(STEP/X).GT.0.3D0 ) STEP=0.3D0*X*(STEP/DABS(STEP))
0021              XMAX=X-STEP
0022              IF( DABS((XMAX-X)/X).LT.EPS ) GO TO 120
0023              GO TO 116
0024          120 X=XMAX
0025              CALL POTOFX(X,POT,POTD,POTDD)
0026              PEAK=ALPHA/X**2+POT
0027              IF( (1/EE).GT.PEAK ) GO TO 135
0028              IF( (1/EE).LE.PEAK ) GO TO 130
            C USE NEWTON'S METHOD TO FIND THE TURNING POINT OF THE ORBIT .
0029          130 X=BE
0030              IF( X.LT.0.9D0 ) X=0.9D0
0031              GO TO 140
0032          135 X=0.9D0
0033          140 CALL POTOFX(X,POT,POTD,POTDD)
0034              STEP=( 1/EE-ALPHA*X**(-2)-POT )/( 2*ALPHA*X**(-3)-POTD )
0035              IF( DABS(STEP/X).GT.0.3D0 ) STEP=0.3D0*X*(STEP/DABS(STEP))
0036              XNEW=X-STEP
0037              IF( DABS((XNEW-X)/X).LT.EPS ) GO TO 150
0038              X=XNEW
0039              GO TO 140
0040          150 XMIN=XNEW
0041              RETURN
0042              END
```

```
FORTRAN IV G                                    POTOFX

0001                  SUBROUTINE POTOFX(X,POT,POTD,POTDD)
0002                  IMPLICIT REAL*8(A-H,O-Z)
                C THIS SEGMENT COMPUTES THE INTERMOLECULAR POTENTIAL AND ITS FIRST TWO
                C DERIVATIVES AT THE POSITION 'X' .
                C ******
                C
0003                  EN=4+9*X
0004                  IF(X.GT.7.D0) GO TO 100
0005                  A=(6/(EN-6))*X**(-EN)
0006                  GO TO 101
0007              100 A=0.D0
0008              101 B=(6/(EN-6))*X**(-6)
0009                  C=( EN/X+9/(EN-6) )
0010                  D=( 6/X+9/(EN-6) )
0011                  E=( 4/X**2+(9/(EN-6))**2 )
0012                  POT=A-(EN/6)*B
0013                  POTD=-A*( C+9*DLOG(X) )+B*C
0014                  POTDD=A*( (C+9*DLOG(X))**2+(E-9) )-B*( C*D+E )
                C
                C ******
0015                  RETURN
0016                  END
```

CONST=	TSTEP=	EPSKT=	SIGVEE=
0.34903301D+02	0.10000000D+00	0.48143379D+00	0.75900725D+00

J=	EKT=	WEKT=
1	0.26356032D+00	0.52175561D+00
2	0.14134031D+01	0.39866681D+00
3	0.35964258D+01	0.75942450D-01
4	0.70858100D+01	0.36117587D-02
5	0.12460801D+02	0.23369972D-04

J=	EEI(J)=	WT(J)=	ALPHA(J)=
1	0.18266551D+01	0.26785955D+00	0.14784475D+01
2	0.34062031D+00	0.47396153D+00	0.63842945D+00
3	0.13386451D+00	0.14401912D+00	0.40023068D+00
4	0.67943367D-01	0.96142072D-02	0.28513542D+00
5	0.38635863D-01	0.82495673D-04	0.21501707D+00

CHAPTER 4

COLLISION-INDUCED ROTATIONAL SCATTERING

In the previous chapter, we considered the collision-induced light scattering by a pair of molecules, neglecting the internal degrees of freedom of the interacting molecules. In this chapter we will consider the way in which higher order polarizabilities can lead to a rotational Raman spectrum from colliding, optically isotropic molecules. The mechanism we shall present is essentially the result of the work done by Buckingham and Tabisz.[1]

To begin, let us consider the form of the interaction of a molecule with an externally applied field $\vec{F}$ and its gradient $\vec{F}'$.[2] The first few multipole moments of the molecule in the applied field are:

$$\mu_\alpha = \mu_\alpha^{(0)} + \alpha_{\alpha\beta} F_\beta + \frac{1}{2} \beta_{\alpha\beta\gamma} F_\beta F_\gamma + \frac{1}{6} \gamma_{\alpha\beta\gamma\delta} F_\beta F_\gamma F_\delta + \cdots + \frac{1}{3} A_{\alpha\beta\gamma} F'_{\beta\gamma} + \frac{1}{15} E_{\alpha\beta\gamma\delta} F''_{\beta\gamma\delta} + \cdots$$

$$\Theta_{\alpha\beta} = \Theta_{\alpha\beta}^{(0)} + A_{\alpha\beta\gamma} F_\gamma + \cdots$$

$$\Omega_{\alpha\beta\gamma} = \Omega_{\alpha\beta\gamma}^{(0)} + E_{\alpha\beta\gamma\delta} F_\delta + \cdots$$

The terms $\mu_\alpha^{(0)}$, $\Theta_{\alpha\beta}^{(0)}$, and $\Omega_{\alpha\beta\gamma}^{(0)}$ represent the permanent dipole, quadrupole and octopole moments of the molecule. The term $\alpha_{\alpha\beta}$ is the usual linear dipole polarizability, while the terms $\beta_{\alpha\beta\gamma}$, $\gamma_{\alpha\beta\gamma\delta}$, ..., which make contributions to the induced dipole moment μ_α that are non-linear in the applied field, are called the hyperpolarizabilities. Just

as the dipole polarizability tensor $\alpha_{\alpha\beta} = \underset{\sim}{\alpha}$ determines the dipole induced in the molecule by the applied field $\vec{F}$, the quadrupole and octopole induced by the field $\vec{F}$ are determined by the tensors $A_{\alpha\beta\gamma} = \underset{\sim}{A}$ and $E_{\alpha\beta\gamma\delta} = \underset{\sim}{E}$. The induced dipole also depends on the gradients of the field, $F'_{\beta\gamma} = \frac{\partial}{\partial x_\beta} F_\gamma$ and $F''_{\beta\gamma\delta} = \frac{\partial^2}{\partial x_\beta \partial x_\gamma} F_\delta$, through the same two tensors. The tensor $\underset{\sim}{A}$ is called the dipole-quadrupole polarizability and $\underset{\sim}{E}$ is called the dipole-octopole polarizability.[3] The multipole expansion, in fact, extends to all orders in the applied field and its gradients.

In our previous discussion of light scattering we only considered the terms $\alpha_{\alpha\beta} F_\beta$, but now we will consider the terms of the multipole expansion including the permanent moments and the tensors $\underset{\sim}{\alpha}$, $\underset{\sim}{A}$ and $\underset{\sim}{E}$. But we are only considering collision-induced scattering from optically isotropic molecules and this results in some simplifications. For molecules of tetrahedral or higher symmetry the polarizability tensor is completely isotropic, $\alpha_{\alpha\beta} = \alpha\, \delta_{\alpha\beta}$. For tetrahedral molecules the first non-vanishing permanent multipole moment is the octopole moment and for octahedral molecules it is the hexadecapole moment. For molecules with a center of symmetry (such as octahedral molecules) the tensor $\underset{\sim}{A}$ also vanishes. Thus the multipole moments of tetrahedral and octahedral molecules in the applied field $\vec{F}$, to our order of approximation, will be:

$$\mu_\alpha = \alpha\, \delta_{\alpha\beta}\, F_\beta + \frac{1}{3}\, A_{\alpha\beta\gamma}\, F'_{\beta\gamma} + \frac{1}{15}\, E_{\alpha\beta\gamma\delta}\, F''_{\beta\gamma\delta}$$

$$\Theta_{\alpha\beta} = A_{\alpha\beta\gamma}\, F_\gamma$$

$$\Omega_{\alpha\beta\gamma} = \Omega^{(0)}_{\alpha\beta\gamma} + E_{\alpha\beta\gamma\delta}\, F_\delta$$

for a tetrahedral molecule, and :

$$\mu_\alpha = \alpha\, \delta_{\alpha\beta}\, F_\beta + \frac{1}{15}\, E_{\alpha\beta\gamma\delta}\, F''_{\beta\gamma\delta}$$

$$\Omega_{\alpha\beta\gamma} = E_{\alpha\beta\gamma\delta}\, F_\delta$$

for an octahedral molecule.

Now let us consider the interaction of a pair of identical tetrahedral molecules with a uniform externally applied field $\vec{F}$. The multipole moments induced on the first molecule will be:

$$^{(1)}\mu_\alpha = {}^{(1)}\alpha\, \delta_{\alpha\beta}\, F_\beta$$

$$^{(1)}\Theta_{\alpha\beta} = {}^{(1)}A_{\alpha\beta\gamma}\, F_\gamma$$

$$^{(1)}\Omega_{\alpha\beta\gamma} = {}^{(1)}\Omega^{(0)}_{\alpha\beta\gamma} + {}^{(1)}E_{\alpha\beta\gamma\delta}\, F_\delta \quad .$$

Just as in the DID model previously discussed, the fields of the induced dipole, quadrupole and octopole on the first molecule will induce an additional dipole moment on the second molecule. Ignoring the octopole terms the total induced dipole on the second molecule will be:

$$^{(2)}\mu_\alpha = {}^{(2)}\alpha\, F_\alpha + {}^{(2)}\alpha \left(T_{\alpha\beta}\, {}^{(1)}\mu_\beta - \frac{1}{3}\, T_{\alpha\beta\gamma}\, {}^{(1)}\Theta_{\beta\gamma} \right) + \frac{1}{3}\, {}^{(2)}A_{\alpha\beta\gamma} \left(T_{\beta\gamma\delta}\, {}^{(1)}\mu_\delta - \frac{1}{3}\, T_{\beta\gamma\delta\varepsilon}\, {}^{(1)}\Theta_{\delta\varepsilon} \right)$$

where $T_{\alpha\beta\gamma} = \nabla_\alpha \nabla_\beta \nabla_\gamma \left(\frac{1}{R}\right)$.

For example:

$$T_{\alpha\beta} = \frac{\partial}{\partial R_\alpha}\frac{\partial}{\partial R_\beta}\left(\frac{1}{R}\right) = \left(3R_\alpha R_\beta - R^2\,\delta_{\alpha\beta}\right)R^{-5}$$

and $T_{\alpha\beta}\,{}^{(1)}\mu_\beta$ is the field at the site of molecule 2 due to the dipole ${}^{(1)}\mu_\beta$ on molecule 1. Similarily, the total induced dipole on molecule 1, to first order, will be

$$\begin{aligned}{}^{(1)}\mu_\alpha = {}&{}^{(1)}\alpha\, F_\alpha + {}^{(1)}\alpha\left(T_{\alpha\beta}\,{}^{(2)}\mu_\beta + \frac{1}{3}T_{\alpha\beta\gamma}\,{}^{(2)}\Theta_{\beta\gamma}\right)\\ &- \frac{1}{3}\,{}^{(1)}A_{\alpha\beta\gamma}\left(T_{\beta\gamma\delta}\,{}^{(2)}\mu_\delta + \frac{1}{3}T_{\beta\gamma\delta\varepsilon}\,{}^{(2)}\Theta_{\delta\varepsilon}\right).\end{aligned}$$

The pair polarizability is given, to lowest order, by:

$$\begin{aligned}{}^{(1,2)}\alpha_{\alpha\beta} = {}^{(1,2)}\alpha_{\beta\alpha} &= \frac{\partial}{\partial F_\beta}\left({}^{(1)}\mu_\alpha + {}^{(2)}\mu_\alpha\right)\\ &= 2\alpha\,\delta_{\alpha\beta} + 2\alpha^2 T_{\alpha\beta} + \frac{1}{3}\alpha\, T_{\alpha\gamma\delta}\left({}^{(2)}A_{\beta\gamma\delta} - {}^{(1)}A_{\beta\gamma\delta}\right)\\ &\quad + \frac{1}{3}\alpha\, T_{\beta\gamma\delta}\left({}^{(2)}A_{\alpha\gamma\delta} - {}^{(1)}A_{\alpha\gamma\delta}\right)\\ &\quad - \frac{1}{9}\,T_{\gamma\delta\varepsilon\eta}\left({}^{(1)}A_{\alpha\gamma\delta}\,{}^{(2)}A_{\beta\varepsilon\eta} + {}^{(2)}A_{\alpha\gamma\delta}\,{}^{(1)}A_{\beta\varepsilon\eta}\right).\end{aligned}$$

If the octopole terms were included, terms involving $\underset{\sim}{E}$ would appear in the expression. The permanent octopole moment would however, only contribute to the polarizability through terms involving the hyperpolarizabilities which we have neglected.[4]

4.1 The Scattered Intensity

The polarizability tensor $\underset{\sim}{A}$ of a tetrahedral molecule is completely specified by the orientation of the molecule and by a single parameter A. The usual molecule-fixed reference frame has the central

atom at the center of a unit cube with the corner atoms of the tetrahedron at alternate corners of the cube. The orientation of the molecule-fixed reference frame with respect to the space-fixed reference frame is specified by the unit vectors $\vec{i}, \vec{j}, \vec{k}$ which lie along the x, y and z axes of the molecule-fixed frame. The tensor $\underset{\sim}{A}_{ww}$ is given in terms of the components $i_\alpha, j_\alpha, k_\alpha$ as:

$$A_{\alpha\beta\gamma} = A\left[i_\alpha j_\beta k_\gamma + i_\alpha j_\gamma k_\beta + i_\beta j_\gamma k_\alpha + i_\beta j_\alpha k_\gamma + i_\gamma j_\alpha k_\beta + i_\gamma j_\beta k_\alpha\right]$$

The scattered intensity is given as usual by the expression:

$$\frac{d\sigma}{d\Omega} = \left(\frac{\omega_s}{c}\right)^4 \lambda_{s_\alpha} \lambda_\beta \lambda_{s_\gamma} \lambda_\delta \left\langle {}^{(1,2)}\alpha_{\alpha\beta}\, {}^{(1,2)}\alpha_{\gamma\delta}\right\rangle$$

where the average $\langle \cdots \rangle$ now extends over all orientations of each molecule individually and over all orientations of one molecule relative to the other. Substituting the ${}^{(1,2)}\alpha_{\alpha\beta}$ derived above and performing the average we obtain the following results:

$$\left\langle \alpha^2_{VV} \right\rangle = \left[(2\alpha)^2 + \frac{4}{3}\left(\frac{36}{15}\right)\alpha^4 R^{-6} + 2\left(\frac{37}{9}\right)\left(\frac{48}{35}\right)(\alpha A)^2 R^{-8} + \left(\frac{1494}{983}\right)\left(\frac{62912}{4725}\right) A^4 R^{-10} \right]$$

$$\left\langle \alpha^2_{VV} \right\rangle = \left[\left(\frac{36}{15}\right)\alpha^4 R^{-6} + 2\left(\frac{48}{35}\right)(\alpha A)^2 R^{-8} + \frac{62912}{4725} A^4 R^{-10} \right] .$$

The term in R^{-6} is just the first order DID result.

The tensor $\underset{\sim}{E}_{ww}$ is also specified by a single parameter E for tetrahedral and octahedral molecules. Including terms involving $\underset{\sim}{E}_{ww}$ in the pair polarizability results in the following additional contributions to the mean square polarizability:

$$\langle \alpha_{VV}^2 \rangle = 2\left(\frac{52}{11}\right)\left(\frac{11}{9}\right)(\alpha E)^2 R^{-10} + K_1 E^4 R^{-12}$$

$$\langle \alpha_{VH}^2 \rangle = 2\left(\frac{11}{9}\right)(\alpha E)^2 R^{-10} + K_2 E^4 R^{-12} \quad .$$

The coefficients of the terms in E^4 have not yet been determined but we may estimate that the ratio of the coefficients of the E^4 and $(\alpha E)^2$ terms is the same as the ratio of the coefficients of the A^4 and $(\alpha A)^2$ terms. By this means we arrive at the estimates $K_1 = 21$ and $K_2 = 12$.

In addition to the orientational average, we must average over the intermolecular separation R. This average will have just the same form as the R-integral in our expression for the zeroth moment:

$$\langle f(R) \rangle = 4\pi \int_0^\infty dR\, R^2\, e^{-\phi(R)/kT}\, f(R) \quad .$$

A Lennard-Jones 6-12 potential with $\epsilon/kT = 0.52$ is fairly representative of the intermolecular potential for the molecules we have studied. With this substitution, the integrals may be evaluated to give the following result for $\langle \alpha_{VH}^2 \rangle$:

$$\langle \alpha_{VH}^2 \rangle = 4\pi \left[\left(\frac{36}{15}\right) \frac{\alpha^4}{\sigma^3} (0.495) + 2\left(\frac{48}{35}\right) \frac{(\alpha A)^2}{\sigma^5} (0.334) \right.$$

$$+ \left(\frac{62912}{4725}\right)\frac{A^4}{\sigma^7}(0.261) + 2\left(\frac{11}{9}\right)\frac{(\alpha E)^2}{\sigma^7}(0.261) + 12\frac{E^4}{\sigma^9}(0.200) \Big] .$$

The values of A and E may be approximated using the bond polarizability model in which the molecule XY_n is represented by n anisotropically polarizable groups, each one symmetric about its XY bond direction.[5] The results of this model are:

$$A = \frac{4}{\sqrt{3}}(\alpha_{\parallel} - \alpha_{\perp})\, R_o \qquad E = -\frac{8}{3}(\alpha_{\parallel} - \alpha_{\perp})\, R_o^2$$

for tetrahedral molecules and:

$$E = 6(\alpha_{\parallel} - \alpha_{\perp})\, R_o^2$$

for octahedral molecules, where $(\alpha_{\parallel} - \alpha_{\perp})$ is the polarizability anisotropy of Y and R_o is its distance from the center of the molecule. Based on this model, the following estimates may be made:[6]

$A_{CH_4} = 1.2\ \text{Å}^4$ $\qquad$ $E_{CH_4} = -1.2\ \text{Å}^5$

$A_{CF_4} = 2.2\ \text{Å}^4$ $\qquad$ $E_{CF_4} = -2.2\ \text{Å}^5$

$A_{SF_6} = 0\ \text{Å}^4$ $\qquad$ $E_{SF_6} = 20\ \text{Å}^5$

Using the values $\sigma = 3.82$ Å and $\alpha = 2.633\ \text{Å}^3$, we may calculate the relative size of the various terms in $\langle \alpha_{VH}^2 \rangle$ for CH_4. Thus:

$$\langle \alpha_{VH}^2 \rangle = 4\pi \Big[1.02 + 1.12 \times 10^{-2} + 6.1 \times 10^{-4} + 5.4 \times 10^{-4} + 3.2 \times 10^{-5}\Big],$$

where the terms in the sum involve α^4, $(\alpha A)^2$, A^4, $(\alpha E)^2$ and E^4, in that order. The contribution of the terms involving A and E to the total intensity is small compared to the DID (α^4) contribution, and the contribution due to the tensor $\underset{\sim}{E}$ is much smaller than that due to $\underset{\sim}{A}$.

4.2 The Spectral Distribution

The calculation of the spectral distribution for collision induced rotational scattering is analogous to the quantum mechanical calculation of the spectrum of the diatomic rotor, except that we must now consider the rotational states of the two molecules in the pair. The transition probabilities are given by the matrix elements:

$$\left| \langle J_1', J_2' \mid {}^{(1,2)}\alpha_{\alpha\beta} \mid J_1, J_2 \rangle \right|^2$$

where ${}^{(1,2)}\alpha_{\alpha\beta}$ is the pair polarizability and J_i, J_i' represent the initial and final state of the i-th molecule. The rotational state J has the normalized symmetric top wavefunction

$$\sqrt{\frac{2J+1}{8\pi^2}}\ D^{J*}_{mK}(\Omega)$$

where $D^J_{mK}(\Omega)$ is the Wigner rotation matrix.[7] The quantum numbers m and K are associated with the projection of the angular momentum J on the space-fixed and molecule-fixed z-axes, respectively. The Euler angles relating the space-fixed and molecule-fixed frames are

represented by Ω. To evaluate the matrix elements, the pair polarizability is written in spherical tensor form. For example, the contribution:

$$\frac{1}{3}\alpha T_{\alpha\gamma\delta}\left({}^{(2)}A_{\beta\gamma\delta} - {}^{(1)}A_{\beta\gamma\delta}\right) + \frac{1}{3}\alpha T_{\beta\gamma\delta}\left({}^{(2)}A_{\alpha\gamma\delta} - {}^{(1)}A_{\alpha\gamma\delta}\right)$$

gives rise to a matrix element of the form:

$$\langle J_1' J_2' \mid D^{3*}_{m2}(\Omega_j) - D^{3*}_{m,-2}(\Omega_j) \mid J_1 J_2 \rangle$$

from which one obtains the selection rules:

$$\Delta J_i = 0 \quad \Delta J_j = 0,\pm1,\pm2,\pm3 \quad J_j+J_j' \geqslant 3 \ .$$

These transitions involve changes of rotational state for one or the other of the molecules in the pair, since this term of the polarizability involves the tensor $\underset{\sim}{A}$ of either one or the other of the molecules. Similarily, the term in the pair polarizability involving products ${}^{(1)}\underset{\sim}{A}\ {}^{(2)}\underset{\sim}{A}$ will give rise to double rotational transitions since it contains the tensors $\underset{\sim}{A}$ for both molecules. Proceeding in this fashion we may obtain the selection rules for transitions corresponding to each term in the pair polarizability. The selection rules corresponding to the various terms in the mean square polarizability $\langle\alpha^2\rangle$ are:

$$\Delta J_i = 0 \quad \Delta J_j = 0,\pm1,\pm2,\pm3 \quad J_j+J_j' \geqslant 3$$

for the term in $(\alpha A)^2$,

$$\Delta J_i = 0,\pm1,\pm2,\pm3 \quad \Delta J_j = 0,\pm1,\pm2,\pm3 \quad J_i+J_i' \geqslant 3 \quad J_j+J_j' \geqslant 3$$

for the term in A^4 ,

$$\Delta J_i = 0 \qquad \Delta J_j = 0,\pm1,\pm2,\pm3,\pm4 \qquad J_j+J_j' \geqslant 4$$

for the term in $(\alpha E)^2$, and

$$\Delta J_i = 0,\pm1,\pm2,\pm3,\pm4 \qquad \Delta J_j = 0,\pm1,\pm2,\pm3,\pm4 \qquad J_i+J_i' \geqslant 4 \qquad J_j+J_j' \geqslant 4$$

for the term in E^4 .

The intensity of the transition $J_1, J_2 \rightarrow J_1', J_2'$ is proportional to:

$$\Gamma(J_1, J_2, J_1', J_2') = \left(\frac{\omega_o \omega_s^3}{c^4}\right) (2J_1'+1)(2J_1+1)(2J_2'+1)(2J_2+1)$$

$$\times \exp(-E(J_1)/kT) \exp(-E(J_2)/kT)$$

where $\hbar\omega_R = \hbar\omega_o - \left[E(J_1') - E(J_1) + E(J_2') - E(J_2)\right]$

and $E(J) = J(J+1)\hbar B$.

To obtain the spectral distribution from the selection rules and the expression for $\Gamma(J_1, J_2, J_1', J_2')$, we compute the position and relative intensity of all the spectral lines arising from a given term of $\langle \alpha^2 \rangle$, and then normalize the intensities of these lines so that the sum of their intensities agrees with results obtained in section 4.1 for total intensity. Finally, we must remember that because of the dependence of the pair polarizability on the intermolecular separation R, each line will be broadened by the translational motion of the molecules in the pair. The pair polarizability contributions governing the rotational scattering fall off faster with R than does the DID

contribution, so that the spectral width of each rotational "line" will be at least as great as the width of the DID spectrum.

The collision induced rotational spectrum for CH_4 may be calculated using the same polarizability parameters as were used in the preceeding section for calculating the total intensity. The spectral lines are broadened to the same width as the DID spectrum. The spectra due to each of the terms $(\alpha A)^2$, A^4, $(\alpha E)^2$ and E^4 are graphed in Figure 4-1. The sum of these contributions gives the total collision induced rotational spectrum for CH_4 and is plotted in Figure 4-2.

While only classical multipole interactions have been considered in computing the collision-induced rotational scattering (CIRS) spectrum all the additional mechanisms discussed in the context of the DID model in section 3-1 may modify the molecular pair polarizability. A short range angle dependent interaction of the electron overlap type, for example, would result in the same selection rules as the multipole interactions, since the selection rules are essentially determined by the molecular symmetry. The spectral distribution of the CIRS spectrum is in turn essentially determined by the selection rules. Additional contributions to the pair polarizability would chiefly affect the total intensity and only secondarily affect the spectral distribution of the CIRS spectrum.

FIGURE 4 - 1

The CIRS Spectra of CH_4 Due to the Terms $(\alpha A)^2$, A^4, $(\alpha E)^2$ and E^4

The CIRS spectra due to the terms $(\alpha A)^2$ (solid line), A^4 (dashed line), $(\alpha E)^2$ (solid line) and E^4 (dashed line) produce successively smaller contributions to the total CIRS spectrum. As usual, the intensity scale is in units of CIS scattering cross section per unit frequency interval (1 cm^{-1}) divide by the scattering cross section of the H_2 S(1) transition under the same conditions, when both gases (H_2 and CH_4) are at unit density (1 mole/liter.) The individual lines of the CIRS spectra have been broadend using the function $\exp(- \frac{|\omega|}{\omega_c})$, where $\omega_c = 15.5$ cm^{-1} is the same as the decay constant in the roughly exponential translational CIS spectrum. The values $A = 1.2$ $\mathring{A}^4$, $E = 1.2$ $\mathring{A}^5$ and $B = 5.25$ cm^{-1} have been used in computing the spectra. The first 20 rotational states have been considered in computing the spectrum, and the number of allowed transitions originating from these 20 states are:

single A transitions	2561
double A transitions	16385
single E transitions	3201
double E transitions	25601

(For CF_4 and SF_6 at least the first 100 and 140 states, respectively, must be considered in computing the CIRS spectrum. The number of transitions involved is prohibitive unless only every 5th of 7th state is considered, since the number of possible double rotational transitions increases as the square of the number of states included.)

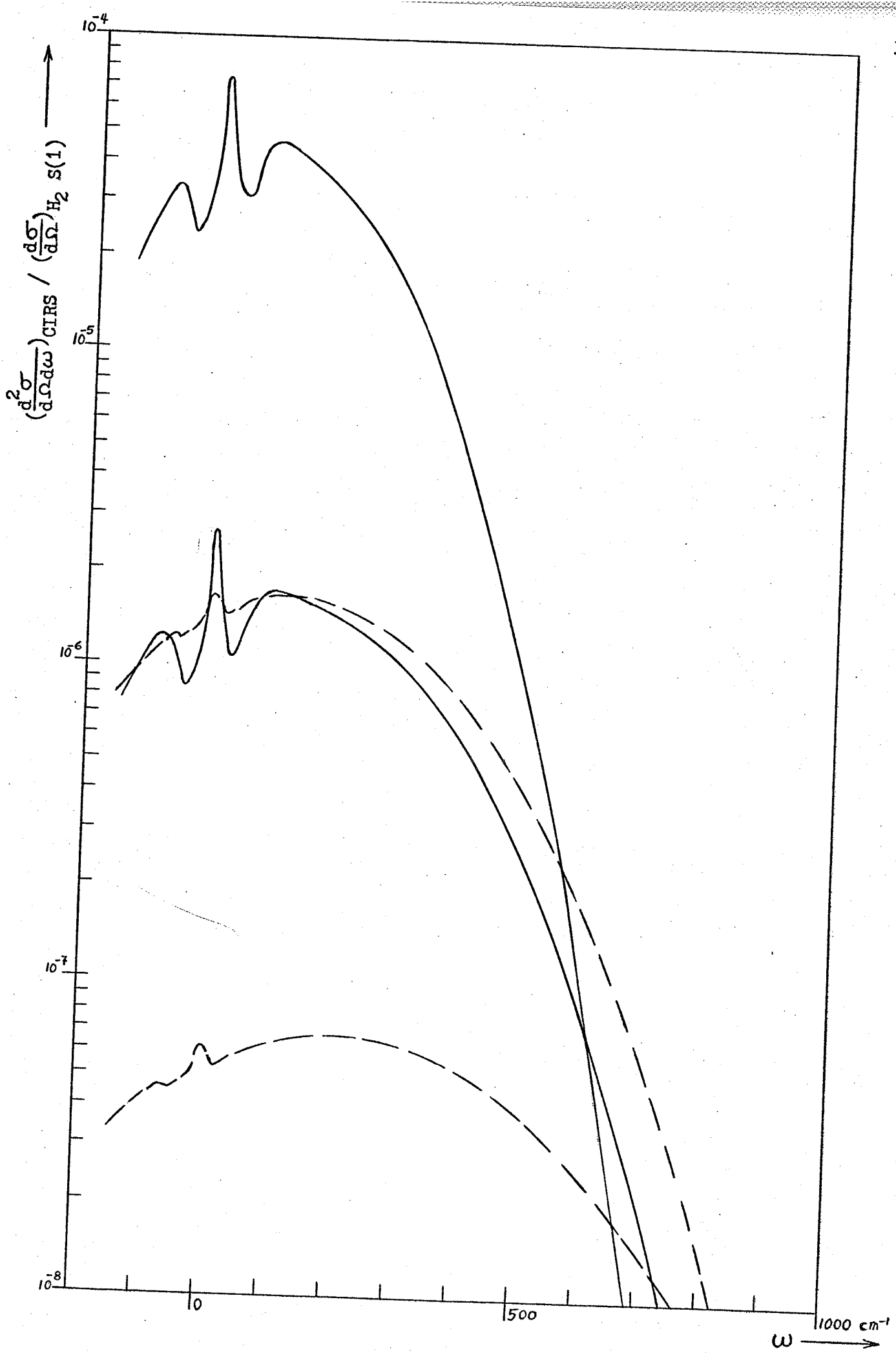
10^{-4}
10^{-5}
10^{-6}
10^{-7}
10^{-8}
$\left(\frac{d^2\sigma}{d\Omega d\omega}\right)_{CIRS} / \left(\frac{d\sigma}{d\Omega}\right)_{H_2\ S(1)}$
0
500
1000 cm^{-1}
ω

FIGURE 4 - 2

The CIRS Spectrum of CH_4

The four components of Figure 4 - 1 have been summed to give the total CIRS spectrum of CH_4. The spectrum is determined chiefly by the A transitions, even in the far tail, for the values of A and E which we have assumed.

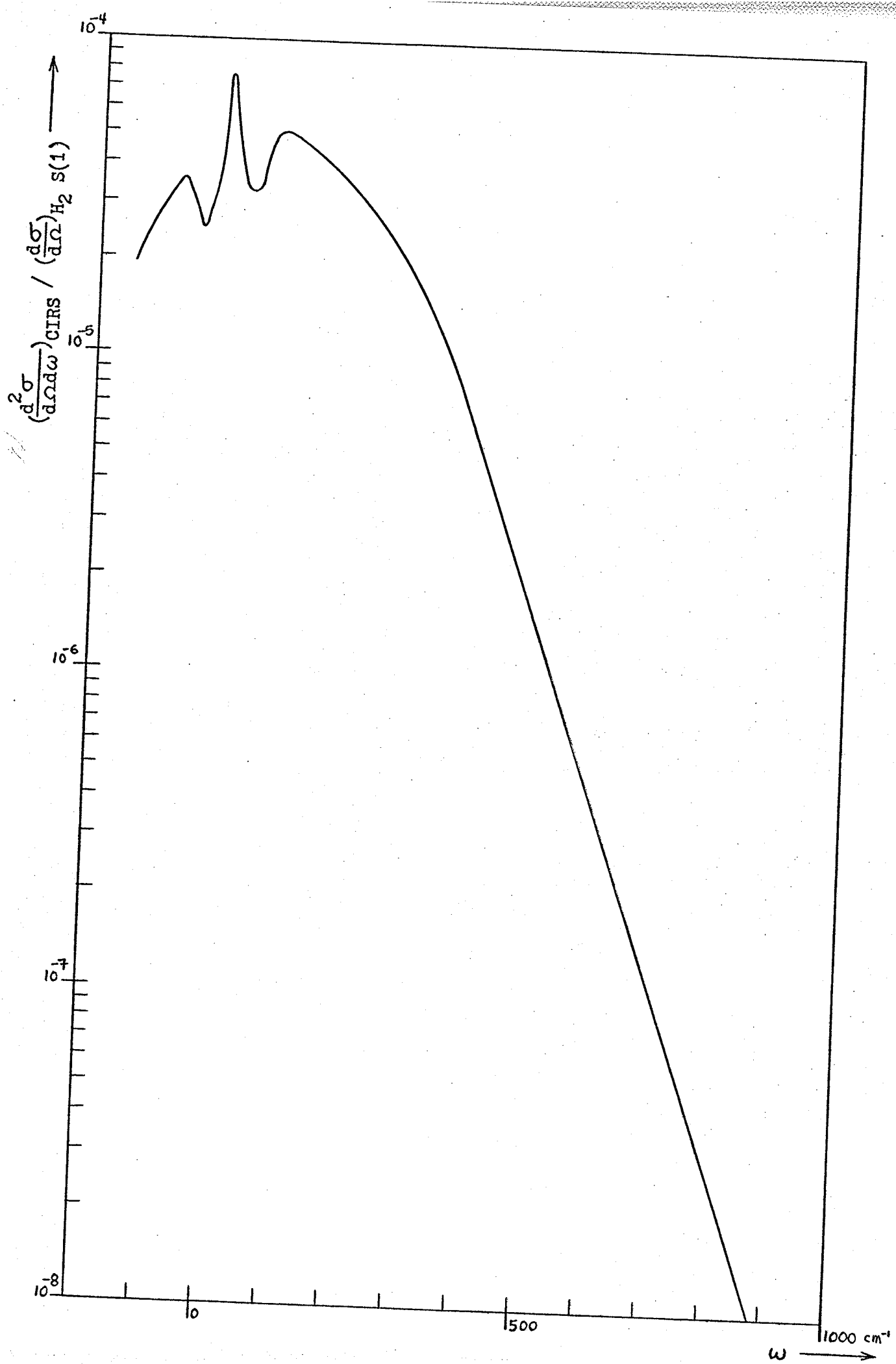
10^{-4}
10^{-5}
10^{-6}
10^{-7}
10^{-8}
$\left(\frac{d^2\sigma}{d\Omega d\omega}\right)_{CIRS} / \left(\frac{d\sigma}{d\Omega}\right)_{H_2\ S(1)}$
0
500
1000 cm^{-1}
ω

NOTES AND REFERENCES

1. The theory of collision-induced rotational Raman scattering is presented in:

   A. D. Buckingham, G. C. Tabisz, Optics Letters 1, 220 (1977)

   A. D. Buckingham, G. C. Tabisz, Mol. Phys. 36, 583 (1978)

2. A. D. Buckingham, Adv. Chem. Phys. 12, 107 (1967)

3. The tensors $\underset{\sim}{\alpha}$, $\underset{\sim}{A}$ and $\underset{\sim}{E}$ are termed the dipole-dipole, dipole-quadrupole and dipole-octopole polarizabilities because the quantum mechanical expressions for them involve $\langle r_\alpha \rangle \langle r_\beta \rangle$, $\langle r_\alpha \rangle \langle r_\beta\, r_\gamma \rangle$ and $\langle r_\alpha \rangle \langle r_\beta\, r_\gamma\, r_\delta \rangle$, respectively; $\langle r_\alpha \rangle$, $\langle r_\alpha\, r_\beta \rangle$ and $\langle r_\alpha\, r_\beta\, r_\gamma \rangle$ are the dipole, quadrupole and octopole transition moments.

4. Light scattering arising from the interaction of the hyper-polarizabilities with the permanent multipole moments has been shown to be negligible in:

   A. D. Buckingham, G. C. Tabisz, Optics Letters 1, 220 (1977).

5. A. D. Buckingham, Adv. Chem. Phys. 12, 107 (1967)

6. A. D. Buckingham, G. C. Tabisz, Mol. Phys. 36, 583 (1978)

7. For example, see Chapter 17 of:

   G. Baym, Lectures on Quantum Mechanics, Benjamin, London, 1973.

CHAPTER 5

THE EXPERIMENT AND DATA ANALYSIS

5.1 The Experiment Design

The experiment consists of sending a beam of light, generated by a laser, through a sample of gas and measuring the intensity and spectral distribution of the light scattered at right angles to the beam direction using a diffraction grating spectrometer — the plan view of the apparatus is presented in Figure 5-1. Since the light is only weakly scattered by the sample, the design of the experiment is mainly concerned with ensuring that the scattered light is bright enough to measure. To understand why the scattered light signal is so weak, we will follow the path of the light in a typical experiment, starting at the laser.

The beam from the Ar - ion laser is directed to the sample cell by means of a series of glass prisms. The polarization of the beam is rotated to the correct orientation and any extraneous polarization compoments are removed by a combination of half-wave plate and Nicol prism polarizer.[1] Finally, the beam is brought to a focus inside the sample cell by mean of a lens. By the time the beam has been transported, polarized and focussed into the cell, it has traversed 20 air-glass interfaces. Not withstanding the fact that all the surfaces have been

FIGURE 5 - 1

Top View of the Experiment Drawn 1/12 Full Scale

1) The other parts of the apparatus are fastened to the surface of a honey-comb core steel table (8 inches thick by 4 feet by 8 feet, weighing about 400 kg). The surface of the table has threaded holes on a 1 inch square gird which facilitates mounting of parts. The table may be floated on 8 inner tubes for vibration isolation and provides a rigid base for all the other components.

2) The light beam scattered by the sample is generated by an Ar-ion laser (built by Coherent Radiation.) The laser has a prism in the resonant cavity to force operation on only one line, usually 4880 Å, and the spectral width is about 0.1 cm^{-1}. The maximum output is about 1 Watt at 30 Amperes tube current (the power supply is mounted underneath the table.) Part of the beam is split off at (2b) and used to monitor and regulate the output of the laser.

3) The beam is directed to the other end of the table and steered by prism (3a) and two prisms at (3b) which are mounted on orthogonal translation stages.

4) A half-wave plate is used to rotate the plane of polarization of the beam, followed by a Nichol prism which removes the undesired polarization component. These parts are mounted on a 1.0 meter triangular steel optical bench.

5) The sample cell assembly is mounted on the optical bench at (5a). The beam is reflected vertically upward by a prism and is focussed by a 10 cm focal length lens placed just below the cell. The equipment for filling the sample cell is contained in the area (5b).

6) The collection optics are mounted on a 0.5 meter optical bench and image the source region onto the entrance slit of the spectrometer. The 20 cm focal length collection and focussing lenses are mounted on

FIGURE 5 - 1 continued

translating stages to allow the image to be focussed and steered. Filters and polarizers may be placed in the collimated beam between the two lenses, as required.

7) The spectrum is scanned by a tandem Czerny-Turner (subtractive dispersion mode) monochromator built by Jarrell-Ash. The two monochromators are mounted one above the other and the light path in the second monochromator is the same as in the first, but in the opposite direction. The focal length of the monochromators is 1.0 m and with 102 mm square gratings of 1180 lines/mm (blazed at 4000 Å) the diffraction limited resolution is about 0.3 cm^{-1}. The light path goes from the (adjustable) entrance slit (7a) to the collimator mirror (7b), the grating (7c), the camera mirror (7d) and then is reflected vertically downward through the intermediate slit (7e). Thereafter, the light retraces its path in the lower monochromator until it is finally deflected to the exit slit (7i). The spectrum is scanned by rotating the gratings about a vertical axis using a stepping motor and a cosecant-bar linkage.

8) The light emerging from the double monochromator is focussed on to the photocathode of an RCA C31034 photomultiplier tube (the combination of the double monochromator and the detector is called the spectrometer) which is mounted in a refrigerated housing (8a). The refrigerator compressor, condensor and temperature controller (evaporator pressure regulator) are mounted at (8b). The C31034 PMT has a (negative electron affinity) GaAs photocathode with a high and relatively constant quantum efficiency throughout the visible spectrum.

9) The experiment is run from this position; the controls for the laser, the spectrometer and the elecronics are all within reach.

10) The electronics are mounted in a standard 20 inch wide rack. They consist of an amplifier and single channel analyzer for processing the PMT pulses, a multichannel scaler which counts the pulses due to photons at the selected frequency shift and a clock for synchronously advancing the stepping drive of the spectrometer and the address of the multichannel scaler.

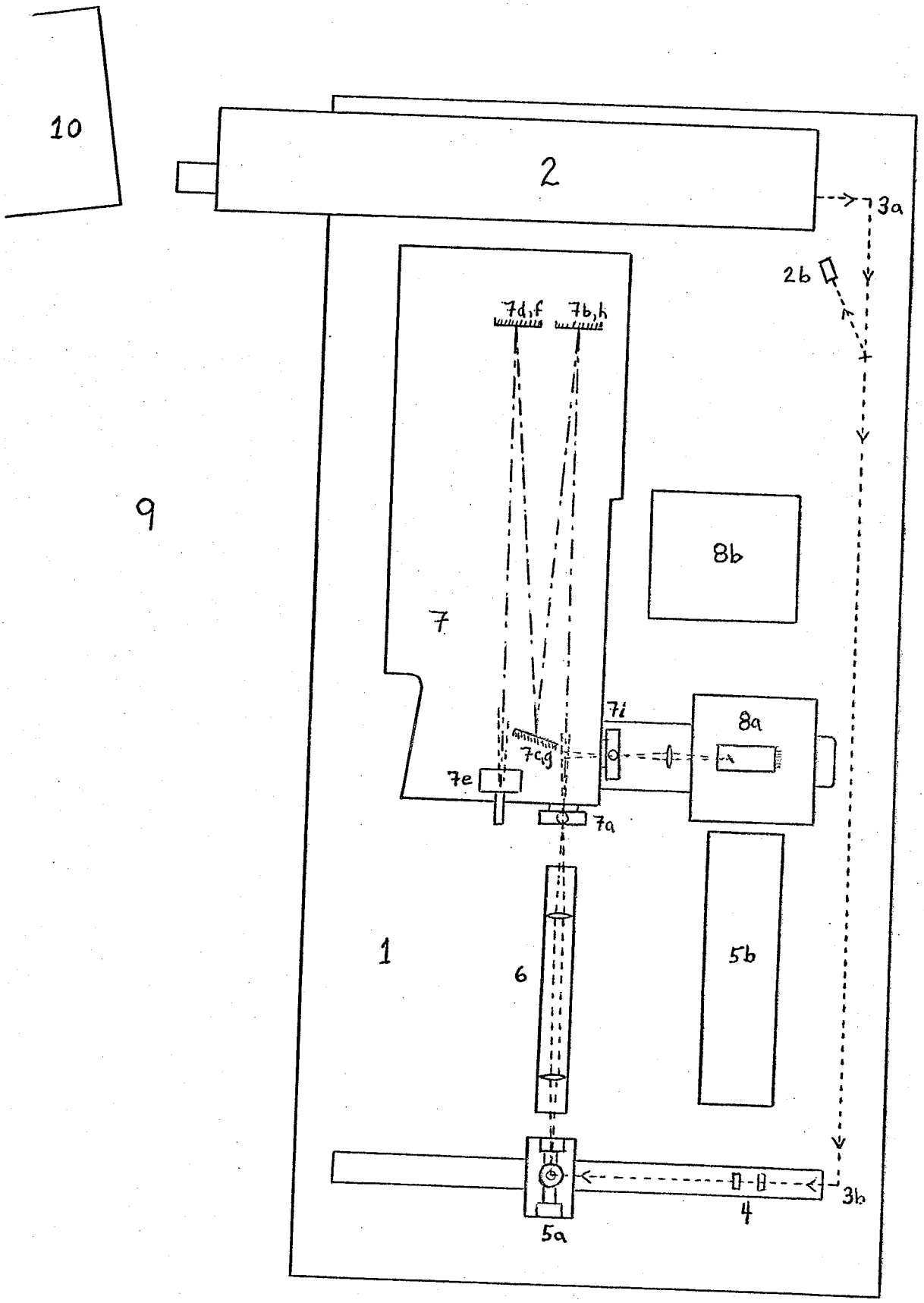
10
2
3a
2b
7d,f
7b,h
9
8b
7
7i
8a
7cg
7e
7a
1
6
5b
3b
4
5a

anti-reflection coated, the intensity of the beam is only one half of its original value by the time the beam has entered the sample — the sample is typically illumimated by a power of 300 mW or 7.5×10^{17} photons/sec at a wavelength of 4880 Å.

Focussing the beam serves to match the width of the scattering region to the width of the entrance slit of the spectrometer. Diffraction makes the focal region of the beam take the form of a cylinder. The diameter and length of the diffraction limited focal cylinder for a 3 mm diameter beam focussed by a 10 cm focal length lens will be:

$$d = 2.4 \lambda \left(\frac{F}{D}\right) = 0.040 \text{ mm}$$

$$l = 16 \lambda \left(\frac{F}{D}\right)^2 = 9 \text{ mm}$$

In fact, the focus is nowhere near being diffraction limited because of the lens aberrations and the wavefront deformation caused by passage through 20 air-glass interfaces and oblique reflection at 4 surfaces. The actual dimensions of the focal cylinder are about 0.2 mm diameter and 10 mm long.[2]

The light scattered by the gas in the focal region is collected by a lens and an image of the source cylinder is formed (with unit magnification) on the entrance slit of the spectrometer. The wavelength dispersion of the spectrometer in the plane of the entrance slit is $\frac{d\lambda}{ds} = 8.26$ Å/mm; the frequency dispersion is $\frac{d\omega}{ds} = -\left(\frac{d\lambda}{ds}\right)\omega^2 = 33.04 \text{ cm}^{-1}/\text{mm} \rightarrow (30.3 \ \mu\text{m/cm}^{-1})$ at $\lambda = 4880$ Å. Thus, a spectral slit width of 3.0 cm^{-1}

corresponds to a physical slit width of 0.090 mm, which is about half the width of the image of the source cylinder. Since we will not use a spectral slit width greater than 3.0 cm^{-1}, the entrance slit will always be fully illuminated but at least half of the light will be wasted. Having the slit narrower than the spot of light does reduce the sensitivity of the apparatus to misalignment of the collection optics which partially compensates for the lost light.

The windows of the sample cell limit the field of view to at most a diameter of 8 mm in the plane of the focussed beam and the edges of this field will be almost totally vignetted. A 5 mm diameter, unvignetted field of view is selected by restricting the height of the entrance slit to 5 mm.

The solid angle over which light is collected is also limited by the spectrometer. The aperture stop of the system is the 10.2 cm square diffraction grating, oriented at 12.5° to the incident light for $\lambda = 4880$ Å. The focal length of the collimator mirror is 100 cm, so that the aperture of the system is $(0.102)^2(0.98) = 1.02 \times 10^{-2}$ steradian (or f/8.8 when expressed as an f/no.)

Now let us calculate how much light is collected by the spectrometer in our experiment. The probability that a photon travelling a unit distance in the sample will be scattered into a unit solid angle about a specified direction is given by the scattering cross section:

$$\left(\frac{d\sigma}{d\Omega}\right)_{VH} = \left(\frac{\omega_s}{c}\right)^4 \frac{1}{15} \left(\frac{\rho}{2}\right)^2 \phi^{(0)} \quad .$$

For our typical experiment we will take the sample to be Ar at a density of 1.5 mole/liter (about 35 atmospheres ar room temperature.) With the value $\phi^{(0)} = 51.5$ Å^9, and allowing for a 10 percent reduction in scattered intensity because of three-body collisions, the cross section per unit volume is:

$$\left(\frac{d\sigma}{d\Omega}\right)_{VH} = \left(\frac{2\pi}{4.88 \times 10^{-7}\,m}\right)^4 \frac{1}{15}\,\frac{1}{2}\left(\frac{1.5(602 \times 10^{23})}{10^{-3}\,m^3}\right)^2 (0.9)(51.5 \times 10^{-90}\,m^9)$$

$$= 3.4 \times 10^{-8}\ m^{-1}\ \text{sterad}^{-1}$$

Taking into account that two independent polarizations (HV and HH) are being observed and that the source image is twice as wide as the opening of the entrance slit, the number of photons which may be collected is

$$2\left(\frac{1}{2}\right)(3.4 \times 10^{-8}\ m^{-1}\ \text{sterad}^{-1})(5 \times 10^{-3}\,m)(1.02 \times 10^{-2}\,\text{sterad})$$

$$\times\ (7.5 \times 10^{17}\ \text{photons/sec}) \quad = \quad 1.3 \times 10^{6}\ \text{photons/sec}$$

However, not all the photons which enter the spectrometer will eventually be detected. After being scattered, each photon must traverse 12 air-glass interfaces (with an average transmission of 98 percent), be reflected from 8 aluminized mirrors (with an average reflectivity of 85 percent) 2 gratings (with individual efficiencies of 78 percent), and finally knock an electron out of the photocathode of the detector (with the overall quantum efficiency for the photocathode and the signal processing electronics being 13 percent) before it is actually detected. The overall detection efficiency of the spectrometer is just:

$(0.98)^{12}\ (0.85)^{8}\ (0.78)^{2}\ (0.13) = 0.014$ count/photon, so that collecting 1.3×10^{6} photons/sec allows us to detect only $(1.4 \times 10^{-2}) \times (1.3 \times 10^{6}) = 1.8 \times 10^{4}$ counts/sec.

Our original intent was to measure the spectral distribution of the scattered light. For small frequency shifts, the Ar collision induced spectrum will have the approximate distribution $I(\omega) = A \exp(-|\omega|/12\ \mathrm{cm}^{-1})$, so that fraction of the photons which will lie within the $3.0\ \mathrm{cm}^{-1}$ pass band of the spectrometer is approximately:

$$\left(\frac{3\mathrm{cm}^{-1}}{12\mathrm{cm}^{-1}}\right) \frac{1}{2} \exp(-|\omega|/12\ \mathrm{cm}^{-1}) \quad .$$

The actual spectrum varies more slowly with ω than the exponential, both for $\omega < 5\ \mathrm{cm}^{-1}$ and for large frequency shifts. Taking into account the spectral distribution and the band pass, we find that the signal at the peak of the spectrum is 1600 counts/sec while at a frequency shift of $120\ \mathrm{cm}^{-1}$ the signal is only 0.6 count/sec. We may note that the background count rate of the photomultiplier tube used to detect the photons is 0.6 count/sec.[3] Thus, the accuracy of spectral measurements at large frequency shifts will be limited by the noise in the background count-rate and by counting statistics for the signal photons (since the photons arrive randomly in time, the uncertainty in the number of photons, N, which will be counted in a fixed time interval is $N^{\frac{1}{2}}$.) It is for this reason that maximizing the scattered light signal is one of the main design objectives in the experiment.

Low frequency spectral measurements meet with a different problem, whose solution is incompatible with the objective of maximizing the signal at large frequency shifts. The problem is that, superimposed on the CIS spectrum at zero frequency shift, there is a strong, narrow line due to so-called "stray" light, which originates from Rayleigh scattering and from light scattering by dust particles. First let us consider the Rayleigh scattering cross section of our Ar gas sample:

$$\left(\frac{d\sigma}{d\Omega}\right)_{VV} = \left(\frac{\omega_s}{c}\right)^4 \rho\, \alpha^2 = (2.8 \times 10^{28}\ m^{-4})(6.02 \times 10^{26}\ m^{-3}) \times (1.642 \times 10^{-30}\ m^3)^2 = 4.2 \times 10^{-5}\ m^{-1}\ \text{sterad}^{-1}$$

The number of Rayleigh scattered photons is

$$\frac{4.2 \times 10^{-5}}{2(3.4 \times 10^{-8})} = 580$$

times the number of photons of both polarizations in the entire CIS spectrum. With a 3 cm^{-1} spectral slit width, the peak intensity of the Rayleigh line will be 12(580) = 6100 times as great as the peak intensity of the CIS spectrum. The fraction of the incident beam which is Rayleigh scattered from the 5 mm long focal region of the beam is $(4.2 \times 10^{-5}) \times (5 \times 10^{-3}) = 2.1 \times 10^{-7}$ sterad $^{-1}$. Now let us consider the light scattering due to dust. If we assume that a dust particle scatters in all directions just 10 percent of the light incident upon it,[4] we find that a <u>single</u> 1 μm diameter dust particle in the focussed beam will scatter:

$$\left(\frac{1}{10}\right)\left(\frac{1}{4\pi}\right)\left(\frac{1\mu m}{200\mu m}\right)^2 = 2 \times 10^{-7}\ \text{sterad}^{-1} ;$$

the scattered intensity due to dust particles easily exceeds the Ray-

leigh intensity unless the most stringent precautions are taken.

Both the Rayleigh scattered light and the light scattered by small dust particles will be polarized in the same plane as the incident light, and the polarization of these components may be used to discriminate against them in the experiment. If I_{VV} is the intensity of the polarized scattered light, and the half-angles of collection and focussing are δ_o and ε_o respectively then it may be shown that the fraction of the polarized light which is visible in the HV + HH scattering geometry is:

$$\frac{I_{HV + HH,\ stray}}{I_{VV}} = \frac{\delta_o^2}{2} + \frac{\varepsilon_o^2}{4} \quad .$$

For then values $\delta_o = (17.6)^{-1}$rad and $\varepsilon_o = (60)^{-1}$rad (f/8.8 and f/30), the "stray" light intensity is $\frac{I_{HV + HH,\ stray}}{I_{VV}} = 1.7 \times 10^{-3}$ of the polarized scattered intensity and the "stray" light peak arising from Rayleigh scattering will be $(6.1 \times 10^{-3})(1.7 \times 10^{-3}) = 10$ times as bright as the CIS spectrum at zero frequency shift in our "typical" experiment. Any effect which tends to depolarized the incident beam, such as stress-induced birefringence of the pressure cell windows, will increase the stray light signal; so also will scattering of the incident beam by dust particles or from the walls of the sample cell increase the stray light.

The stray light due to scattering from the cell walls may be reduced to negligible proportions by anti-reflection coating and carefully cleaning the windows of the cell, blackening the interior surfaces of the cell, using field stops around the incident beam and in front of the collection arm window and by using a blackened, off-axis wedge as a backdrop for the

focal region of the beam. Dust scattering can be reduced to manageable proportions by flushing and filling the cell through a series of sintered metal filters, the finest blocking all particles larger than $5\mu m$ in diameter. In order to reduce dust scattering to a small fraction of the Rayleigh scattered intensity, sub-micron pore sized bacteriological filters would be necessary but probably not sufficient — the interior surfaces of the sample cell and pressure equipment are just too complicated to be adequately cleaned of all dust. The stray light intensity at zero frequency shift is typically 30 times the peak intensity of the CIS spectrum, so that about $\frac{1}{2}$ or $\frac{2}{3}$ of the stray light is due to dust.

Since the stray light peak is from 10 to 100 times as bright as the peak of the CIS spectrum, depending on the sample molecule and the conditions of observation, it is in no case possible to recover information about the CIS spectrum underlying the instrumentally broadened stray light peak by any sort of subraction technique. The greater part of the total CIS intensity lies at small frequency shifts. In order to obtain information about the behavior of the CIS spectrum near $\omega = 0$, which is essential for determining $\phi^{(0)}$, the spectral slit width must be narrow compared to the spectral width of the CIS spectrum. It is also essential that the intensity of the stray light transmitted by the spectrometer be very small when the pass band is shifted away from $\omega = 0$. This is achieved by using two monochromators in tandem; the shape of the pass band for the Jarrell-

Ash double monochromator is shown in Figure 5-2 for two choices of the slit width. The transmission of an intense narrow spectral line just outside the instrumental pass band falls by a factor of about 10^3 per cm^{-1}; for frequency shifts of a few hundred wavenumbers the transmission is about 10^{-9} of its peak value.

Another limitation which appears when making measurements at small frequency shifts is the finite dynamic range capability of the signal processing electronics. The electronics have been optimized for low signal conditions (photon counting) and at count rates of 10^4 counts/sec or more the "dead-time" losses must be considered. (Dead time losses will be discussed briefly in section 5.3.) At count rates of 10^6 Hz or greater the photomultiplier tube may be damaged. When the signal from the far tail of the spectrum is large enough to be measured, then the peak intensity of the CTS spectrum will usually strain the dynamic range capability of the apparatus, and the Rayleigh line will be so bright that the collected light must be attenuated with a filter.

The one good thing we can say about the Rayleigh line is that it provides a reliable frequency reference. The line appears at precisely zero frequency shift and is so narrow that its spectrum is always instrumentally broadened by our equipment.

The experiment has two conflicting goals: measurement of the very weak spectrum at large frequency shifts and measurement of the spectrum near

FIGURE 5 - 2

Band Pass Profile of the Spectrometer

The intensity of the signal transmitted by the spectrometer is plotted as a function of the frequency shift of the center of the pass band from the frequency of a very narrow spectral line incident on the entrance slit. (The narrow spectral line is obtained by shining the beam of the Ar-ion laser onto the slit through a ground glass screen and filters.) The response functions for two spectral slit widths are plotted: 0.3 cm^{-1} (diffraction limit) and 3.0 cm^{-1}. With all slits set to the same physical width, the "ideal" band pass function is triangular with a full width at baseline equal to twice the spectral slit width; outside this region the transmission should fall abruptly to zero. The measured band pass profile is a good approximation to the ideal. With 3.0 cm^{-1} slits, the transmitted intensity at larger frequency shifts is:

$\Delta\omega(cm^{-1})$	I	$\Delta\omega(cm^{-1})$	I
10	180	30	9
15	57	50	7
20	25	100	3
25	17	200	3

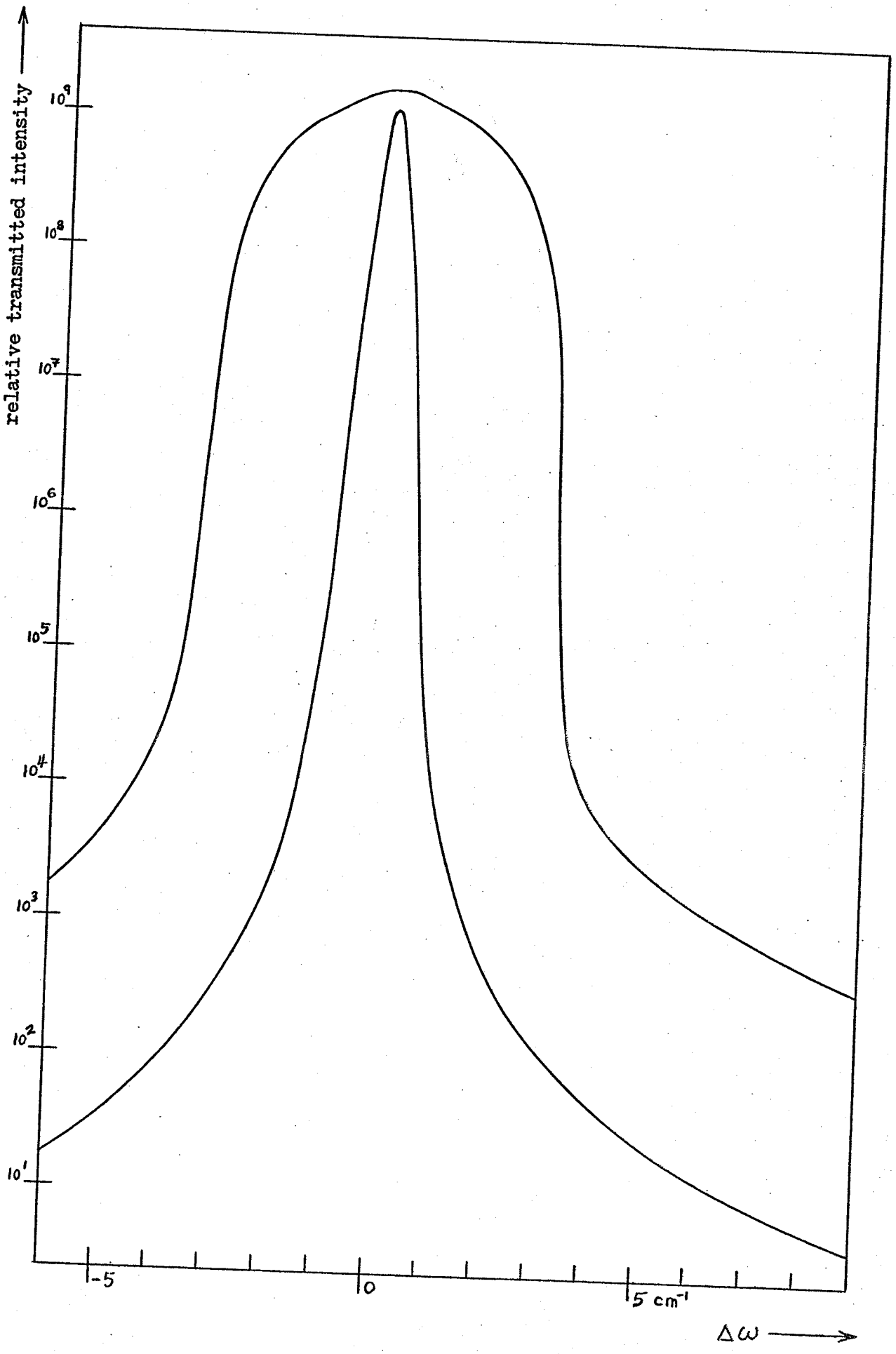
relative transmitted intensity
10^9
10^8
10^7
10^6
10^5
10^4
10^3
10^2
10^1
-5
0
5 cm^{-1}
$\Delta\omega$

$\omega = 0$ in spite of the bright Rayleigh line. To obtain the CIS spectrum near $\omega = 0$ we must use a narrow spectral slit width so that only a small portion of the spectrum is obliterated by the instrumentally broadened Rayleigh line. However, the light entering the spectrometer will be proportional to the slit width, because the slit is always fully illuminated by the too-wide image of the focal region of the incident beam. Also, the fraction of the light entering the spectrometer which will be transmitted to the detector is proportional to the spectral slit width, since the CIS spectrum is much broader than the pass band of the instrument. Thus, the detected signal will increase as the square of the spectral slit width, and measurements at large frequency shifts will be favored by wide slits. The only way to reconcile these conflicting requirements is to make separate scans with narrow and wide slits, for the small and large frequency shift regions of the spectrum respectively.

5.2 Sample Preparation

The desired spectral measurements require the preparation of gas samples at room temperature and with pressures in the range of 10 to 100 atmospheres. The sample handling equipment is arranged to allow the cell to be purged, gases to be purified and filtered as necessary, and mixed gas samples of controlled composition to be prepared. The apparatus is comprised of the sample cell and "thermal compressor", tanks of gas and

a vacuum system, two pressure gauges, and various valves , filters, piping and fittings. The components are mostly manufactured by the American Instrument Company (AMINCO) and are intended for high pressure applications (for example, the piping and its 60^{o} coned connections are designed for operation at internal pressures of 100,000 pounds per square inch or 7000 atmospheres, while the sample cell is designed to operate at up to 700 atmospheres.) The schematic arrangement of the components is shown in Figure 5-3.

The "thermal compressor" consists of a thick walled stainless steel vessel which may be cooled by immersion in liquid nitrogen. The gas sample to be compressed is admitted to the thermal compressor and liquified therein. At this point, the liquified sample can be purified by fractional distillation. The sample where this was most necessary was CF_4. The CF_4, as it comes from the supply cylinder, is contaminated with 0.2 mole percent of air. Using the difference in the vapor pressures of N_2, O_2 and CF_4 at and around the boiling temperature of liquid nitrogen, most of the N_2 and O_2 may be removed with a vacuum pump, limited eventually by the solubility of N_2 and O_2 in liquid CF_4. The purity may be easily improved to 0.05 mole percent of air, and by repeated melting and freezing of the CF_4 and prolonged pumping on the liquid CF_4 held in a bath at the temperature of liquid oxygen, the impurity concentration may be reduced to 0.005 mole percent of O_2. The assay of the impurity concentration is

FIGURE 5 - 3

Schematic of the Sample Handling Equipment

Elbow, "tee" and "cross" connections are indicated as E, T and X. Valves are indicated as V. The filters are made of sintered copper or stainless steel. The internal volume of some of the components are 32.3 cm^3 for the sample cell with its liner installed, 9.1 cm^3 for the 0 - 3000 psi (Bourdon tube) pressure gauge and 2.4 cm^3 for the plumbing between the cross (X) and the cell. The internal volume of the thermal compressor is 105 cm^3 but this can be reduced by inserting an aluminum cylinder.

The sample cell is shown sectioned, looking towards the window facing the collection optics (the cell is shown 0.3 times full scale.) The laser beam travels vertically upwards through the cell, and the fused silica windows are shown "hatched." The sample cell is essentially a solid block of stainless steel which has been cross-bored with 1 inch diameter holes. The blackened aluminum liner has not been indicated.

The placement of the 0 - 3000 psi gauge shown in the diagram is very poor -- it should be placed on the inlet side of the sample cell instead, if an internal intensity standard of H_2 gas is to be used.

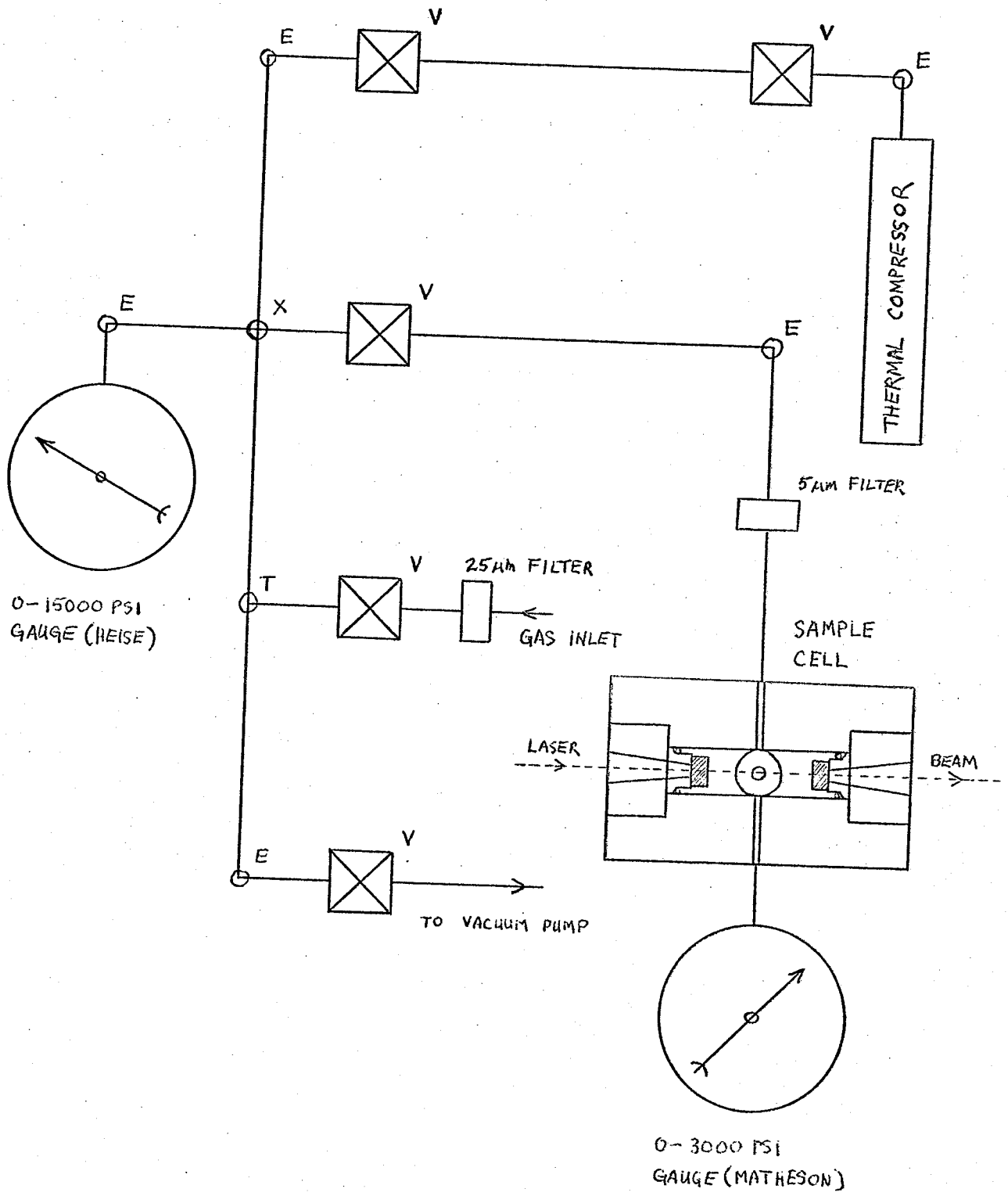
E
V
V
E
THERMAL COMPRESSOR
E
X
V
E
5μm FILTER
0-15000 PSI
GAUGE (HEISE)
T
V
25μm FILTER
GAS INLET
SAMPLE
CELL
LASER
BEAM
E
V
TO VACUUM PUMP
0-3000 PSI
GAUGE (MATHESON)

readily done spectroscopically, using the intensity of their pure rotation Raman lines to determine the concentration of N_2 and O_2 in a low density gas sample of CF_4. After being purified, the pressure of the sample is increased by valving off the thermal compressor and allowing it to warm to room temperature. The liquified sample evaporates and the final pressure is determined by the fraction of the thermal compressor's internal volume which was filled by liquid. Pressures of up to 1000 atmospheres at room temperature may be obtained in this way (the gas density may be as high as the liquid density.)

The sample obtained from the thermal compressor are invariably dustier than the samples obtained directly from the supply cylinders. The thermal compressor was only necessary for preparing CF_4 and CD_4, so the other gas samples were prepared directly from the supply cylinders. Cylinders of UHP Ar and CH_4 contain gas at 150 atmospheres (the Ultra-High Purity grade is of 99.999 mole percent and 99.97 mole percent purity for Ar and CH_4 respectively); SF_6 (with 0.06 mole percent O_2 as an impurity) is supplied as a liquid at 23 atmospheres; H_2 was "prepurified" grade of 99.95 percent minimum purity. All the gases except CD_4 were obtained from Matheson; CD_4 was obtained from Merck, Sharpe and Doheme with an isotopic purity of 99 percent. In the case of CD_4, a leaky coupling between the gas bottle and the sample handling apparatus resulted in contamination of the CD_4 by 0.8 mole percent air. (Ten grams of CD_4 cost $500 and was just enough to fill the sample cell to 80

atm. Fractional distillation would have resulted in too large a loss of CD_4 to be afforded.)

The preparation of the sample for an experiment begins by repeatedly purging (with H_2) and evacuating the entire gas handling system except the thermal compressor. Then, the system is filled with 1 atmosphere of H_2 gas and the pressure is measured with a mercury barometer. The density of the H_2 us calculated from its temperature and pressure. Now the sample gas may be introduced on top of the H_2. If a series of measurements are to be made at successively higher sample densities, then the sample for each measurement is made by adding more gas to the previous sample and recording the total pressure. The density of the H_2 gas, which serves as an internal standard for determining the scattered light intensity, is fixed by the amount initially added to the system.

The H_2 density in the sample is higher than the initial density of H_2 in the system because the sample gas, when it is first added, sweeps the H_2 contained in the piping into the sample cell. The small internal diameter of the pipes (the piping has a 1.5 mm internal diameter and a typical length of 50 cm) prevents mixing of the sample gas and H_2 gas in the lines when the sample gas is first introduced. Diffusional mixing through the piping at pressures of a few atmospheres is so slow that all the H_2 which has been swept into the cell remains there. The result is

that the density of H_2 in the sample cell is increased by about 8 percent, for our apparatus.

Some care must be exercised in the placement of components in the gas handling system. In one configuration, the second pressure gauge was attached to the sample cell at a port opposite the gas inlet. The internal volume of the gauge was comparable to that of the cell, and the result of this arrangement was that part of the H_2 in the cell was swept into the gauge each time sample gas was added. Diffusional mixing between the gas in the gauge and in the cell is negligible, and the net result is that the H_2 internal standard in the cell is diluted by some indeterminate factor each time sample gas is added to the system. Under these circumstances, the H_2 internal standard becomes virtually useless — this is clearly a situation to be avoided.

Presuming that the concentration of H_2 in the sample is known, the final step in sample preparation is to calculate the concentration of each constituent of the sample from its total pressure and temperature. Two pressure gauges (with accuracies of ± 1 atm and ± 0.5 atm) were used to measure the total pressure of the sample with an accuracy of ± 0.3 atmosphere. The sample contains 1 - 10 percent H_2 and usually less than 0.1 percent impurities. For purposes of calculating the sample density, we will ignore the impurities and treat the sample as a binary mixture of H_2 and the sample gas, denoted as X.

As a first approximation, we will assume that each gas separately obeys the van der Waals equation of state:

$$(P + a\rho^2)(1 - b\rho) = \rho RT$$

where P and ρ have units of atmospheres and moles/liter, respectively. The equation of state of this mixture will be approximated by the expression:

$$\left[P + a_X \rho_X^2 + 2 \left(\frac{a_X + a_{H_2}}{2} \right) \rho_X \rho_{H_2} + a_{H_2} \rho_{H_2}^2 \right] \cdot \left[1 - b_X \rho_X - b_{H_2} \rho_{H_2} \right] = (\rho_X + \rho_{H_2}) RT \quad .$$

This may be further approximated as:

$$(P' + a_X \rho_X^2)(1 - b_X \rho_X) = \rho_X RT$$

where $P' = P - P_{H_2} + P''$

$$= P - P_{H_2} + (b_X \rho_X P_{H_2} - b_{H_2} \rho_{H_2} P) + (a_X + a_{H_2}) \rho_X \rho_{H_2} + a_{H_2} \rho_{H_2}^2 \quad .$$

We may calculate ρ_{H_2} with sufficient accuracy, from P_{H_2} and T using the van der Waals equation of state for H_2 since the H_2 density is low. Next, we obtain an approximate value for ρ_X which will enable us to compute P", the pressure due to H_2 - X interactions. Since the uncertainty in the measurement of the total pressure P is on the order of 0.3 atm while the value of P" is usually in the range of 0.1 - 0.2 atm, it is quite adequate to use very approximate densities in evaluating P".

Finally, we compute ρ_X as the density of the pure component X at temperature T and pressure $P' = P - P_{H_2} + P''$. For this step we use an equation of state for the gas which better describes its behavior than the

van der Waals equation of state. For CH_4 and CF_4 the Beattie-Bridgeman equation of state was solved iteratively to obtain ρ_X.[5] The entire calculation can be iterated until a self-consistent value of ρ_X is obtained, if this is necessary.

5.3 The Data Analysis

Once a series of spectra have been obtained from samples of known density and composition, the data must be reduced to a form which is directly comparable with the theoretical predictions. The binary CIS spectrum is obtained from the raw data by applying instrumental corrections, accounting for the effect of impurities in the sample and by fitting a virial expansion to the measured intensities. We will discuss the data analysis steps in the same order in which they are applied to the data.

5.3.1 Dead Time

The processing of the pulse generated by the electronics in response to the detection of a photon by the photomultiplier tube requires a finite amount of time. If two photons, both of which are detected, arrive with a separation less than the so-called "dead time" of the electronics, only one event will be counted. The photons in the light signal being measured arrive randomly in time and so the pulses due to detected photons will be randomly distributed in time as well. The probability that a second

pulse will follow any given first pulse within the dead time interval and therefore not be counted, is just proportional to the mean pulse rate. The fraction of the pulses which will be counted is given by:

$$\frac{r'}{r} = 1 - \beta r$$

where r' = count rate and r = pulse rate. When the dead time losses are small ($r'/r \geq 0.9$), this relation may be inverted to give the pulse rate in terms of the count rate:

$$r \simeq r' (1 + \beta r') \quad .$$

The rate limiting component is our data handling electronics is the multichannel scaler, which counts the number of pulses that arrive while the spectrometer is set at a particular frequency and stores the total in the appropriate memory address or channel. The dead time is $\beta = 2.52$ μsec and the dead time losses increase linearly for count rates up to 80 KHz. Count rates near the peak of the CIS spectrum often reach 40 KHz (10 percent dead time losses) when the apparatus has been optimized for measuring the weak light signal in the far tail of the spectrum. The measured intensities will be affected long before the distortion of the spectral shape becomes apparent. In all critical work, the CIS peak count rate is kept below 2 KHz so that dead time losses are less than 0.5 percent.

5.3.2 Spectral Response

The probability that a photon entering the spectrometer will be detected depends on both its frequency and its polarization. The components which make the largest contributions to the polarization dependence of the instrumental response are the diffraction gratings; the slits and the photocathode surface, which is inclined to the direction of the light, both make substantial additional contributions. As for the frequency dependence of the instrumental response, every component in the light path makes a significant contribution. Accordingly, one must be careful about making changes to the apparatus after the overall response of the system has been measured.

The measurement of the frequency response of the spectrometer for unpolarized light was done using a tungsten ribbon lamp as a light source. The lamp had been calibrated by the National Research Council of Canada (NRCC) lab against a secondary standard. The relative sensitivity of the spectrometer to light polarized parallel to and perpendicular to the entrance slit (and the rulings of the diffraction gratings) was measured by placing a polaroid before the entrance to the spectrometer. The sensitivity of the spectrometer to light polarized perpendicular to the grating rulings is about three times as great as for light polarized parallel to the rulings. Since our measurements of the CIS spectrum were made in the HV + HH geometry, and the intensity of the components

FIGURE 5 - 4

Relative Response Function of the Spectrometer

The relative spectral response is plotted for 3.0 cm^{-1} (upper curve) and 0.5 cm^{-1} spectral slit width of the spectrometer. Zero frequency shift occurs at 20492 cm^{-1} (4880 Å.) The curve for 3.0 cm^{-1} spectral slit width is characteristic of the response for slits wider than 1.0 cm^{-1}. For slits narrower than 1.0 cm^{-1} the relative spectral response becomes dependent on slit width. The relative response plotted in the graph is in units of counts per mW of incident light, within the fixed wavelength bandpass of the instrument.

Since the spectral slit width, for a fixed physical slit width, is proportional to ω^2, and the number of photons per mW is proportional to ω^{-1}, the plotted response curves must be multiplied by ω^3 to obtain the relative response of the instrument in counts per incident photon per unit frequency interval.

The relative response functions for 3.0 cm^{-1} and 1.0 cm^{-1} slits are then:

$$R(\text{counts/photon} - cm^{-1}) = \left(\frac{\omega_o - \Delta\omega}{\omega_o}\right)^3 \left(1 - 0.0442 \left(\frac{\Delta\omega}{1000}\right) - 0.0308 \left(\frac{\Delta\omega}{1000}\right)^2\right)$$

and $$R(\text{counts/photon} - cm^{-1}) = \left(\frac{\omega_o - \Delta\omega}{\omega_o}\right)^3 \left(1 - 0.0645 \left(\frac{\Delta\omega}{1000}\right) - 0.0222 \left(\frac{\Delta\omega}{1000}\right)^2\right) ,$$

respectively, in the range $\Delta\omega = -200 \longrightarrow +1000\ cm^{-1}$, where $\omega_o = 20492 cm^{-1}$.

The spectral response is flat largely because of the flat spectral response of our photomultiplier tube.

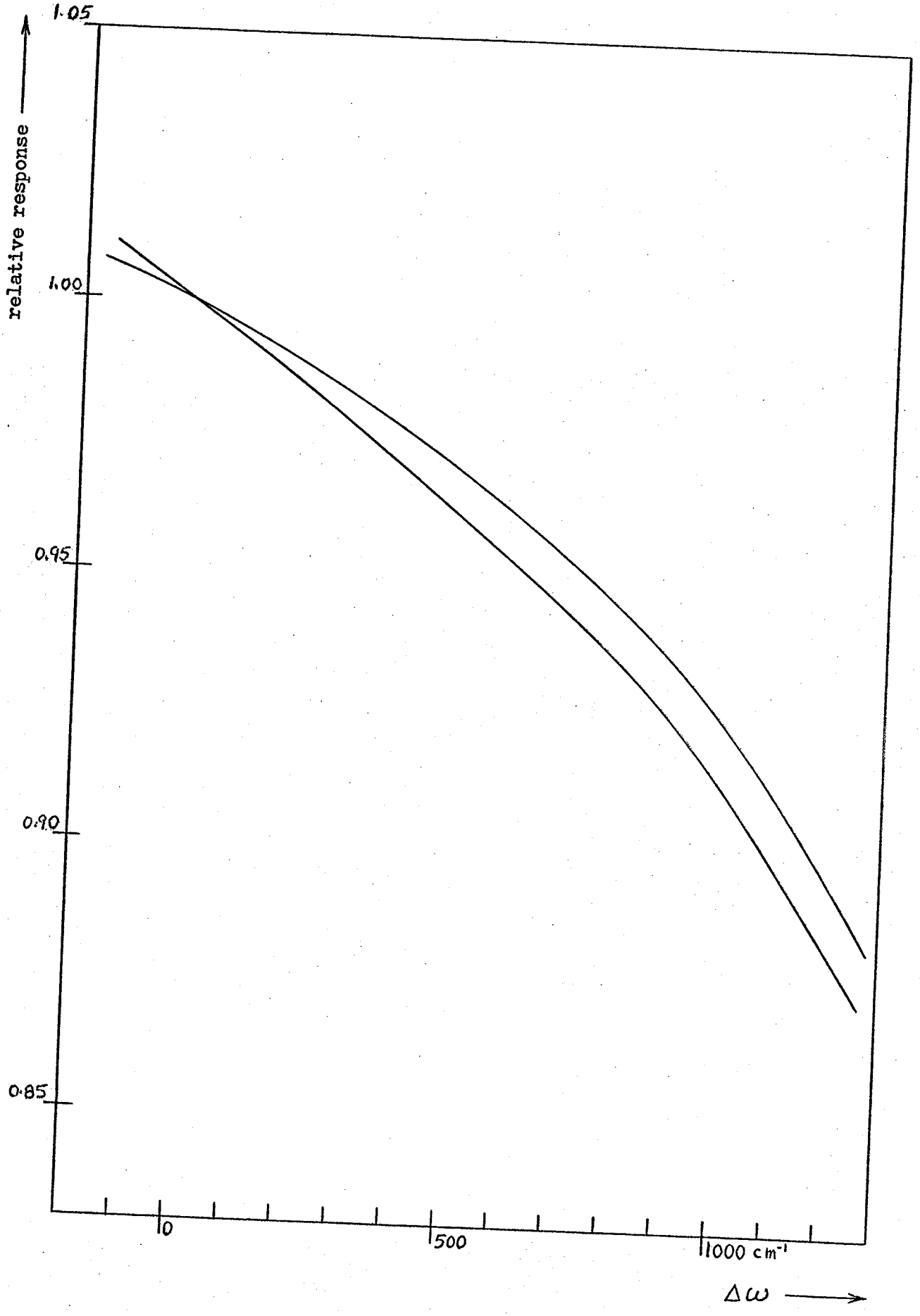
relative response
1.05
1.00
0.95
0.90
0.85
0
500
1000 cm⁻¹
Δω

I_{HV} and I_{HH} are equal by symmetry, we need only apply the correction for the frequency response of the spectometer to unpolarized light. The relative response of the system in the frequency region of interest for our light scattering measurements is presented in Figure 5-4. Note that the relative response is given in terms of counts/mW for a fixed slit width. The spectral slit width is proportional to ω^2 for a fixed physical slit width and the number of photons per mW is inversely proportional to ω. Thus, to obtain the relative response in counts per photon and per unit frequency interval, with a fixed physical slit width, we must multiply the relative response values in the figure by ω^3.

5.3.3 The Spectrum Due to Impurities

The only significant impurities in the samples studied were N_2 and O_2. These impurities will result in a weak rotational Raman spectrum being superimposed on the CIS spectrum. If the impurity concentration in a given sample is known, then the pure rotation spectrum of the impurity may be calculated, suitably pressure broadened, and subtracted from the CIS spectrum. The rotational Raman spectrum for N_2 and O_2 was calculated at the end of Chapter 2. The concentration of N_2 and O_2 may be assayed spectroscopically by comparing the intensity of the rotation lines of N_2 and O_2 in a low pressure sample (of measured density) to the intensity of the S(1) line of a sample of H_2 (of measured density.) The

pressure broadened lines may be taken to have Lorentzian profiles, with a width which is the sum of the spectral slit width and the width due to pressure broadening.

5.3.4 The H_2 - X CIS Spectrum

The major constituents of the sample being studied are H_2 and X and its CIS spectrum will consist of contributions arising from X - X, H_2 - X and H_2 - H_2 collisions. Because of the low concentration of H_2 and its small polarizability, we will ignore the H_2 - H_2 spectrum as being to weak to concern us. The H_2 - X CIS spectrum however, will make a small but significant contribution to the total intensity. Since we are interested in the binary CIS spectrum due to X - X collisions only, we will subtract the H_2 - X spectrum. And since the intensity of the H_2 - X spectrum is only a few percent of the X - X intensity, a rough approximation to the real H_2 - X spectrum will be sufficient for our purposes.

The zeroth moment of the binary CIS spectrum for the mixture will be, in the DID approximation:

$$\phi^{(0)} = 4\pi\left\{\rho_X^2 \frac{36\alpha_X^4}{\sigma_X^3}\int_0^\infty x^{-4} g_X(x)\,dx + 2\rho_X\rho_{H2}\frac{36\alpha_X^2\alpha_{H_2}^2}{(\sigma_X^3\sigma_{H_2}^3)^{\frac{1}{2}}}\int_0^\infty x^{-4} g_{H_2-X}(x)\,dx + \rho_{H_2}^2\frac{36\alpha_{H_2}^4}{\sigma_{H_2}^3}\int_0^\infty x^{-4} g_{H_2}(x)\,dx\right\}/(\rho_{H_2}+\rho_X)^2 \quad .$$

$$\frac{I_{H_2\text{-}X}}{I_{H_2\ S(1)}} = \frac{\left(\frac{\omega_s}{c}\right)^4 \frac{\rho_{H_2}\rho_X}{30}\ 2\ \frac{36\alpha_{H_2}^2\ \alpha_X^2}{(\sigma_{H_2}^3\ \sigma_X^3)^{\frac{1}{2}}} \int_0^{\infty} x^{-4}\ g_{H_2}(x)\ dx}{\left(\frac{\omega\omega_s^3}{c^4}\right)\frac{\rho_{H_2}}{10}\ (0.662)(2/5)(\alpha_{\parallel} - \alpha_{\perp})_{H_2}^2} = B\rho_X$$

expressed in terms of the H_2 S(1) rotation line intensity. The H_2 - H_2 CIS spectrum may be represented as $I(\omega) = A \exp(-\omega/50\ cm^{-1})$, on the Stokes side. The collision time for H_2 - X collisions is determined by the inverse square root of the reduced mass of the colliding pair. The decay constant of the H_2 - X spectrum is inversely proportional to the collision time, and is about 36 cm^{-1} for the molecules studied. For the purpose of subtracting the H_2 - X CIS spectrum, we will approximate it by an exponential spectral profile whose integrated intensity is given by the DID model.

5.3.5. Separation of the Two-Body and Three Body Components

After removing the contributions due to the impurities N_2, O_2 and H_2, the intensity of the CIS spectrum may be represented by a power series expansion in density:[6]

$$I(\omega) = I^{(2)}(\omega)\ \rho_X^2 + I^{(3)}(\omega)\ \rho_X^3 + I^{(4)}(\omega)\ \rho_X^4 + \ldots$$

The leading term is $I^{(2)}(\omega)\ \rho^2$ since the CIS spectrum arises from the interactions of at least two molecules. Over the range of densities

we have used in our experiments, the spectrum is adequately expressed in terms of just the two-body and three-body terms. When the four - body term becomes important, it will appear first at small frequency shifts. The two and three body spectra are obtained from a series of spectra at different densities by first normalizing the intensities to the H_2 S(1) line intensities, then multiplying by ρ_{H_2} / ρ_X^2, and then finally fitting a straight line of the form $A + B\rho_X$ at each separate frequency. The coefficients of the fit are just $I^{(2)}(\omega)$ and $I^{(3)}(\omega)$.

5.3.6. The Zeroth Moment

The zeroth moments of the two body and three body spectra may be obtained by integrating $I^{(2)}(\omega)$ and $I^{(3)}(\omega)$. However, it is preferable to obtain the zeroth moments by fitting $I^{(2)} + I^{(3)}\rho_X$ to a plot of $I(\rho)/\rho^2$ versus ρ, where $I(\rho)$ is the integrated intensity of the spectrum obtained from the sample with density ρ. The advantage of this method is that each spectrum is represented by a single point so that it is easier to critically assess the quality of the fit in terms of statistical and systematic uncertainties.

The measurement of the zeroth moment is difficult because the central part of the spectrum which contributes most of the total intensity, is partially obscured by the Rayleigh line. Unless the spectrum is scanned with sufficiently high resolution, the extrapolation of the spectrum to

FIGURE 5 - 5

Extrapolation to Zero Frequency for the CIS Spectrum of Ar

The number of counts per channel (10 sec per channel) of an experimental Ar CIS spectrum is plotted versus channel number (4 channels per cm^{-1}, the full spectrum consists of 256 channels.) The Ar sample is at a pressure of 120 atm. at room temperature (5.3 mole/liter) and the spectral slit width used in the scan was 0.5 cm^{-1}. The CIS spectrum may be followed down to a frequency shift of 1 cm^{-1}. The extrapolation which we have used for frequency shifts below 1 cm^{-1} is shown by the line; the extrapolation is not expected to introduce gross errors in the determination of the zeroth moment.

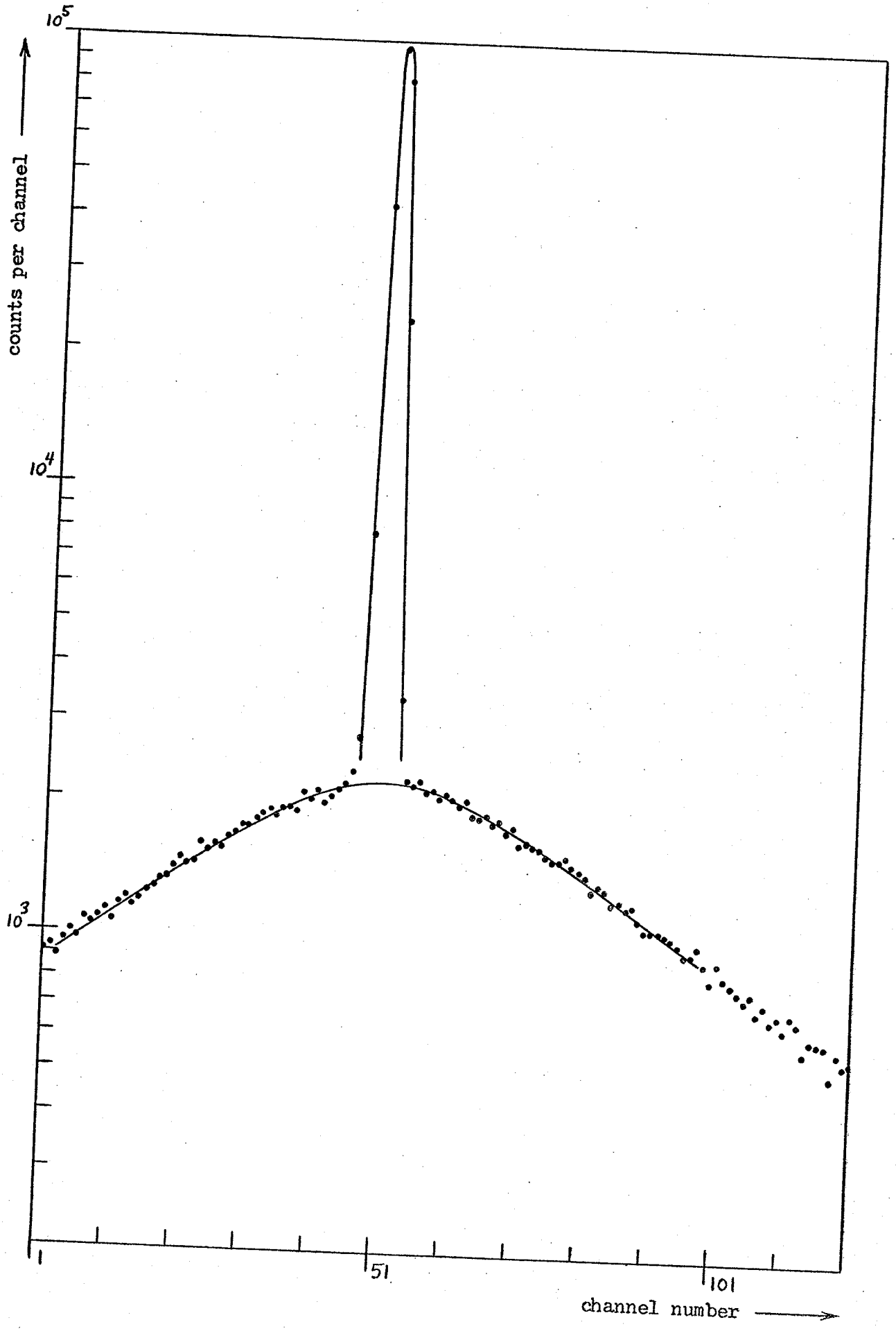
10^5
counts per channel
10^4
10^3
1
51
101
channel number

FIGURE 5 - 6

Determination of the Zeroth Moment of the Ar CIS Spectrum

The graph is of $I(\rho)/\rho^2$ versus ρ, where ρ has units of mole/liter and $I(\rho)/\rho^2 = \phi^{(0)}$ has units of Å^9. The $\phi^{(0)}$ is related to the integrated intensity of the Ar spectrum by:

$$\phi^{(0)}(\rho) = \frac{I(\rho)}{\rho^2} = \frac{(119.2)\,\rho_{H_2}\ (\text{mole/liter})}{\rho^2\ (\text{mole}^2/\text{liter}^2)} \frac{\left(\frac{d\sigma}{d\Omega}\right)_{Ar\ CIS}}{\left(\frac{d\sigma}{d\Omega}\right)_{H_2\ S(1)}}$$

where the H_2 S(1) rotation Raman line has been used as an internal standard for determining the intensity of the Ar CIS spectrum. The plotted values of $\phi^{(0)}(\rho)$ have been corrected for effects such as H_2 - Ar scattering. The zero density intercept gives the intensity due to binary collisions, while the downward slope of the line gives the negative, three-body contribution to the scattered intensity. The line is $\phi^{(0)}(\text{Å}^9) = 54.2 - 3.71\rho\,(\text{m/l})$. The crosses, filled and open circles represent spectra taken at different times and of different quality.

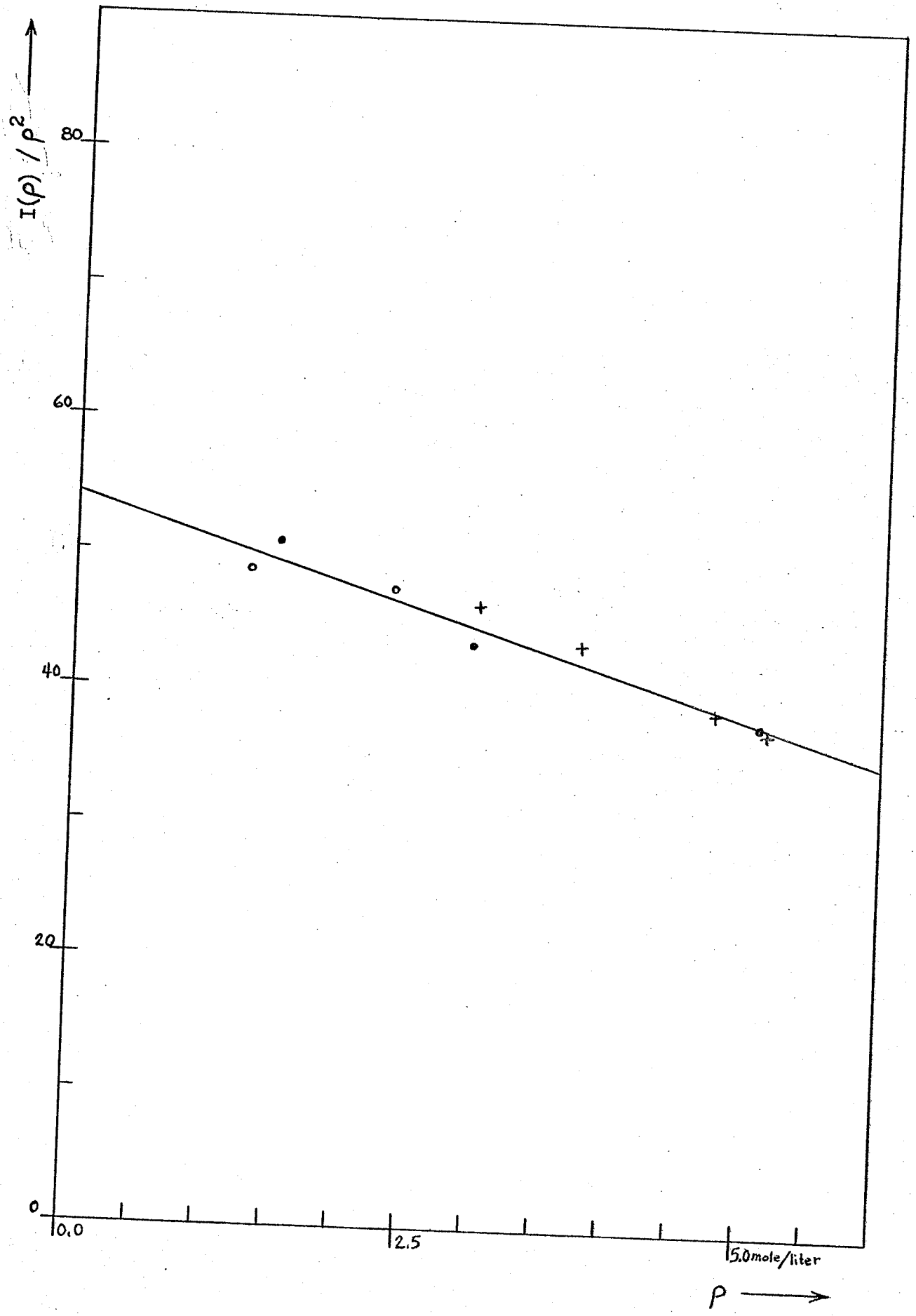
I(ρ) / ρ²
80
60
40
20
0
0.0
2.5
5.0 mole/liter
ρ

zero frequency shift will be unreliable. The narrow slit width required for high resolution, however, greatly reduces the observed intensity, and eventually counting statistics will limit the accuracy of the integrated intensity measurement. The small frequency shift region of an Ar spectrum scanned at high resolution is presented in Figure 5-5. The extrapolation to zero frequency shift for this spectrum will contribute only a small uncertainty to measurement of the integrated intensity. For the high resolution Ar spectra measured at lower densities, it is usually the counting statistics and not the extrapolation which limits the accuracy of the integrated intensity. The plot of I/ρ^2 versus ρ for Ar is given in Figure 5-6. A straight line is an adequate representation of the data, which justifies the neglect of the four-body contribution to the intensity. For the molecules we have studied, the zeroth moment is at least five times as large as for Ar; this makes the measurement of the zeroth moment for the molecules much easier than for Ar.

The results of our measurements of the zeroth moments may be summarized as:

Molecule	
Ar	$\phi^{(0)} = 54.2 - 3.17\rho$
CH_4	$\phi^{(0)} = 296 - 24.7\rho$
CF_4	$\phi^{(0)} = 277 - 17.6\rho$
SF_6	$\phi^{(0)} = 1212 - 342\rho$

where $\phi^{(0)}$ is given in units of Å^9 and ρ is given in units of mole/liter. The first term is due to binary collisions while the second is due to three body collisions. The uncertainty of the measurements is about ± 5 to ± 15 percent, increasing down the table.

5.3.7. Comments on Absolute Intensity Measurements

The interpretation of the CIS spectrum is much easier when we know the absolute scattering cross section as well as the shape of the spectrum. However, measurements of the absolute scattered intensity with an accuracy of 5 percent or better are quite difficult to make. They are most easily performed by comparing the intensity scattered by the sample to the intensity scattered by some standard — in our case H_2 gas. A number of laboratories have made measurements of the zeroth moment of the CIS spectrum of Ar, and the results have been in the range of 0.5 to 0.8 times the calculated DID result for $\phi^{(0)}$.[7] The results disagree with each other and with the theoretical predictions.

The disagreement between the various measurements of $\phi^{(0)}$ for Ar has prompted our group, and the group headed by Barocchi, at CNR Firenze, Italy, to make independent determinations of $\phi^{(0)}$ for Ar. We have used the internal standard method, where a measured amount of H_2 is present in the sample, and the measurements of the intensity scattered by the sample and by the standard are measured at the same time. This eliminates the effect of focussing or alignment changes in the optics.

Barocchi uses the external standard method, where the cell is filled first with pure H_2 for the standard measurement, and then filled with a pure gas sample for all the other measurements. This eliminates the interaction between sample and H_2 molecules which must be accounted for in the internal standard method. A decisive factor in choosing the internal standard method in our case is the fact that the experimental room is not temperature stabilized. Variations in room temperature require that the tracking of the two halves of the tandem monochromator be adjusted every day and sometimes for every measurement, when one is operating at high resolution ($0.5\ cm^{-1}$.)

Since the H_2 S(1) rotation line appears at a large frequency shift from the CIS spectrum, it is necessary to know the spectral response function of the spectrometer. We have measured the spectral response of our instrument using a calibrated tungsten lamp; Barocchi has used a black body source for this purpose.

The results for the zeroth moments of the two-body CIS spectrum of Ar are 54.2 ± 3 Å^9 for our lab and 48.8 ± 3 Å^9 for Barocchi's lab.[8] The two results agree with each other and have an average of 51.5 Å^9, which is 1.2 times the calculated DID value of $\phi^{(0)}$. These results are clearly inconsistent with the measurements reported by previous workers. We may suggest several reasons for error in the previous reports:

1) The variation in spectral sensitivity between zero frequency

shift and the position of the H_2 S(1) line has not been taken into account.

2) The effect of the negative three-body contribution to the total scattered intensity has not been taken into account. At 40 atmospheres (about 15 mole/liter) the three body contribution is already 10 percent of the two body intensity. The intensity of the spectrum becomes inconveniently low for Ar if the density is reduced much below this value.

3) Usually only the Stokes side of the spectrum is measured because the spectrum is symmetric about zero frequency shift, except for the Boltzmann factor. The zeroth moment includes the entire spectrum and if only the Stokes side is used in computing $\rho^{(0)}$, the result will be too small by a factor of two.

Unless one has the specific intent of making accurate absolute intensity measurements, the results are likely to be affected by systematic errors due to features of the experiment which are of little consequence when only the spectral shape is desired. As a final consideration, we must note that the absolute intensity measurements we have made can be no more accurate than the value of $(\alpha_{\parallel} - \alpha_{\perp})_{H_2} = 0.314$ Å^3 that we have assumed for our internal standard. The experimental value of $(\alpha_{\parallel} - \alpha_{\perp})^2$ for H_2 is 6 percent larger than the corresponding result obtained by a careful theoretical calculation, so that the absolute intensities we have obtained may be systematically too large by this amount.[9]

NOTES AND REFERENCES

1. Crystal optics as well as other topics in optics which pertain to the design of the apparatus are treated in:
M. Born, E. Wolf, Principles of Optics, Pergamon, Oxford, 1970
A. Nussbaum, R. A. Phillips, Contemporary Optics for Scientists and Engineers, Prentice-Hall, Englewood Cliffs, 1976 .

2. If aberrations can be controlled, then it is desirable to reduce the diameter of the diffraction limited focal cylinder by shortening the focal length of the focussing lens, since this will result in an increase in the collected light. See:
J. J. Barrett, N. I. Adams, J. Opt. Soc. Am. 58, 311 (1968)
R. L. Schwiesow, J. Opt. Soc. Am. 59, 1285 (1969)

3. The photomultiplier tube must be electromagnetically shielded and cooled to about -40°C to reduce the background count rate, due mainly to thermionic emission from the photocathode at room temperature, to this level. A substantial part of the count rate of the cooled tube is due to light generated by cosmic rays and natural radioactivity of the glass envelope. The rest is generated by thermionic and field emission of electrons and by other processes occurring inside the tube itself. For a discussion of the properties of photoemissive detectors see:
A. H. Sommer, Photoemissive Materials, Wiley, New York, 1968 .
The cooler for the PMT is similar to that described in:
A. L. Broadfoot, Appl. Opt. 5, 1259 (1966) .
The optimization of the signal to noise ratio in photon counting with photomultipliers is discussed in:

A. T. Young, Appl. Opt. 8, 2431 (1969) .

4. The Mie scattering cross section for particles with a radius greater than or equal to the incident light wavelength is approximately equal to the geometric cross sectional area. For particles with $r < \lambda$, the scattering cross section is approximately $(\pi r^2)(\frac{r}{\lambda})$. For large particles the scattered light peaks in the forward direction, but for particles much smaller than the wavelength, the angular distribution becomes very broad.

5. The Beattie-Bridgeman equation of state has the form $P = RT(1-\varepsilon)\rho^2 (B + 1/\rho) - A\rho^2$ where $A=A_o(1-a\rho)$, $B=B_o(1-b\rho)$ and $\varepsilon = c\rho T^{-3}$. The density may be obtained by the iteration

$$\rho = \frac{P}{C_1 + C_2\rho + C_3\rho^2 + C_4\rho^3}$$

where $C_1 = RT$

$C_2 = R(B_oT - c/T^2) - A_o$

$C_3 = aA_o - RB_o(c/T^2 + bT)$

$C_4 = RB_obc/T^2$.

The PVT relations for CH_4, CF_4 and SF_6 are given by:

Douslin, Harrison, Moore, McCullough, J. Chem and Eng. Data 9, 358 (1964)

Douslin, Harrison, Moore, McCullough, J. Chem. Phys. 35, 1357 (1961)

MacCormack, Schneider, J. Chem. Phys. 19, 845 (1951)

For Argon the PVT data was obtained from the NBS circular:

Gosman, McCarty, Hurst, Thermodynamic Properties of Ar from the Triple Point to 300°K at Pressures to 1000 Atmospheres,

National Bureau of Standards (NSRDS-NBS27) 1969

The CD_4 equation of state is very similar to that for CH_4. The differences in the second virial coefficients for CH_4 and CD_4 are measured by:

Thomaes, Steinwinkel, Mol. Phys. 5, 307 (1962)

The PVT data for H_2 and H_2-Ar mixtures are given in:

Michels, de Graaff, Wassenaar, Levelt, Louwerse, Physica 25, 25 (1959)

Zandbergen, Beenakker, Physica 33, 343 (1967)

A comprehensive list of references for PVT data is found in:

Mason, Spurling, The Virial Equation of State, International Encyclopedia of Phys. Chem. and Chem. Phys., Topic 10, Vol 2, 1969

6. The virial expansion of the CIS spectrum is considered, for example, by

J. P. McTague, W. D. Ellenson, L. H. Hall, J. de Phys. (Paris) 33, C1-241 (1972)

7. The results are:

a) McTague et al 25.7 ± 2.5 Å^9

b) Buckingham, Dunmur (Kerr Effect) 30.2 ± 4.4 Å^9

c) Lallemand 33.5 ± 5.0 Å^9

d) Thibeau et al 27.7 ± 1.2 Å^9

where:

a) J. P. McTague, W. D. Ellenson, L. H. Hall, J. de Phys. (Pairs) 33, C1-241 (1972)

b) A. D. Buckingham, D. A. Dunmur, Trans. Faraday Soc. 64, 1776 (1968)

c) P. Lallemand, J. de Phys. (Paris) 32, 119 (1971)

d) M. Thibeau, G. C. Tabisz, B. Oksengorn, B. Vodar, J. Quant. Spectrosc. Rad. Transfer 10, 839 (1970)

8. F. Barocchi, M. Zoppi, Physics Letters 66A, 99 (1978)

9. The experimental result is from:

N. J. Bridge, A. D. Buckingham, Proc. Roy. Soc. A295, 334 (1968)

The calculation is by:

W. Kolos, L. Wolniewicz, J. Chem. Phys. 46, 1426 (1967)

CHAPTER 6

DISCUSSION AND CONCLUSIONS

In the previous chapters, the theoretical framework for the discussion of collision-induced light scattering was presented. In this chapter, we will compare the theoretical predictions with the observed spectra and draw our conclusions.

The first comparison we will make is between the spectra computed using the point DID model, $\beta(x)=x^{-3}$, and the experimentally observed spectra for Ar, CH_4, CF_4 and SF_6. The spectra are plotted in Figures 6-1,2, 3 and 4. The computed spectra agree well with the observations in terms of the spectral shape, especially considering that there are no free parameters involved. This agreement in the gross features of the spectral distribution arises because the spectral width is determined by the molecular diameter and velocity; the spectral shape is relatively insensitive to the form of the pair polarizability function. However, the intensity of the calculated spectrum does not agree with the observed spectrum; the error bars on the measurements have a width of the order of ± 10 percent while the discrepency between the theory and experiment is of the order of $\pm$ 100 percent. It would seem that the simple point DID model is not a sufficiently good approximation to $\beta(x)$. We will consider refinements of the DID model shortly.

The comparision we just made was limited to the low and intermediate frequency regions of the spectrum. If we continue into the high frequency shift region, we find an abrupt change in the shape of the observed spectra for all the molecules, which the DID model can-

FIGURE 6 - 1

Comparison of the Experimental and the Calculated DID CIS Spectrum for Ar

The experimental measurements are indicated by dots (plotted every 2 cm^{-1}.) The spectrum calculated using the DID model, $\beta(x) = x^{-3}$, is shown by the solid line. The dashed line (near zero frequency shift) is the calculated spectrum ignoring the contribution of bound dimers. The bound dimer spectrum is somewhat too narrow while the unbound dimer spectrum is somewhat too wide. However, the overall shape of the calculated spectrum agrees remarkably well with the observed spectral shape.

The intensity calculated using $\beta(x) = x^{-3}$, (the other parameter values used are given in Table 3 - 2) is $\phi^{(0)}_{ttl} = 42.7$ $Å^9$ ($\phi^{(0)}_{free} = 37.5$ $Å^9$) as compared with the measured value $\phi^{(0)} =$ 51.5 $Å^9$ for Ar. The calculated intensity is slightly smaller than the observed intensity.

The intensity scale is in units of the CIS scattering cross section per unit frequency interval (1 cm^{-1}) divided by the scattering cross section of the H_2 S(1) transition under the same conditions, when both gases (H_2 and Ar) are at unit density (1 mole/liter.)

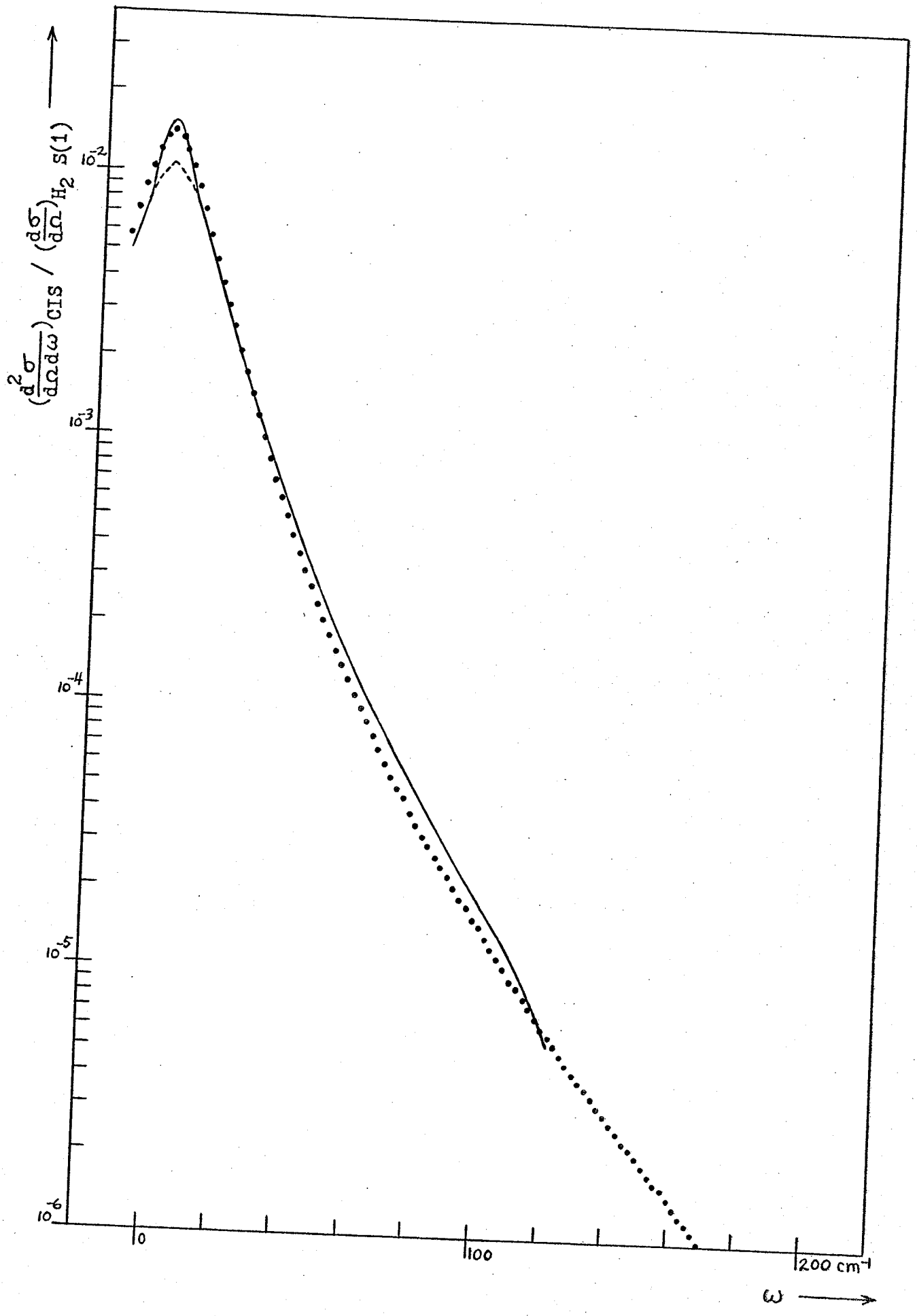
$(\frac{d^2\sigma}{d\Omega d\omega})_{CIS} / (\frac{d\sigma}{d\Omega})_{H_2\ S(1)}$
10^{-2}
10^{-3}
10^{-4}
10^{-5}
10^{-6}
0
100
200 cm^{-1}
ω

FIGURE 6 - 2

Comparison of the Experimental and Calculated DID CIS Spectrum for CH_4

The experimental measurements are indicated by dots (plotted every 4 cm^{-1}.) The spectrum calculated using the DID model, $\beta(x) = x^{-3}$, is shown by the solid line. The dashed line (near zero frequency shift) is the calculated spectrum ignoring the contribution of bound dimers. The bound dimer spectrum is too narrow, while the unbound dimer spectrum is too wide. Past 180 cm^{-1} the shape of the observed spectrum changes abruptly.

The intensity calculated using $\beta(x) = x^{-3}$ is $\phi^{(0)}_{ttl} = 249.9$ $\mathring{A}^9$ ($\phi^{(0)}_{free} = 191.7$ $\mathring{A}^9$) as compared to the measured value of $\phi^{(0)} = 296.2$ $\mathring{A}^9$ ($\phi^{(0)} = 291.2$ $\mathring{A}^9$ when the CIRS contribution is subtracted.) The observed intensity is slightly larger than the calculated value.

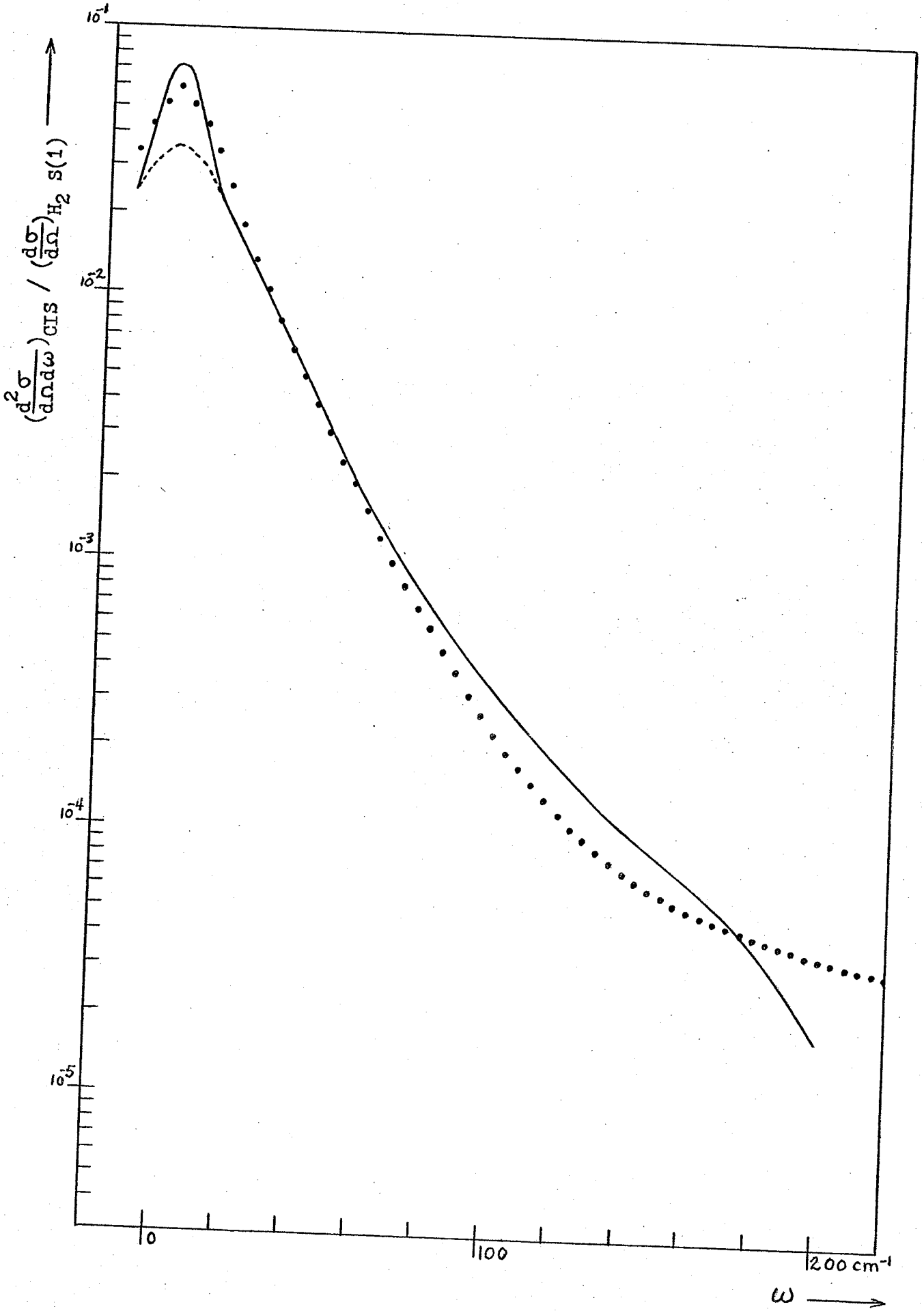
10^{-1}
10^{-2}
10^{-3}
10^{-4}
10^{-5}
$(\frac{d^2\sigma}{d\Omega d\omega})_{CIS} / (\frac{d\sigma}{d\Omega})_{H_2\ S(1)}$
0
100
200 cm^{-1}
ω

FIGURE 6 - 3

Comparison of the Experimental and Calculated DID CIS Spectrum for CF_4

The experimental measurements are indicated by dots (plotted every 1 cm^{-1}.) The spectrum calculated using the DID model, $\beta(x) = x^{-3}$, is shown by the solid line. The dashed line (near zero frequency shift) is the calculated spectrum ignoring the contribution of bound dimers. The bound dimer spectrum is somewhat too narrow, but the overall shape of the calculated spectrum agrees very well with the observed shape. Past 60 cm^{-1} the shape of the observed spectrum changes abruptly.

The intensity calculated using $\beta(x) = x^{-3}$ is $\phi^{(0)}_{ttl} = 142.1$ $Å^9$ ($\phi^{(0)}_{free} = 128.8$ $Å^9$) as compared to the measured value of $\phi^{(0)} =$ 277 $Å^9$ ($\phi^{(0)} = 271.5$ $Å^9$ when the CIRS contribution is subtracted.) While the shape is correctly predicted, the predicted intensity much too small.

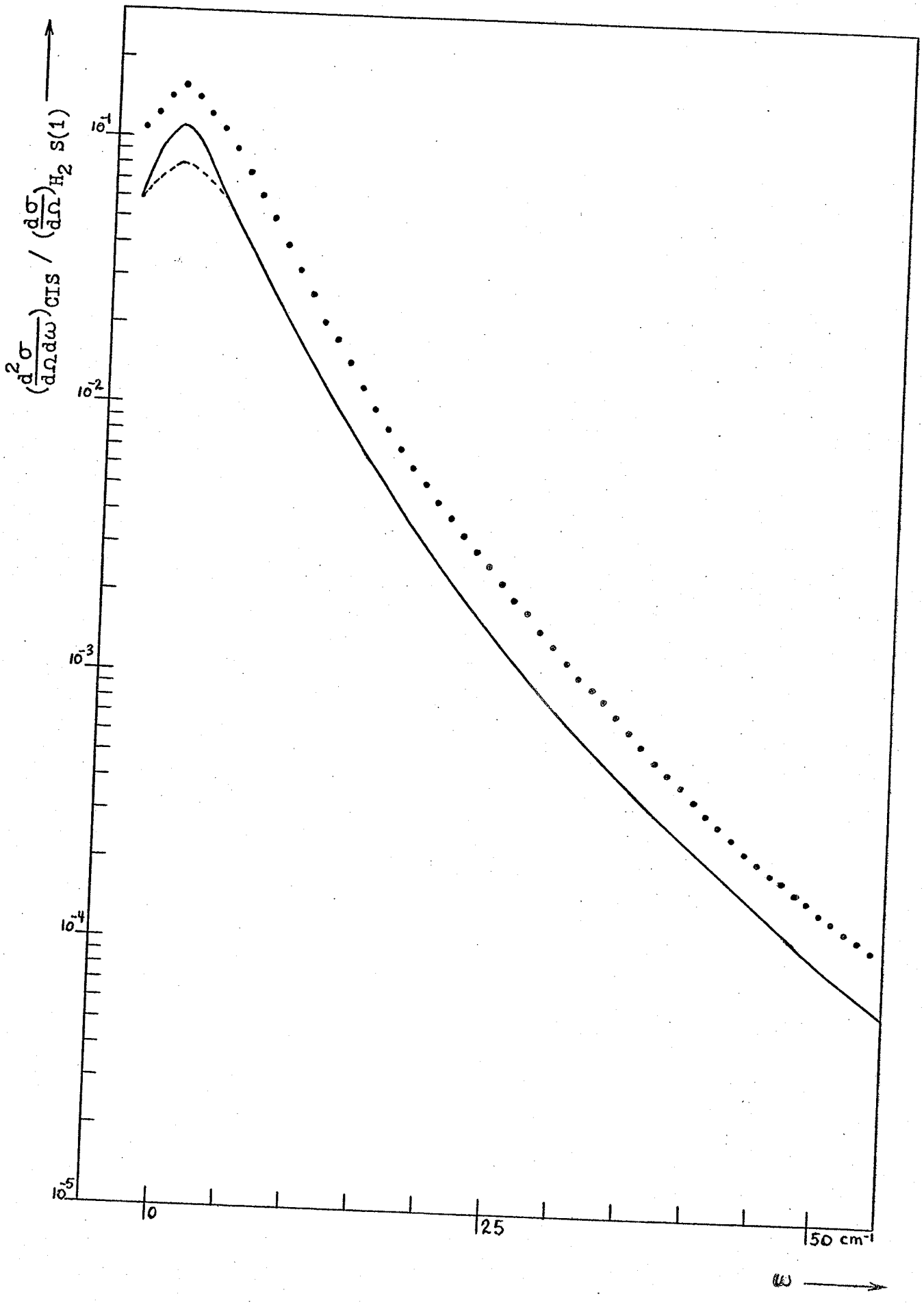
$(\frac{d^2\sigma}{d\Omega d\omega})_{CIS} / (\frac{d\sigma}{d\Omega})_{H_2\ S(1)}$
10^{-1}
10^{-2}
10^{-3}
10^{-4}
10^{-5}
0
25
50 cm^{-1}
ω

FIGURE 6 - 4

Comparison of the Experimental and Calculated DID CIS Spectrum for SF_6

The experimental measurements are indicated by dots (plotted every 1 cm^{-1}.) The spectrum calculated using the DID model, $\beta(x) = x^{-3}$, is shown by the solid line. The dashed line (near zero frequency shift) is the calculated spectrum ignoring the contribution of bound dimers. The bound dimer spectrum and the unbound dimer spectrum are both too narrow. Past 40 cm^{-1} the shape of the observed spectrum changes abruptly.

The intensity calculated using $\beta(x) = x^{-3}$ is $\phi^{(0)}_{ttl} = 574.5$ $Å^9$ ($\phi^{(0)}_{free} = 460.6$ $Å^9$) as compared to the measured value of $\phi^{(0)} =$ 1212 $Å^9$ ($\phi^{(0)} = 1188$ $Å^9$ when the CIRS contribution is subtracted.) Both the width and intensity of the predicted spectrum are smaller than the experimentally measured values.

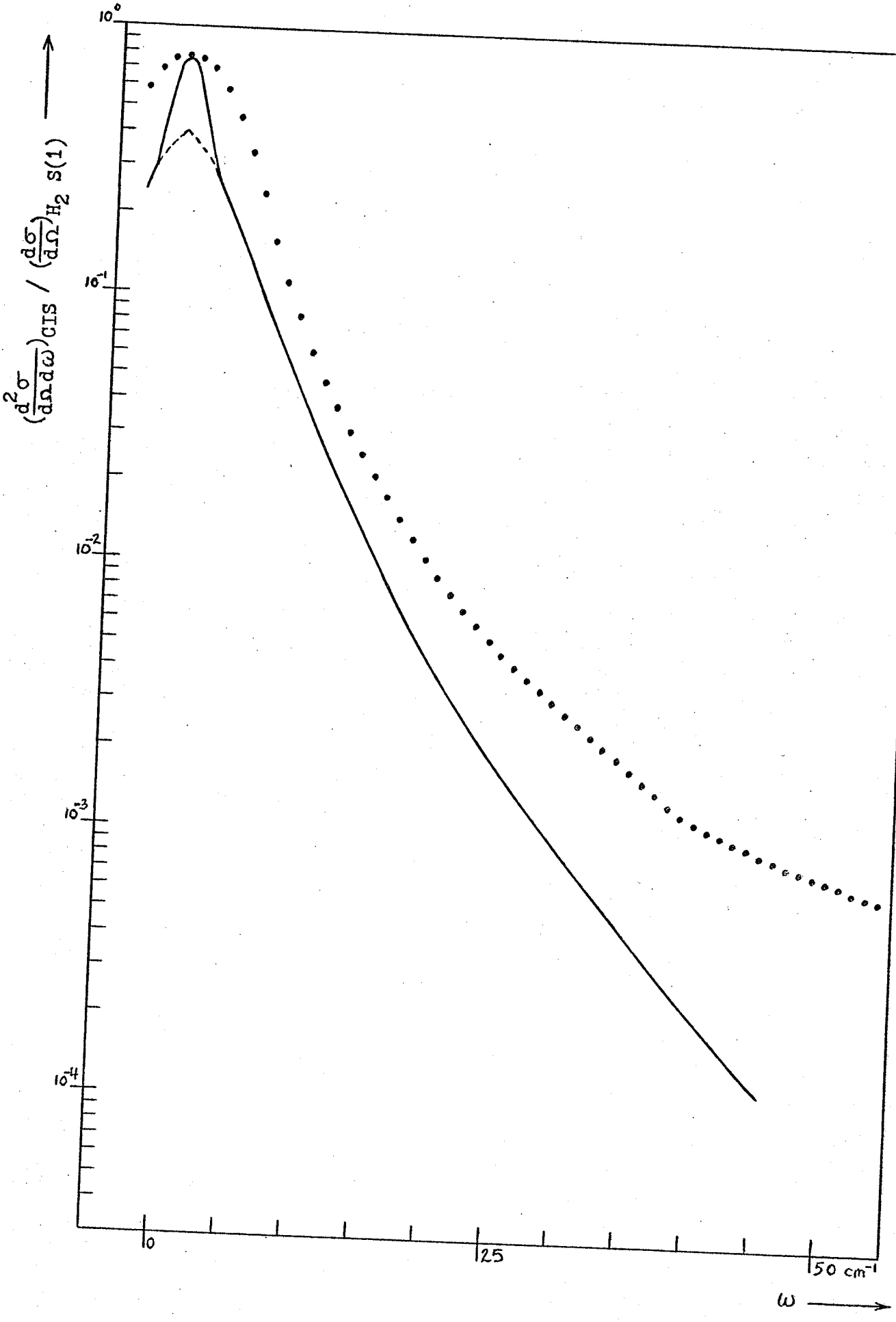
10^{0}
10^{-1}
10^{-2}
10^{-3}
10^{-4}
$(\frac{d^2\sigma}{d\Omega\, d\omega})_{CIS} / (\frac{d\sigma}{d\Omega})_{H_2\ S(1)}$
0
25
50 cm^{-1}
ω

not account for at all. In fact, a different mechanism, collision-induced rotational scattering, takes over from the translational CIS mechanism. This change is suggested by the fact that a high frequency tail is present for all the molecules, but not for Ar. We may confirm our surmise about the nature of the high frequency tail by making an isotopic substitution. As we have said before, the frequency spread of the translational CIS spectrum is essentially determined by the molecular diameter and velocity. The frequency spread of the CIRS spectrum on the other hand, depends on the moment of inertia of the molecule. Consider the pair of molecules CH_4 and CD_4, with masses 16 amu and 20 amu respectively. The molecular velocity of a CD_4 molecule will be $(16/20)^{\frac{1}{2}} \approx 0.89$ times the velocity of a CH_4 molecule with the same energy. All the other properties of these molecules, such as their polarizability, diameter and intermolecular potential, are very similar. Except for a slight shift to lower frequencies, the CD_4 translational CIS spectrum should be identical to that of CH_4. The moment of inertia of CD_4, however, is twice as large as that of CH_4. The frequency of all rotational transitions for CD_4 will be reduced by a factor of two from the CH_4 rotational transition frequencies and so the entire CIRS spectrum will be shifted down in frequency by a factor of two. The spectra of CH_4 and CD_4, obtained under the same conditions, are compared in Figure 6-5. At small frequency shifts the two spectra are almost identical. The high frequency tail of the spectrum however, is drastically different for the two molecules. This is the clear signature of collision-induced rotational scattering in the far tail of the CH_4 and CD_4 spectra.

Having demonstrated that CIRS actually contributes to the observed

FIGURE 6 - 5

Comparison of CH_4 and CD_4 Spectra

The raw data for scans of a CH_4 spectrum (dots) and a CD_4 spectrum (crosses) under the same conditions are plotted in this figure. The samples were both at a pressure of 75 atmospheres at $22^{\circ}C$ and the spectra were scanned with 3.0 cm^{-1} slits at a speed of 20 sec/ch (1 channel = 2 cm^{-1}). Every second point has been plotted (every 4 cm^{-1}), and the background count rate has been indicated by the dashed line at the bottom of the graph. The sharp peak at 354 cm^{-1} is the H_2 S(0) line (H_2 gas at 1 atm has been added to the samples as an internal intensity standard.)

From $0 \rightarrow 60$ cm^{-1} the CH_4 and CD_4 spectra are very similar with the CD_4 spectrum being slightly narrower, as expected. From $60 \longrightarrow 180$ cm^{-1} the CD_4 spectrum bulges upward -- this is due to the presence of 0.8 mole percent air as a contaminant in the CD_4 (see Figure 2 - 2b,c for the shape of the N_2 and O_2 rotational spectra.) Past 200 cm^{-1} the contaminant spectrum no longer interferes with the measurement of the CIS spectrum. At large frequency shifts the spectral profiles for CH_4 and CD_4 are quite different; the CH_4 spectrum bends sharply upwards at 200 cm^{-1}, but the CD_4 does not. The CH_4 spectrum is much more intense at large frequency shifts than the CD_4 spectrum, as is predicted by the CIRS theory.

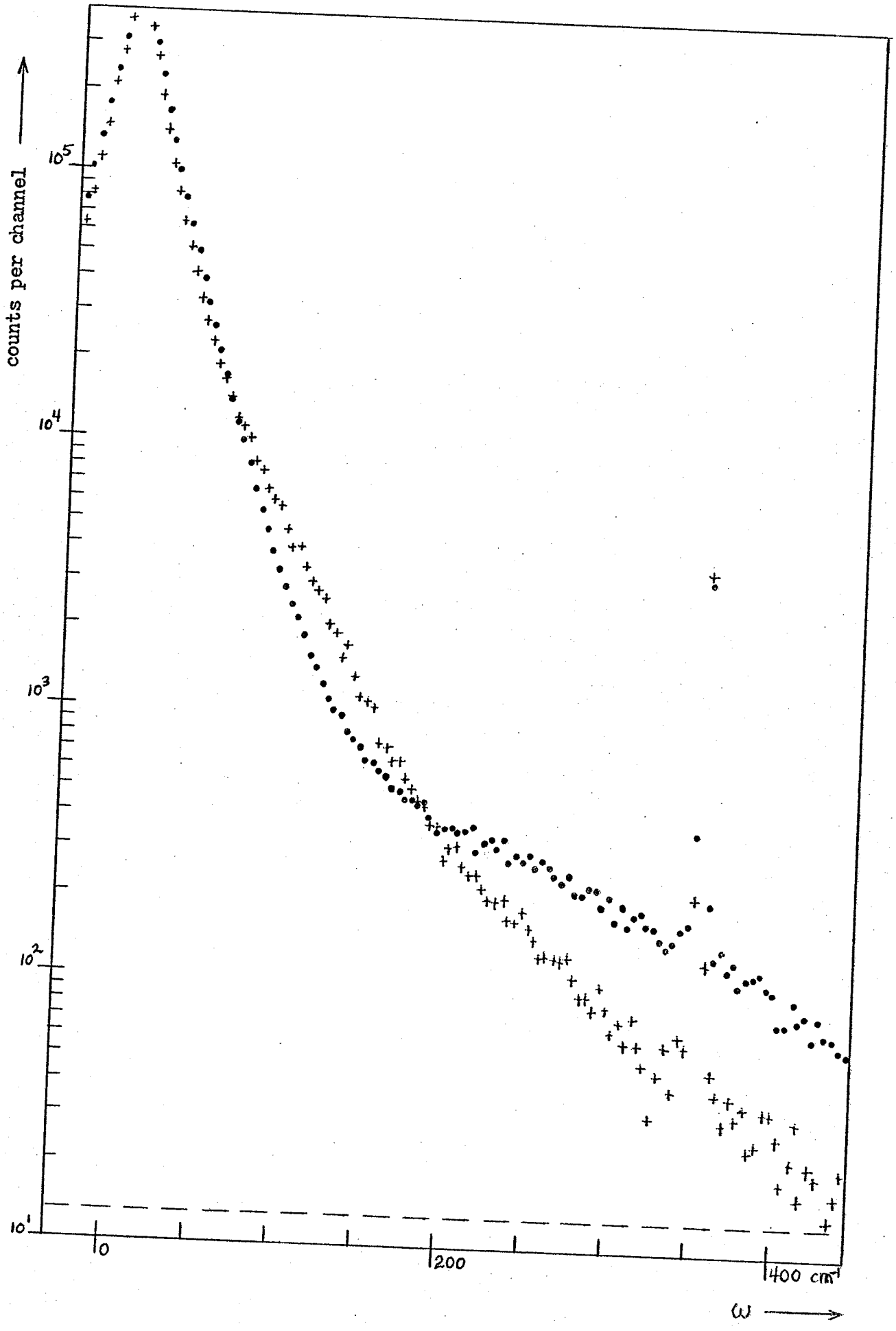
counts per channel
10^5
10^4
10^3
10^2
10^1
0
200
400 cm^{-1}
ω

spectrum we will now compare the computed CIRS spectra with the observed spectra of the molecules CH_4, CD_4, CF_4 and SF_6. The spectra are plotted in Figures 6-6, 7, 8 and 9. The bond polarizability values of A and E from Chapter 4, and the values 5.25, 2.63, 0.185 and 0.0867 cm^{-1} for the rotational constants $\tilde{B}$, have been used in calculating the spectra. The total intensity of the CIRS spectrum is 1.7, 2.5 and 5 percent of the total intensity of the CIS spectrum for CH_4, CF_4 and SF_6 respectively. For both CH_4 and CD_4, the calculated CIRS spectrum agrees very well with the observed high frequency tail of the spectrum. However, at very high frequencies, the calculated CH_4 spectrum becomes too weak compared to the measured spectrum. In the cases of CF_4 and SF_6, the results are less satisfactory. For CF_4 and SF_6 there is only a short range of frequencies where the CIRS spectrum clearly contributes to the observed spectrum. For both CF_4 and SF_6, the observed intensity at large frequency shifts is greater than can be accounted for by our calculation.

This excess intensity at high frequencies appears only in the molecular spectra, so it is most likely that the scattering mechanism is rotational. The frequency shift of this spectral tail lies in the range which can be produced by double rotational transitions involving the tensor $\underset{\sim}{E}$. The bond polarizability model was used to obtain estimates of A and E, and for the estimated values of E the contribution of single and double E transitions to the overall CIRS spectrum is small (except of course for SF_6, where A = 0.) If the values of E which we have used were underestimated by a factor of about 2.5, then the double E transitions would be able to account for the far tail for CH_4 and CD_4. For CF_4, the slope of the far tail

FIGURE 6 - 6

Comparison of the Experimental and the Calculated CIRS Spectrum for CH_4

The experimental measurements are indicated by the dots (plotted every 10 cm^{-1} to 200 cm^{-1}, then every 20 cm^{-1} to 460 cm^{-1} and then at 550, 640 and 730 cm^{-1}), while the upper curve is the DID calculation shown in Figure 6 - 2. The lower curve is the CIRS spectrum calculated for CH_4 with A = 1.2 $\mathring{A}^4$ and E = - 1.2 $\mathring{A}^5$. The CIRS calculation begins to fall below the experimental measurements past 400 cm^{-1}. The contribution of the terms in E to the calculated CIRS spectrum is very small for the chosen values of A and E.

The intensity scale is in units of the CIS scattering cross section per unit frequency interval (1 cm^{-1}) divided by the scattering cross section of the H_2 S(1) transition under the same conditions, when both gases (H_2 and CH_4) are at unit density (1 mole/liter).

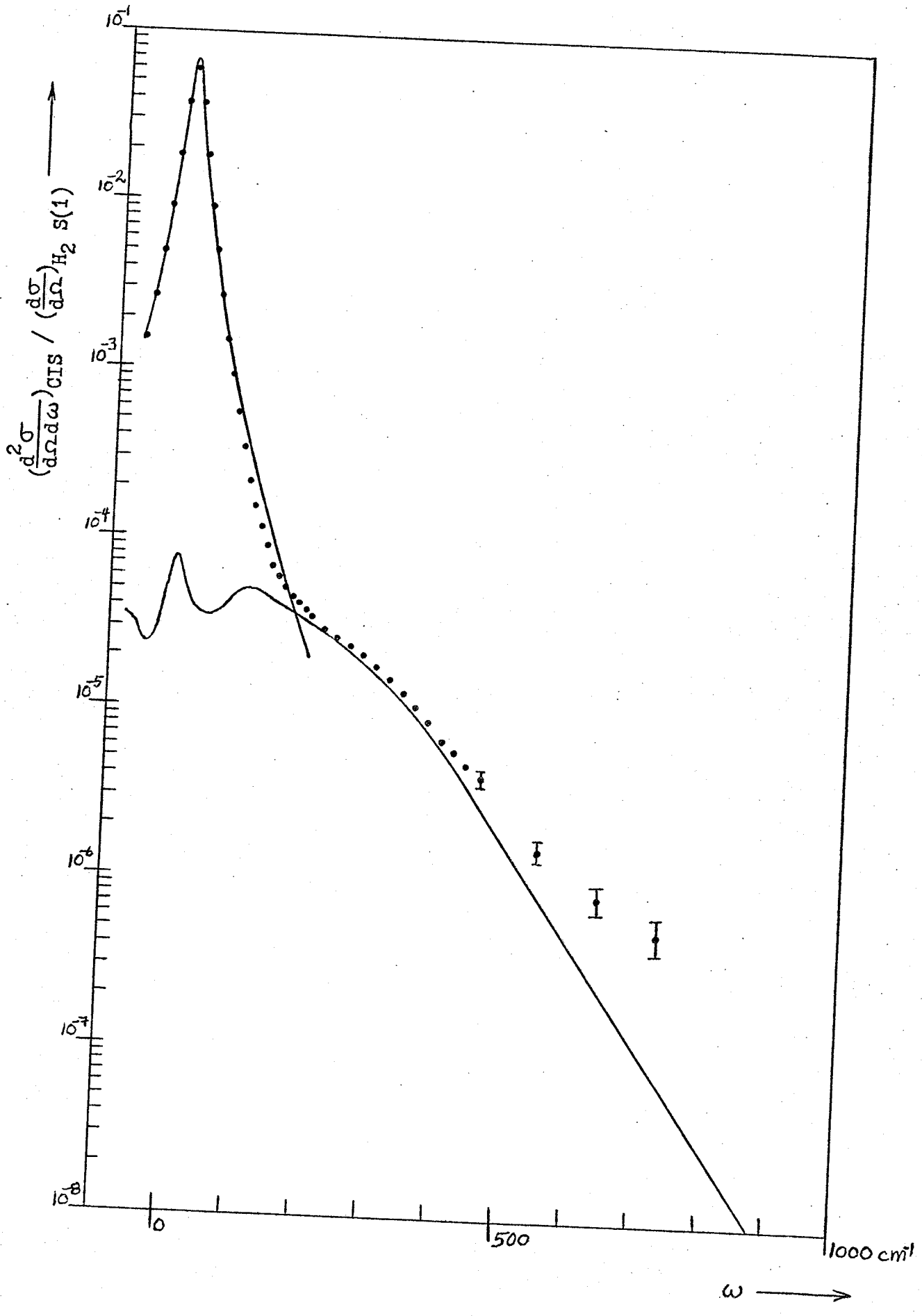
10^{-1}
10^{-2}
10^{-3}
10^{-4}
10^{-5}
10^{-6}
10^{-7}
10^{-8}
$(\frac{d^2\sigma}{d\Omega\, d\omega})_{CIS} / (\frac{d\sigma}{d\Omega})_{H_2\ S(1)}$
0
500
1000 cm^{-1}
ω

FIGURE 6 - 7

Comparison of the Experimental and the Calculated CIRS Spectrum for CD_4

The experimental measurements are indicated by the dots (plotted every 10 cm^{-1} to 200 cm^{-1}, and every 20 cm^{-1} thereafter), while the upper curve is the DID calculation shown in Figure 6 - 2, but with the frequency scale compressed by a factor of 0.9 . The lower curve is the CIRS spectrum calculated for CD_4 with A = 1.2 $\mathring{A}^4$ and E = -1.2 $\mathring{A}^5$. The CIRS calculation agrees well with the experiment, though it seems to fall somewhat below the measurements past 300 cm^{-1}. The contribution of the terms in E to the calculated CIRS spectrum is very small for the chosen values of A and E.

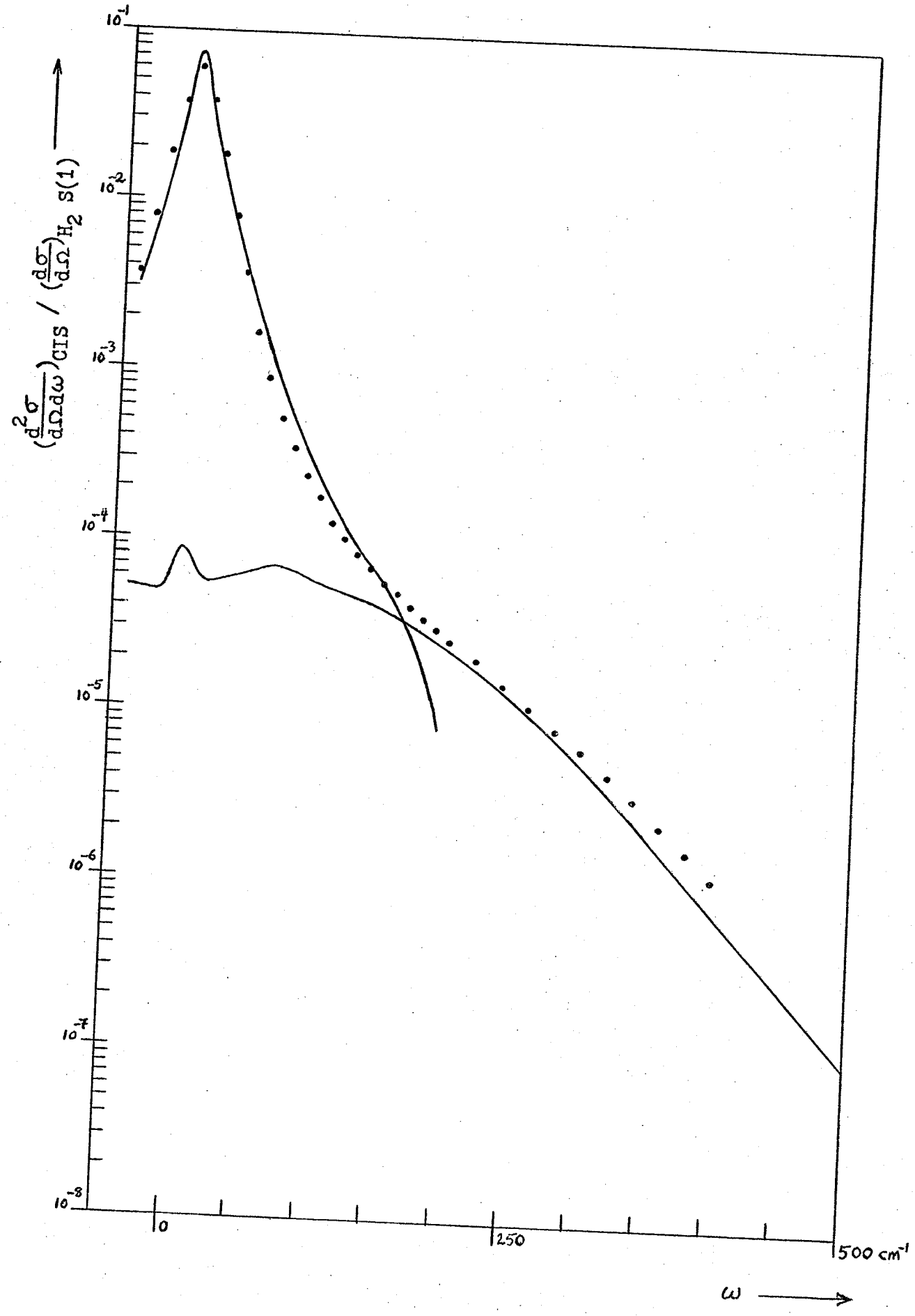
10^{-1}
10^{-2}
10^{-3}
10^{-4}
10^{-5}
10^{-6}
10^{-7}
10^{-8}
$(\frac{d^2\sigma}{d\Omega d\omega})_{CIS} / (\frac{d\sigma}{d\Omega})_{H_2\ S(1)}$
0
250
500 cm^{-1}
ω

FIGURE 6 - 8

Comparison of the Experimental and the Calculated CIRS Spectrum for CF_4

The experimental measurements are indicated by the dots (plotted every 2 cm^{-1} to 60 cm^{-1}, and every 10 cm^{-1} thereafter), while the upper curve is the DID calculation of Figure 6 - 3. The lower curve is the CIRS spectrum calculated with A = 2.2 $Å^4$ and E = -2.2 $Å^5$. From 60 to 80 cm^{-1} the calculated CIRS spectrum lies near the experimental measurements, but for larger frequency shifts the observed intensities are far larger than the calculated values. The contribution of the terms in E to the calculated CIRS spectrum is small for the chosen values of A and E.

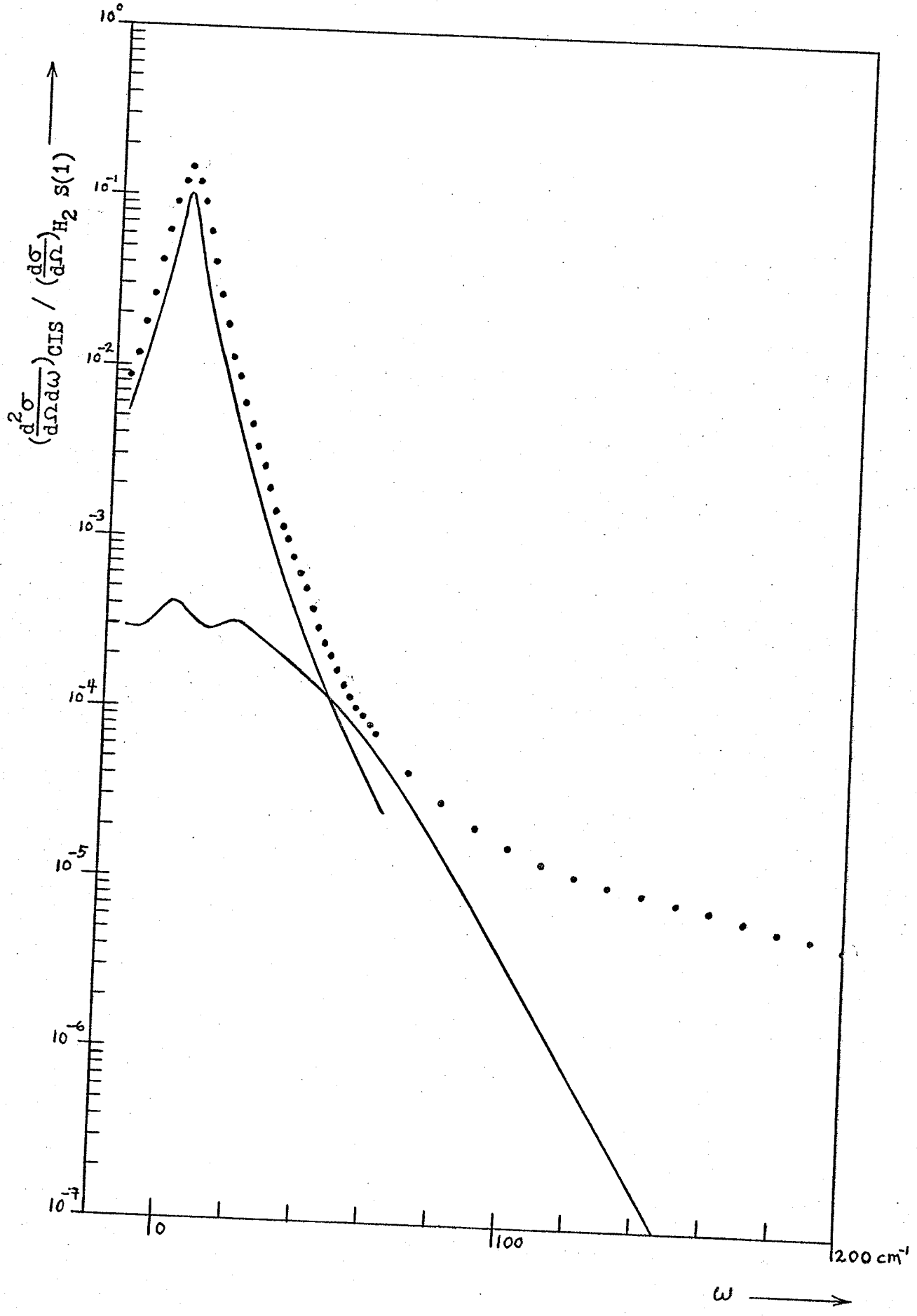
10^{0}
10^{-1}
10^{-2}
10^{-3}
10^{-4}
10^{-5}
10^{-6}
10^{-7}
$\left(\frac{d^2\sigma}{d\Omega d\omega}\right)_{CIS} / \left(\frac{d\sigma}{d\Omega}\right)_{H_2\ S(1)}$
0
100
200 cm^{-1}
ω

FIGURE 6 - 9

Comparison of the Experimental and the Calculated CIRS Spectrum for SF_6

The experimental measurements are indicated by the dots (plotted every 2 cm^{-1} to 40 cm^{-1}, and every 10 cm^{-1} thereafter), while the upper curve is the DID calculation of Figure 6 - 4. The lower curve is the CIRS spectrum calculated with A = 0 $Å^4$ and E = 20 $Å^5$. From 30 to 70 cm^{-1} the calculated CIRS spectrum agrees with the experimental measurements, but for larger frequency shifts the calculated spectrum falls below the measured spectrum. The calculated CIRS spectrum is almost completely due to the E^4 term.

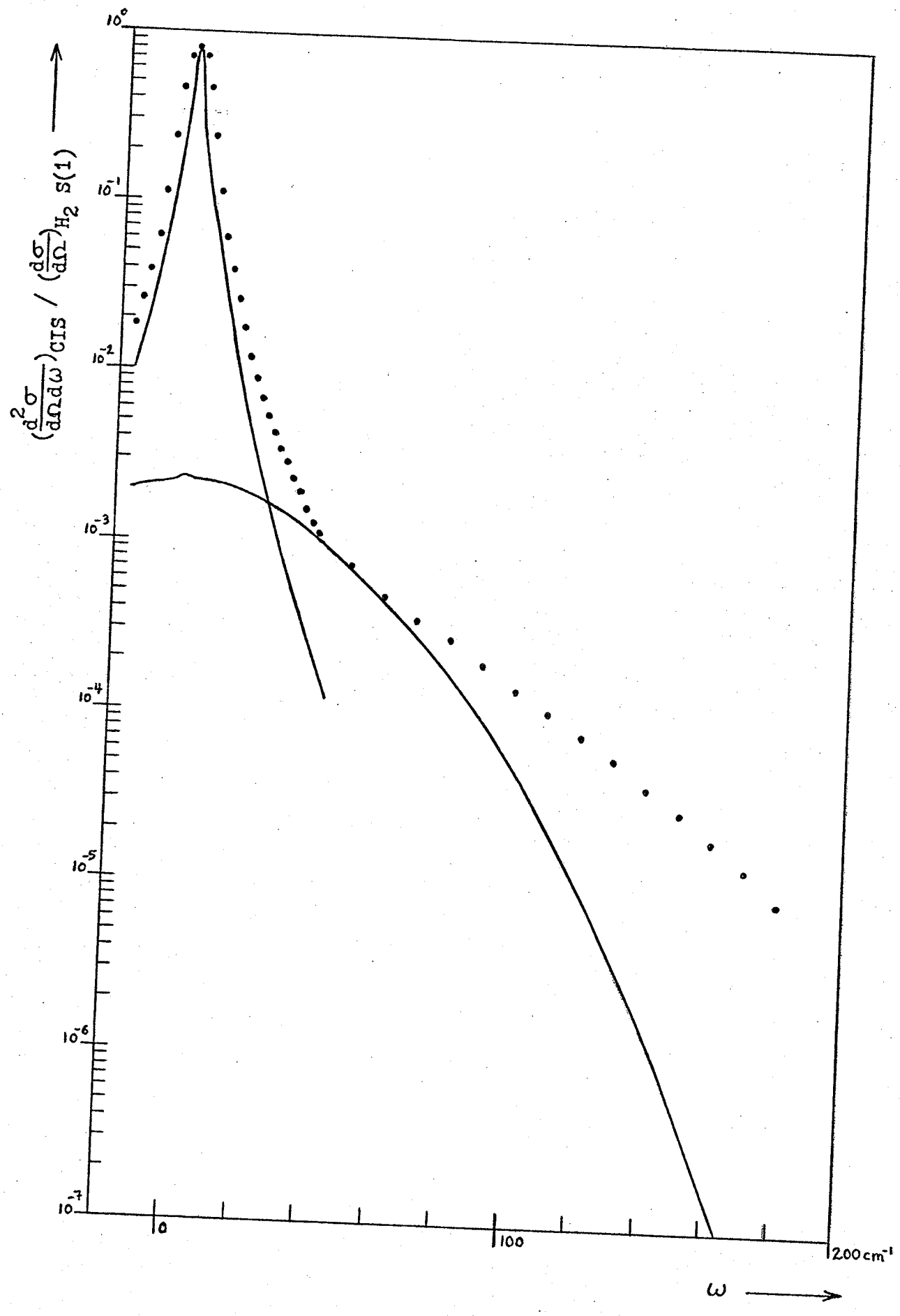
10^{0}
10^{-1}
10^{-2}
10^{-3}
10^{-4}
10^{-5}
10^{-6}
10^{-7}
$(\frac{d^2\sigma}{d\Omega d\omega})_{CIS} / (\frac{d\sigma}{d\Omega})_{H_2\ S(1)}$
0
100
200 cm^{-1}
ω

is too shallow to be accounted for only by double E transitions. In the case of SF_6, one has to invoke the next higher order polarizability, since the calculated SF_6 CIRS spectrum is already all due to the double E transitions.

Unfortunately, the present experimental results for CD_4 do not extend far enough in frequency to rule out, by comparison between the CH_4 and CD_4 spectra, the possibility that the excess intensity at very high frequencies is due to a translational CIS mechanism. The very high freqency tail of the spectrum may, in that case, arise either from the effect of a very short range contribution to the pair polarizability, such as frame distortion, or from the break-down of our classical correlation function calculation. The tail in the CH_4 (Stokes) spectrum, for example, corresponds to collisions where the energy of the molecules is increased by more than 3 kT. Since our calculation does not incorporate the four-fold energy change of the CH_4 molecules during these collisions when determining the trajectories, it will probably be incapable of predicting the correct spectrum at such high frequencies. In that event, the classical calculation of the spectrum will have to be replaced with one based on the quantum mechanical description of light scattering.

We will now return to consider the translational CIS spectrum and some modifications of the simple DID model of the pair polarizability. In the point DID model, the polarizability anisotropy is given by the series $\beta(x) = x^{-3} + (\frac{\alpha}{\sigma^3})\, x^{-6} + \ldots$ (recall that $\beta(r) = (\frac{6\alpha^2}{\sigma^3})\, \beta(x)$.) A perturbation calculation[1] for the diatom $(He)_2$ gives the asymptotic form of $\beta(x)$ as:

$$\beta(x) = x^{-3} + 2.52 \left(\frac{\alpha}{\sigma^3}\right) x^{-6} \quad .$$

When we adjust the coefficient of the x^{-6} term of $\beta(x)$ for Ar so that the calculated $\phi^{(0)}$ agrees with the measured value (see Table 3-2) the form of $\beta(x)$ is:

$$\beta(x) = x^{-3} + 0.1147\, x^{-6} + 3.71 \left(\frac{\alpha}{r_m^3}\right) x^{-6} \quad .$$

This result for Ar is quite plausible in the light of the result of the calculation for $(He)_2$. Repeating this proceedure for CH_4, and taking account of the CIRS contribution, we get:

$$\beta(x) = x^{-3} + 0.1355\, x^{-6} + 2.32 \left(\frac{\alpha}{\sigma^3}\right) x^{-6}$$

which is again reasonable in the light of the $(He)_2$ result.

For CF_4 and CF_6, the corresponding expressions for $\beta(x)$ are:

$$\beta(x) = x^{-3} + 0.7723\, x^{-6} = x^{-3} + 28.13 \left(\frac{\alpha}{\sigma^3}\right) x^{-6}$$

$$\beta(x) = x^{-3} + 0.7231\, x^{-6} = x^{-3} + 27.06 \left(\frac{\alpha}{\sigma^3}\right) x^{-6} \quad .$$

For both CF_4 and SF_6, the coefficient of the x^{-6} term is about 10 times as large as expected on the basis of the $(He)_2$ result. It is not clear at first whether this abrupt increase in the coefficient of x^{-6} is reasonable. The main feature which distinguishes CF_4 and SF_6 as a group from He, Ar and CH_4, is just that there are F atoms on the outside of the molecule.[2]

In Figure 6-10 we have plotted the spectra computed for Ar with three values of the coefficient of the x^{-6} term; the coefficient has values of 0, 2.5 and 15 times the value of the coefficient of x^{-6} term for the point DID model. Since the translational scattering calculation ignores internal structure, the behavior of the Ar spectra as the coefficient of x^{-6} increases, should be representative of the

FIGURE 6 - 10

The Effect of a Short Range Term in the Pair Polarizability Upon the Calculated Spectral Profile

Three spectra calculated for Ar using the pair polarizability function $\beta(x) = x^{-3} + A\, x^{-6}$ are plotted (only the unbound dimer spectra are shown.)

A	$\phi^{(0)}_{free}$ (Å^9)	$\phi^{(0)}_{ttl}$ (Å^9)
0.6879	98.2	111.1
0.1147	45.3	51.5
0.0000	37.5	42.7

The spectral profile swings upward as A increases, so that the spectrum becomes relatively more intense at high frequencies when the short range component of $\beta(x)$ becomes larger. However, no abrupt changes in shape are introduced by the short range term.

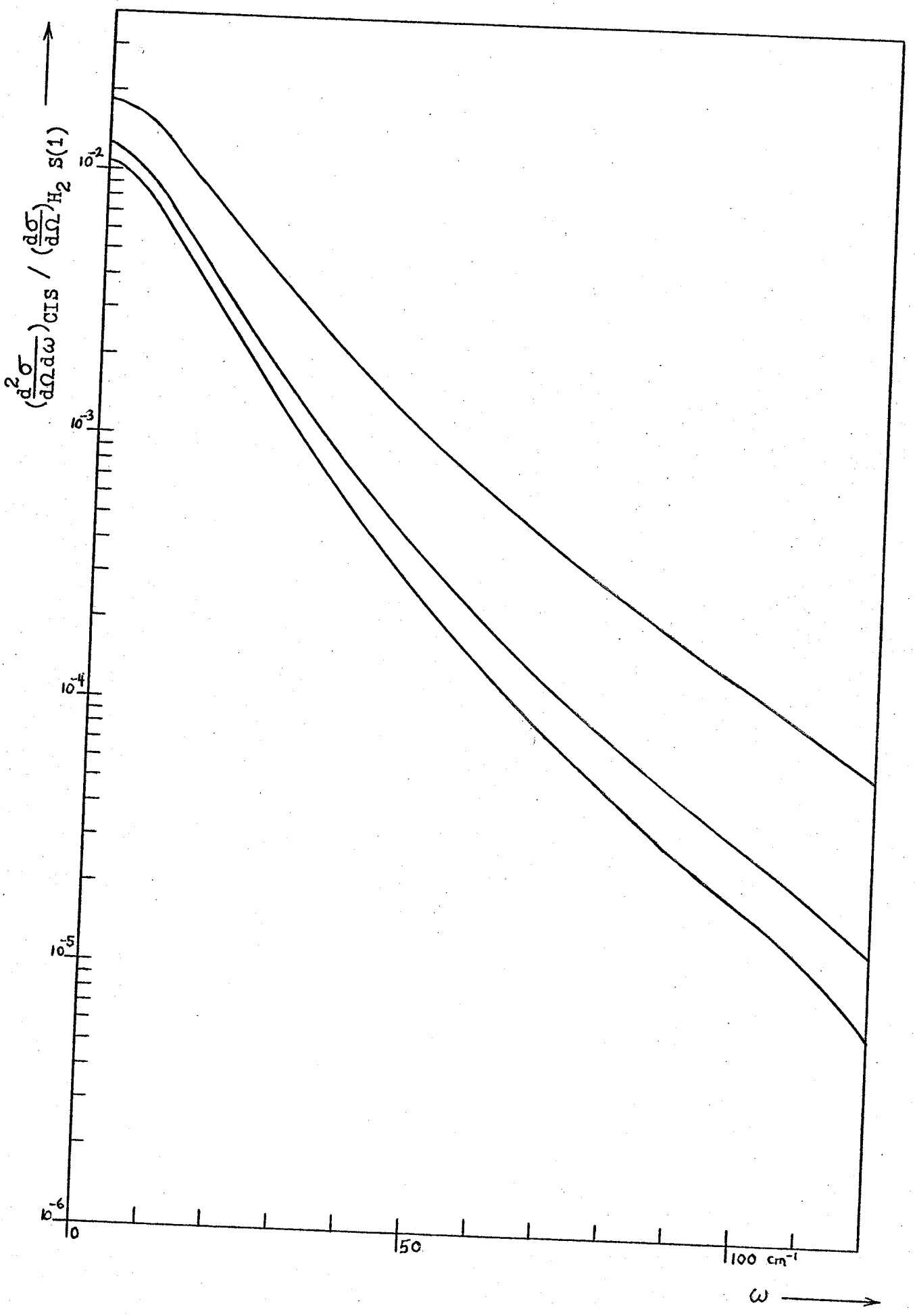
$(\frac{d^2\sigma}{d\Omega d\omega})_{CIS} / (\frac{d\sigma}{d\Omega})_{H_2\ S(1)}$
10^{-2}
10^{-3}
10^{-4}
10^{-5}
10^{-6}
0
50
100 cm^{-1}
ω

behavior of the molecular spectra under the same circumstances. The successive Ar spectra become relatively more intense at high frequencies as the short range component of $\beta(x)$ gets larger, but the dominant change in the spectra is just the increase in intensity at all frequencies. The spectral shape is relatively insensitive to the form of $\beta(x)$. The large x^{-6} term needed to account for the excess intensity in the case of CF_4 and SF_6 cannot be ruled out on the basis of the spectral shape since the spectral shape is only weakly affected by the inclusion of the x^{-6} term.

The large short range term in $\beta(x)$ for CF_4 and SF_6 may in fact arise because of the inadequacy of the point DID model in describing the interaction of these molecules. The point DID model is satisfactory for large intermolecular separations, but for close encounters, the induced fields may vary greatly over a molecular diameter. The electric field at the center of the molecule will be smaller than its value near the colliding edge, so that the point DID model, which considers the fields at the center of the molecule, will underestimate the interaction. In the case of CF_4 and SF_6, the interaction between molecules in a collision may be localized at the impacting fluorine atoms rather than at the center of the molecule. This would account for the unexpectedly large x^{-6} term in $\beta(x)$ when the interaction is expressed in terms of the distance from the molecular center.[3]

The spectrum calculated for Ar with $\beta(x) = x^{-3}$ has an intensity greater than the observed value at large frequency shifts. Inclusion of the short range x^{-6} term will make the disagreement between theory and experiment at large frequency shifts even worse. A mechanism which decreases $\beta(x)$ at short ranges would counteract the tendency for the

high frequency shift part of the spectrum to become relatively too bright. One such mechanism is the so-called electron overlap interaction. When two colliding molecules come close enough together for their electron clouds to partially overlap, the electrons will be compressed into a smaller volume against the effects of their electrostatic repulsion and the Pauli exclusion principle, and the molecules will be strongly repelled. The compression of the electron clouds also results in a reduction in the polarizability of the molecule. Since the repulsive force between the molecules decreases exponentially with their separation, we may expect that the change in the pair polarizability of the molecules due to electron overlap will also decrease exponentially with distance.

To see the effect of electron overlap on the shape of the spectrum we have included in $\beta(x)$ a term which falls exponentially with distance at the same rate as the repulsive part of the intermolecular potential.[4] The size of this negative contribution was chosen arbitrarily to be equal to one half the value of the x^{-6} term at the distance of closest approach in collisions at room temperature. The exponential term sharply reduces $\beta(x)$ at short ranges as can be seen in Figure 6-11. Spectra computed with the inclusion of this term are plotted in Figures 6-12 and 6-13 for Ar and CH_4, along with the corresponding spectra computed with the inclusion of only an x^{-6} term. The total intensity for each of the computed spectra is just equal to the observed zeroth moment of the appropriate molecule. There are no abrupt changes in the shape of the spectrum accompanying the changes in $\beta(x)$. The relative intensity at high frequencies is reduced in the expected fashion by the inclusion of the electron overlap term,

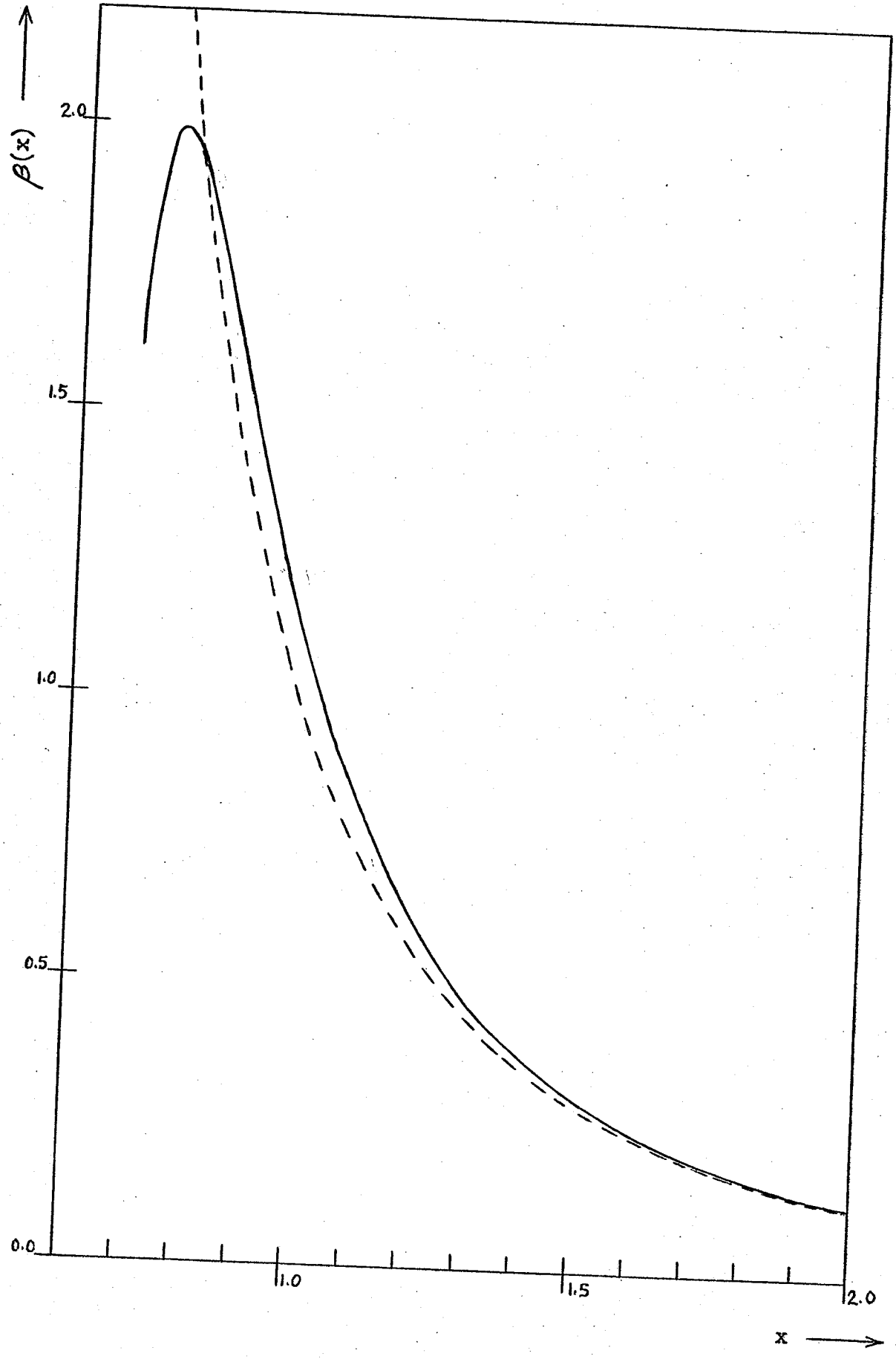
β(x)
2.0
1.5
1.0
0.5
0.0
1.0
1.5
2.0
x

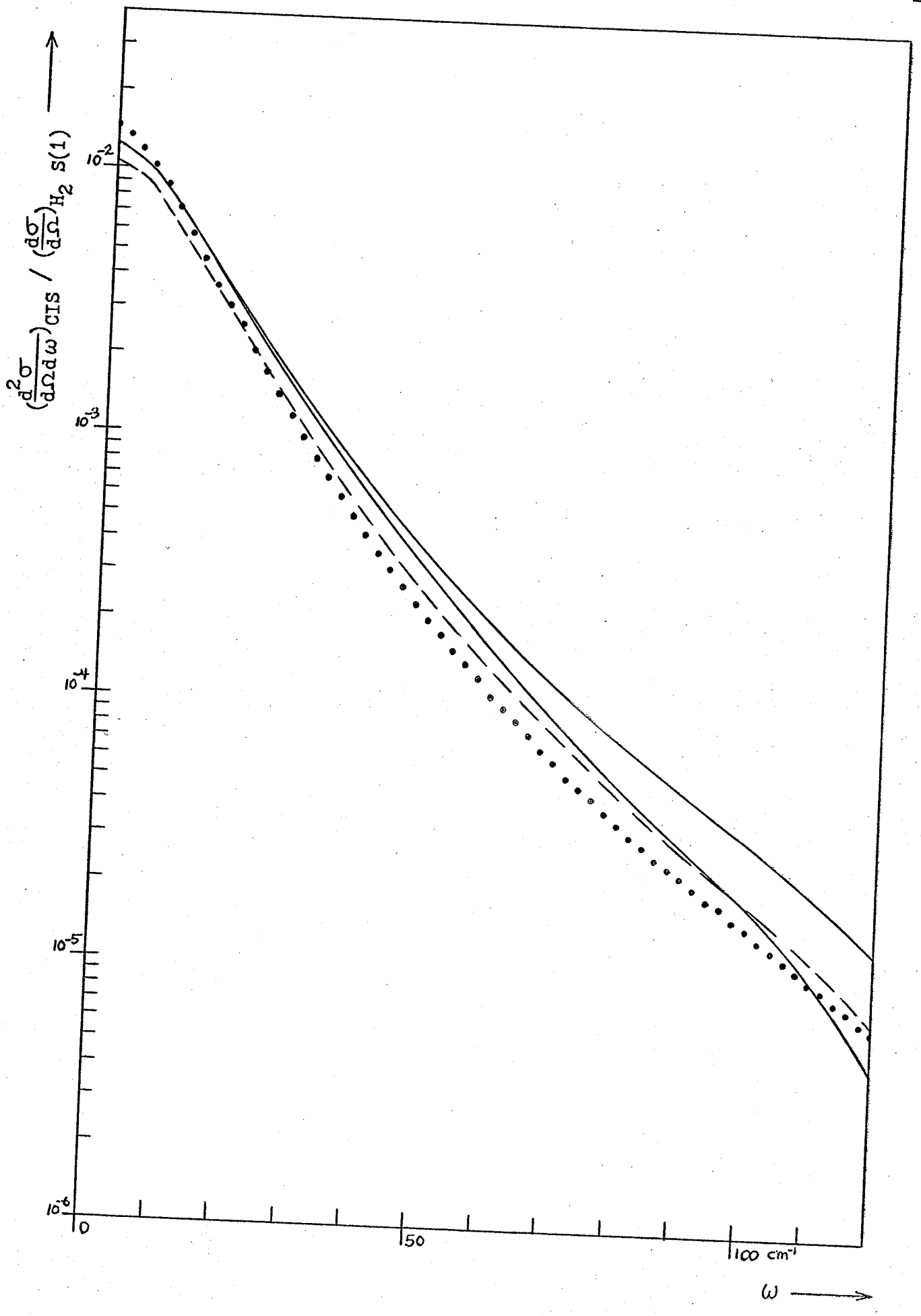
$(\frac{d^2\sigma}{d\Omega d\omega})_{CIS} / (\frac{d\sigma}{d\Omega})_{H_2\ S(1)}$
10^{-2}
10^{-3}
10^{-4}
10^{-5}
10^{-6}
0
50
100 cm^{-1}
ω

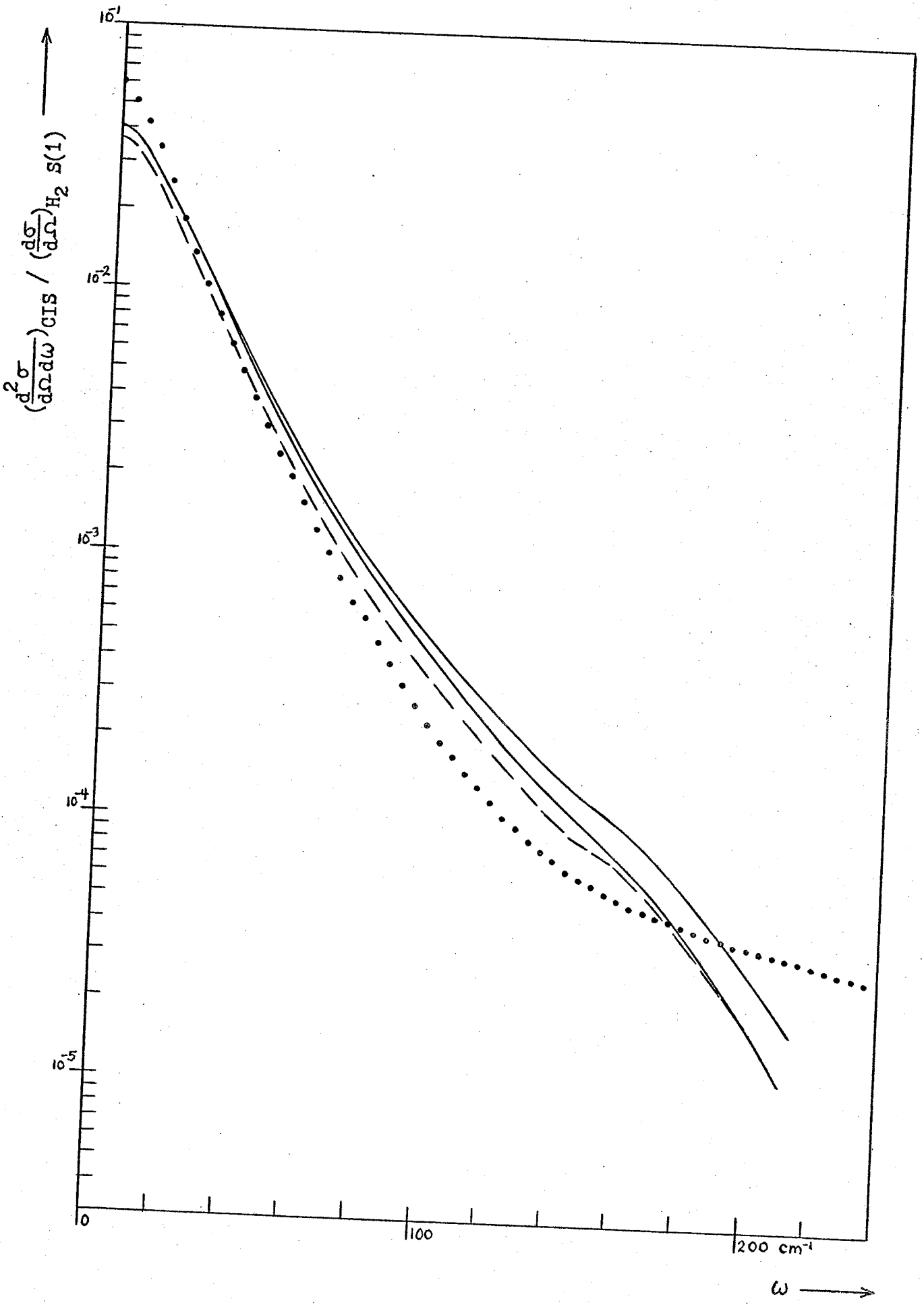
10^{-1}
10^{-2}
10^{-3}
10^{-4}
10^{-5}
$(\frac{d^2\sigma}{d\Omega d\omega})_{CIS} / (\frac{d\sigma}{d\Omega})_{H_2\ S(1)}$
0
100
200 cm^{-1}
ω

and for both Ar and CH_4, the spectra are too intense only in the intermediate frequency region. By a suitable choice of the three parameters in $\beta(x)$, the calculated spectra may be forced to better fit the observations; but to decide whether the resulting parameter values are meaningful, one really requires a better theoretical understanding of the form of $\beta(x)$. It must not be forgotten, for example, that the detailed shape of the scattered light spectrum depends on the form of the intermolecular potential as well as the pair polarizability.

Our conclusions, drawn from the study of the translational CIS spectrum, may be summarized as follows:

a) The simple DID model of the pair polarizability yields a good first approximation to the spectral shape. The spectral shape is relatively insensitive to the form of $\beta(x)$, depending mainly on the collision dynamics.

b) The experimentally observed zeroth moment, $\phi^{(0)}_{expt}$, is larger than the value, $\phi^{(0)}_{DID}$, calculated using the DID model; for the atom and molecules that we have studied, $\phi^{(0)}_{expt}$ is in the range 1.2 to 2.2 times $\phi^{(0)}_{DID}$.

c) In order to account for the discrepency between the observed and calculated intensities, the pair polarizability function must be modified. The additional contributions to $\beta(x)$ which have been considered seem to be short range — for example second order DID, electron overlap and frame distortion. Inclusion of such short range terms tends to increase the intensity at intermediate and high frequencies, making the shape of the calculated spectrum deviate further from the shape of the observed spectrum than it does for the simple

DID model. This tendency is partially countered by the negative electron overlap term. The spectral shape seems to favor a long range form for $\beta(x)$.

d) While the scattered intensity is sensitive to the form of $\beta(x)$, experimentally it is difficult to obtain information about the form of $\beta(x)$ because the measured quantity has been averaged over all the values of x accessible to the colliding molecules. Working over a wide range of temperatures would enable one to select the range of x values being probed in the collisions; the information about the form of $\beta(x)$, obtained from measurements of $\phi^{(0)}$ versus T, would be particularily valuable because it is independent of the theoretical models of $\beta(x)$.

e) Finally, short range terms in $\beta(x)$ do not cause abrupt changes in shape of the spectrum but only tend to smoothly shift the intensity to higher frequencies. The spectra of all the molecules show an abrupt change in the slope of the CIS spectrum at high frequencies. Translational CIS mechanisms cannot account for the intensity at high frequencies.

From the study of the high frequency spectral tails which occur in the CIS spectra of molecules, we may draw the following conclusions:

a) The spectral component which appears (abruptly) at high frequencies in the CIS spectra of molecules is due to collision-induced rotational scattering (CIRS) which arises from the higher order polarizability tensors of the molecules. The high frequency spectra are well accounted for, in intensity and shape, by the CIRS spectra calculated using reasonable parameter estimates.

b) The magnitude of the lowest order polarizability contributing to

the CIRS spectrum may be determined from the spectral measurements. For the molecules we have studied:

$$\left|A_{CH_4}\right| = \left|A_{CD_4}\right| = 1.2 \pm 0.1 \text{ Å}^4$$

$$\left|A_{CF_4}\right| = 2.2 \pm 0.2 \text{ Å}^4$$

$$\left|E_{SF_6}\right| = 20 \pm 2 \text{ Å}^5$$

c) At very high frequencies, the calculated CIRS spectrum falls below the measurements. This appears to be due to the effect of the next higher order polarizability tensors. For CH_4 the excess intensity at very high frequencies may be accounted for, in intensity and shape, by the double E transitions. This allows us to estimate the value of E for CH_4 as:

$$\left|E_{CH_4}\right| = \left|E_{CD_4}\right| = 3.0 \pm 0.5 \text{ Å}^5 .$$

d) For CF_4, we cannot properly extimate E from the data because we cannot ascribe all the intensity excess over the A transitions to the E transitions — as a rough estimate we may take $\left|E_{CF_4}\right| = 10 \pm 5 \text{ Å}^5$. For both CF_4 and SF_6, the very far tail is too broad to be accounted for by the double E transitions, so it would seem that the dipole-hexadecapole polarizability tensor must be invoked to describe this part of the spectrum.[5]

e) The CIRS spectrum not only accounts for the high frequency tails of the molecular CIS spectra, but it also provides a straightforward method for experimentally determining the magnitudes of the higher order molecular polarizabilities.

NOTES AND REFERENCES

1. P. J. Certain, P. R. Fortune, J. Chem. Phys. 55, 5818 (1971)

2. The polarizabilities of He, Ar, CH_4, CF_4 and SF_6 are 0.2051, 1.642, 2.633, 2.85 and 4.470 $Å^3$, respectively. The molecular diameters (the parameter σ of the L-J 6-12 potential) are 2.57, 3.43, 3.68, 4.70 and 5.51 Å . The C-H, C-F and S-F bond lengths are 1.091, 1.33, and 1.59 Å in CH_4, CF_4 and SF_6; the molecular diameter σ as determined by the intermolecular potential is about 1.7 times the diameter of the molecular frame for each of these molecules. The atomic and molecular masses are 2, 40, 16, 88 and 146 amu. On the basis of the polarizability, size and mass of the atoms and molecules, they do not seem to divide into two distinct groups even though there is a clear progression to larger size and polarizability as one goes down the list.

3. When we say that the interaction is localized at the F atoms we do not mean this too literally; we only wish to draw attention to the fact that the electron density is less centrally peaked for CF_4 and SF_6 than for Ar and CH_4. This may make the effect of the finite molecular size upon the scattered intensity relatively larger for CF_4 and SF_6 than for Ar and CH_4.

4. For the repulsive core potentials calculated for the inert gas atoms, see:

   A. A. Abrahamson, Phys. Rev. 130, 693 (1963) .

5. We have used a multipole expansion to describe the angle-

dependent interaction between two molecules which allows the CIRS spectrum. A model which represents a diametrically opposite viewpoint, is to represent the angle-dependent interaction as being due to (point dipole) atom-atom interactions between the outer atoms comprising the two colliding molecules (see: R. A. Stuckart, C. J. Montrose, T. A. Litovitz, Symposia Faraday Soc. 11, 94 (1977).) While the scattering by such an atom-atom interaction would be much smaller than for the induced quadrupole and octopole interactions we have considered, it could very well compete with the induced hexadecapole interactions; for tetrahedral and octahedral molecules the atom-atom and hexadecapole polarizabilities will both involve moments of the 5-th rank (see: A. D. Buckingham, G. C. Tabisz, Mol. Phys. 36, 583 (1978).)